Effects of Microemulsion and Shut-in Time on Well Performance: A Comparative Field, Laboratory and Simulation Study

by

Taregh Soleiman Asl

A thesis submitted in partial fulfillment of the requirements for the degree of

Master of Science

in

PETROLEUM ENGINEERING

Department of Civil and Environmental Engineering

University of Alberta

© Taregh Soleiman Asl, 2020

Abstract

Montney Formation is well-known as a world-class unconventional resource, covering approximately 130,000 km^2 located on the border between the provinces of Alberta and British Columbia. In last decade, horizontal drilling and hydraulic fracturing technologies have been the key to unlock the hydrocarbon production from these unconventional resources. However, the oil recovered through the hydraulic fracturing is low, and only between 5-10 % of the Original Oil in Place (OOIP) is recovered. Using EOR methods in unconventional resources is necessary to recover the remaining oil.

In this research, we analyzed flowback and post-flowback production data from a horizontal well in the Montney Formation, which was fractured with water containing a microemulsion additive as an EOR while fracturing method. This well was shut-in for 7 months after 5 months of post-flowback production. Oil and gas rates were significantly increased after the shut-in (700% increase), suggesting a reduction in matrix-fracture damage.

To investigate the reasons behind this enhancement, we performed a series of imbibition oil-recovery tests to investigate how the presence of (i) capillary suction (ii) osmotic pressure (iii) salts precipitation reduces formation damage at the fracture-matrix interface, resulting in improved oil displacement from matrix during the tests. Next, we measured dynamic liquid-liquid contact angles for oil droplets on the rock surface by gradually adding ME to the aqueous phase to mimic the mixing of injected fracturing fluid with reservoir brine.

In addition to the experiments, to further investigate the effects of the shut-in on the spontaneous imbibition oil recovery, we simulated three-phase production using the actual reservoir geological model. We attempt to match the production data before and after the shut-in period. To match the data, we had to account for the reduction in oil and gas relative permeabilities due to water blockage by using transmissibility multipliers for the fracture-

matrix interblocks. Additionally, we perform sensitivity analysis to determine the optimum shut-in time for this well. The objective functions for determining this optimum shut-in time are net present value (NPV) and cumulative hydrocarbon production.

Combined analyses of field, laboratory and simulation results suggest that: (i) imbibition of fracturing water containing ME solution during extended shut-in periods reduces phase trapping near fracture face; (ii) osmotic pressure is a key driving force for improved oil recovery during imbibition oil-recovery, (iii) capillary pressure is an additional driving force if the aqueous phase preferentially wets the rock surface and (iv) extended soaking time of the well, enhances the hydrocarbon relative permeability and decreases the water blockage at fracture-matrix interblock.

Preface

This research is original work by Taregh Soleiman Asl. Some parts of the thesis in Chapter 3, 5 and 6 have been published or presented as:

1) Soleiman Asl, T., Habibi, A., Ezulike, O. D., Eghbalvala, M., & Dehghanpour, H. (2019, January 29). The Role of Microemulsion and Shut-in on Well Performance: From Field Scale to Laboratory Scale. Society of Petroleum Engineers. doi:10.2118/194363-MS.

2) SPE-19998-MS will be published in the Unconventional Resources Conference (Calgary, Sep 2020).

Dedicated to my beloved parents

Acknowledgment

Table of Contents

List of Tables

List of Figures

Chapter 1

1) Introduction

In this chapter, we present an overview and background of the unconventional resources, recent drilling and fracturing development, Enhanced Oil Recovery (EOR) using chemical additives , extended shut-in time, and low-salinity water EOR. We introduce the case study along with field observations and describe the research objectives and scope of the work**.**

1.1   Overview and background

1.1.1 Unconventional Resources and Hydraulic Fracturing

Different forecasts expecting a gap between the supply and demand of oil and gas in the future. With the sacristy of finding new high-quality and high-permeability reservoirs, the unconventional reservoirs are becoming a very important source to provide the world demands of energy. However, until the end of the last decade, extracting the oil and gas from these unconventional resources was difficult and not economic. The main turning point of the production from the unconventional reservoirs, was the development of horizontal drilling and combining it with the multistage hydraulic fracturing operations, which made the exploitation of the unconventional resources economically feasible. Due to the latest completion technologies, unconventional resources in North America have received a lot of attention recently (Holditch 2003, Franz and Jochen. 2005, Clarkson and Pedersen 2011).

1.1.2 Horizontal Drilling

Hydraulic fracturing is a process in which a fluid is injected into the well with high rates and pressure to exceed the reservoir rock strength. The first time the hydraulic fracturing was used in 1949 to stimulate the oil and gas production from the wells (Montgomery and Smith. 2010). It became the basic requirement for an economic development of the tight oil and gas reservoirs since 1968 (Gandossi 2013). However, the main target was to fracture the entire production zone and create a larger contact area between the fractures and matrix. Using long horizontal wells along with multistage hydraulic fracturing allows to achieve this target. Creating multistage fractures in the ultra-low permeability reservoirs requires high-pressure injection of a fracturing fluid such as slickwater or crosslinked gel (Yu and Sepehrnoori 2013, Rahman et al.2014).

1.1.3 EOR Methods in the Low-Permeability Reservoirs

During the primary oil-recovery after hydraulic fracturing of a tight-oil reservoir, only less than 10% of the Original Oil in Place (OOIP) is recovered (Clark. 2009). Obviously, there is a huge volume of residual oil which requires application of enhanced oil-recovery (EOR) methods to be extracted. In other words, the remaining oil is a big prize to be claimed using the best EOR method in the low permeability reservoirs. One of the recommended methods is "EOR while fracturing", by adding chemical additives to the fracturing water (Neog and schechter. 2016, Chevalier et al. 2018, Tangirala and Sheng. 2019). In this technique, the fracturing fluid is treated with the chemical additives such as surfactants or microemulsion, and is injected to the wellbore at high rate and pressure (Palisch and Handren. 2010). The main objective of adding surfactants to the fracturing fluid is 1) to reduce the interfacial tension (IFT) between oil and water in the reservoir and 2) to alter reservoir-rock wettability (Samuel et al.2000, Sheng 2015, Yan et al.2016).

1.1.4 Effects of Microemulsion and Extended Shut-in time on Oil-recovery

Water blockage is a phenomenon that occurs near the matrix-fracture interface during the hydraulic fracturing, due to the large amount of the injected fracturing water that may leak-off from the fractures into the reservoir matrix and trap in small pores. This phenomenon is considered as formation damage which may results in fracturing-fluid loss into the matrix along with lower oil-recovery from the reservoir (Bennion et al.1996, Longoria et al.2015). Adding microemulsions to the fracturing fluid is considered as a solution to decrease the water blockage by reducing the s interfacial tension (IFT) of oil-water system. Adding microemulsion to fracturing fluid allows the solubilization of the trapped water into the hydrocarbon, thus minimizing the water blockage (Negin et al.2016, Wijaya 2019). In addition to lowering the IFT, microemulsions are well-known as effective agents for wettability alteration to increase the wetting affinity of rock towards water and enhance the spontaneous imbibition of water into the matrix, and allow the counter current imbibition of the oil into the fracture (Alvarez and schechter 2017). Along with using microemulsions, extended shut-in time is another technique to reduce the water blockage. In this mechanism, the well is shut-in after the fracturing process for longer times, allowing the water to further imbibe into the matrix and reduce the water saturation near the matrix-fracture interface (Ghanbari and Dehghanpour 2016).

1.1.5 Low-salinity water Injection

Soaking a well with low-salinity water is an important EOR method in tight and shale oil reservoirs. In this method, osmotic pressure acts as an extra driving force in addition to the capillary forces to expel the oil out by counter-current imbibition (Brodie and Jerauld 2014). This pressure is a result of the chemical osmosis process occurs in the reservoir. During chemical-osmosis, water moves from a low-salinity side to a high-salinity side through a semipermeable membrane to reach salinity equilibrium in both sides. In the reservoir clay can act as semi-permeable membrane in the chemical osmosis process (Fakcharoenphol et al.2014).

1.1.6 Research Gap

A great deal of researches and studies have been performed in last decade to evaluate the effects of using microemulsions and surfactants in unconventional plays, during EOR processes (Kathel and Mohanty 2013, Bera and Mandal 2015, Shen et al.2018, Druetta and Picchioni 2019). Moreover, several studies were conducted to investigate the effect of using low-salinity water and the role of the osmotic pressure on oil-recovery of tight-oil reservoirs (McGuire et al.2005, Sandengen et al.2016, Teklu et al.2018). However, most of these studies did not consider combining the field observations with the laboratory experiments and focused only on one of them. In addition, there is no clear picture in the literature about the relationship between capillary pressure and osmotic pressure, and what is their combined role in the enhance oil recovery.

1.2 Case Study

As a case study in this thesis, we considered the Montney Formation, which is an unconventional resource play, located in the Western Canadian Sedimentary Basin (WCSB).

1.2.1 Well Shut-in Effect on Production

A horizontal well drilled in the Montney Formation and fractured using water containing a micremulsion (ME) additive. This well was put on production immediately after completion process. **Fig. 1-1** shows the production profile of this well. It was put on flowback for 33 days using a jet pump and shut-in for 2 months before reopening it for post-flowback production. The well remained on post-flowback production for 5 months, having high water rate and low oil and gas rates. This well was then shut-in for 6 months for surface facility completion and pipeline construction, before reopening with gas lift instead of jet pump to minimize water cut. **Fig. 1-2** shows that shut-in period significantly affects the instantaneous oil and gas rates by increasing them to higher values than those before the shut-in time. Different hypotheses are

proposed to explain this interesting enhancement in oil and gas rates after the shut-in, and they will be evaluated in this dissertation.
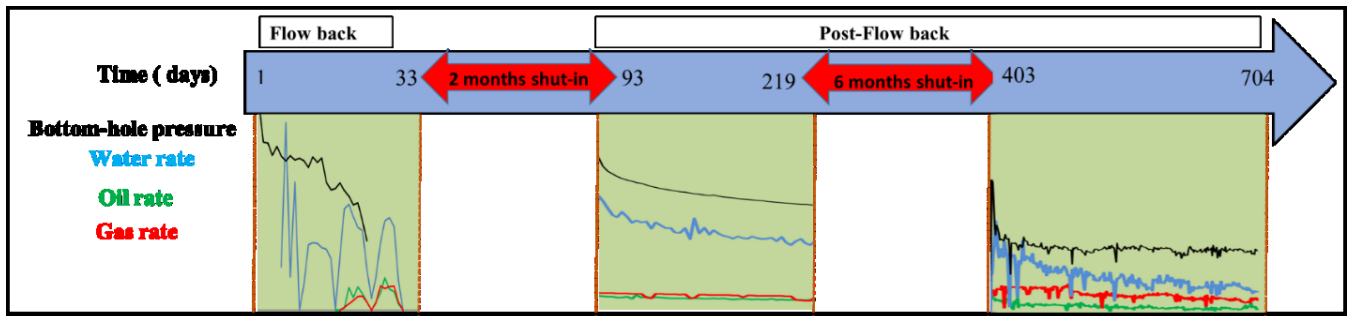
Figure 1-1- Production profile of the target well from immediate production after fracturing job using jet pump to gas lift after 6 months of shut-in.
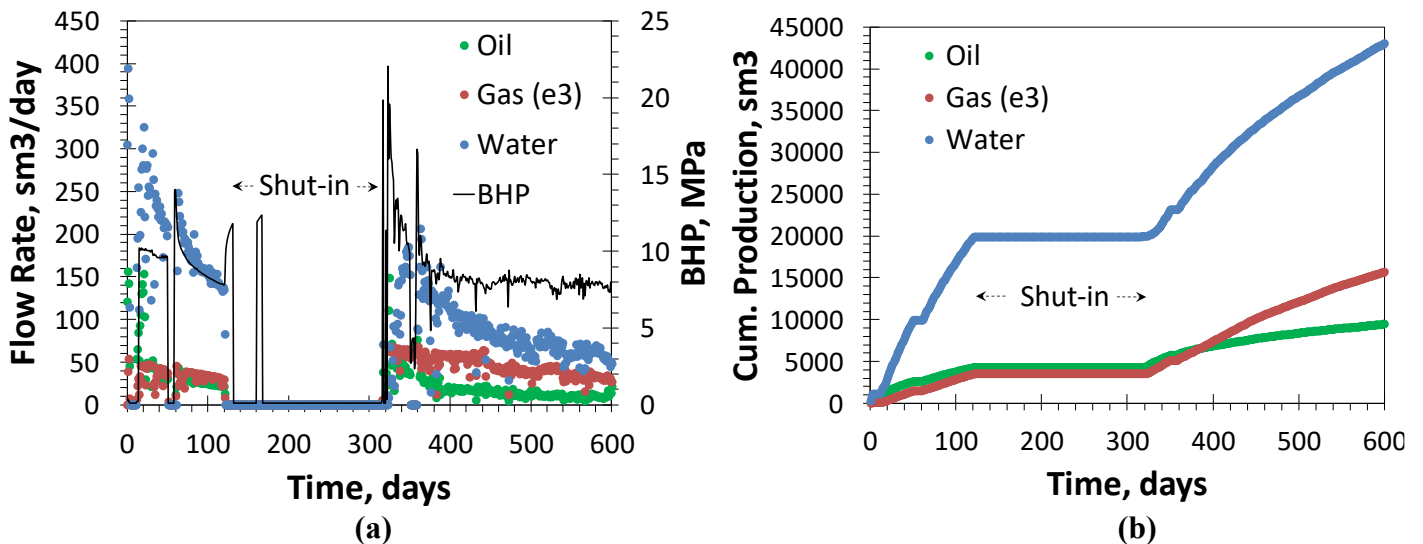
Figure 1-2- Post-flowback production data. (a) Oil, gas, and water flow rate and bottom-hole pressure. (b) Cumulative production.

1.3 Objective and Scope of Work

Different questions are raised about the enhancement of hydrocarbon rates after the well shut-in: 1) is this enhancement due to the extended shut-in time, 2) what happened in matrix-fracture interface during the shut-in period, 3) what is the main reason behind the hydrocarbon production increase after the shut-in, the ME additive or the pressure buildup 4) what is the role of osmotic pressure on hydrocarbon production. Three different hypotheses are proposed to explain the improved oil and gas production rate after shut-in period: 1) reduction of water blockage and formation damage near the matrix-fracture interface 2) capillarity and wettability alteration that lead to counter-current imbibition of fracturing fluid and 3) role of clays and

osmosis pressure on oil displacement from matrix to fractures. To evaluate these hypotheses, I performed a comprehensive study in this thesis as follows:

i)   Data-driven analyses on flowback and post-flowback field data to quantitatively and qualitatively evaluate how shutting a well fractured with water containing ME affects hydrocarbon production.

ii) Spontaneous imbibition oil-recovery tests with different scenarios to simulate rock-fluid interactions during the shut-in period, and evaluate the effect of ME and salinity on oil recovery

iii) New methods of dynamic contact-angle measurements along with IFT tests to evaluate the changes in wettability and interfacial properties as a result of adding ME to an oil-water system

iv) Numerical methods for calculating the osmotic pressure to prove the contribution of osmosis pressure in addition to capillarity pressure.

v)   Reservoir simulation by using the geological reservoir model, to history match the actual field production and pressure data.

1.4   Thesis Structure

This research is divided into 8 chapters. The organization of these chapters are as follows:

In Chapter 1, we present an overview and background of the unconventional resources, recent drilling and fracturing development, EOR using chemical additives, extended shut-in time, and low-salinity water EOR. We introduce the case study along with field observations and describe the research objectives and scope of the work.

In Chapter 2, we present the relevant literature including a brief overview of the Montney Formation, hydraulic fracturing, role of chemical additives in EOR, spontaneous imbibition of the fracturing fluid, and the chemical-osmosis effect.

In Chapter 3, we present the key observations of field production data during different production stages, along with the data analysis of the production history of the well.

In Chapter 4, we analyze the petrophysical properties such as porosity and permeability of the core plugs of the target well along with two adjacent wells by using the results of different laboratory measurements conducted on the core plugs.

In <u>Chapter 5</u>, we simulate the actual geological model of the reservoir, to investigate the effect of the extended shut-in time on the well performance.

In <u>Chapter 6</u>, we conduct experiments to understand the change in the oil-water-rock interactions in the laboratory-scale and compare it with the field-scale.

In <u>Chapter 7</u>, we calculate the capillary and osmotic pressures, to understand the contribution of each one on oil-recovery mechanism.

In <u>Chapter 8</u>, we present the conclusions and the recommendations.

Chapter 2

2) Literature Review

In this chapter, we firstly review the specifications of the Montney Formation followed by importance on oil production in North America, followed by the role of the latest technologies in development of the tight oil and gas plays. Then the relevant literature including the EOR by using chemical additives, spontaneous imbibition dominated with capillary pressure, role of the extended shut-in time on hydrocarbon production, and finally the effect of osmosis effect on oil recovery are reviewed.

2.1   Montney Tight-Oil Formation

Montney Formation belongs to Lower to Middle Triassic era (approximately 240 million years) located in Western Canadian Sedimentary Basin. It is known as a world-class unconventional resource, covering approximately 130,000 km^2 located on the border between the provinces of Alberta and British Columbia (**Fig 2-1**). The lithology of the Montney Formation is mainly siltstone and contains small fractions of sandstone. Its depth ranges between 500m to 4500m, and the thickness can be up to 300 m (NEB 2013). This change in depth along the Montney Formation forms variety of hydrocarbons including oil, natural gas, and dry gas. The marketable hydrocarbon-in-place of the Montney is estimated to be 4,274 Tcf of natural gas and 268 billion bbl of oil and natural gas liquids. The average Total organic Carbon (TOC) content of the Montney is estimated between 0.1 to 3.6 wt% with average of 0.8 wt% (Rivard et al. 2014). The rock mineralogy is mainly quartz, dolomite, feldspar, and clay minerals. Average porosity is around 10% and extremely low permeability ranges from 0.0005 to 0.003 mD (Rivard et al. 2014).
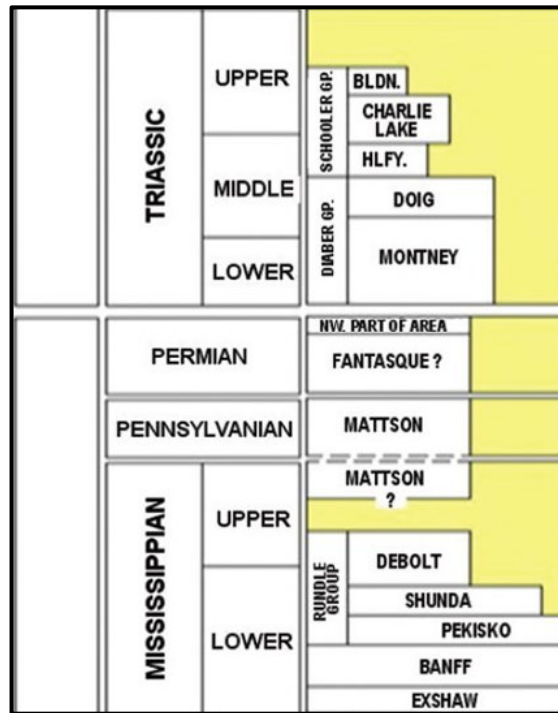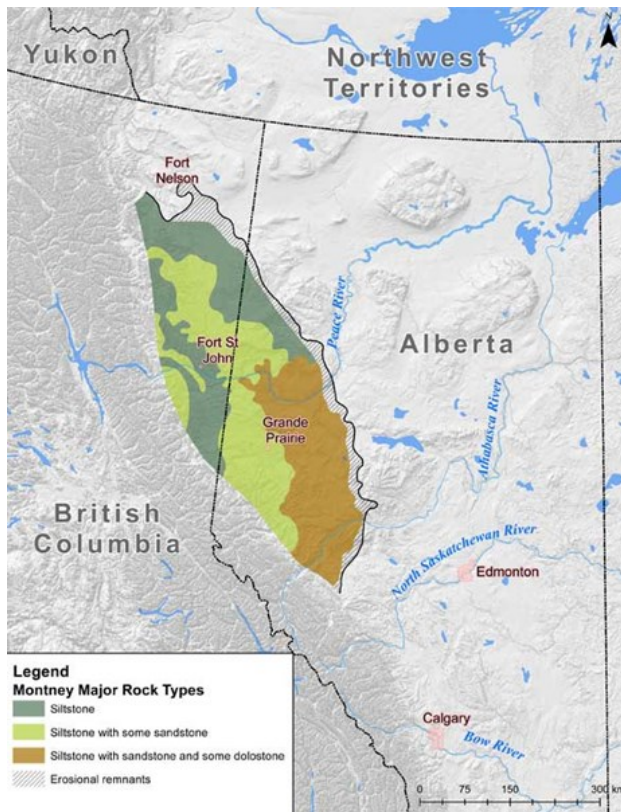
Figure 2-1- The geographic and stratigraphic location of the Montney Formation (NEB et al. 2013, Nieto et al. 2013).

Oil and gas exploration in the Montney Formation has started since 1950s, mainly focusing on the conventional reservoirs. However, Montney remained undeveloped until 2005, when new technologies such as horizontal drilling and hydraulic fracturing were developed and made economic exploitation of the unconventional resources feasible (NEB 2013).

2.2   Horizontal Drilling and Hydraulic Fracturing Developments

Increasing global energy demand and decreasing hydrocarbon production from conventional reservoirs have motivated the industry to explore new ways to produce hydrocarbon from unconventional resources (He et al. 2015). Over the last decade, the combined horizontal drilling with multistage hydraulic fracturing have been the key to unlock the hydrocarbon production from the unconventional resources (Desai 2014, He et al. 2015). This development raised the interest in the unconventional shale and tight oil and gas resources in North America (Shaoul et al. 2011, Vengosh et al.2013). The unlocked resources by hydraulic fracturing boosted the natural gas reservoirs of the North America to approximately 3 quadrillion cubic feet and increased the oil production 10 times more than that from conventional reservoirs (Desai 2014). Hydraulic fracturing was first applied in the U.S. petroleum industry in the late

1940`s as an Enhanced Oil Recovery (EOR) technique, which led to 75% increase in the oil production of vertical wells (Montgomery and Smith 2010). In hydraulic fracturing, after drilling and perforating the well, a fluid with high pressure is injected until the formation rock is fractured, then the fractures are extended over the course of fluid injection, creating a high permeability zone in the reservoir (Haimson and Fairhurst. 1969). The first time that the hydraulic fracturing was combined with the horizontal drilling was in the 1990s, to produce oil from the shale reservoirs (King 2010).

Horizontal drilling helps to reduce number of wells compared to the drilled vertical wells. A multi-well pad with several horizontal wells, occupies a smaller surface area and is able to access long distances down the reservoir by different hydraulic fracturing stages. These hydraulic fracturing stages can create a large contact area between the horizontal well and the reservoir matrix (**Fig 2-2**). For a typical hydraulic fracturing operation with water as the fracturing fluid, approximately between 10,000 to 70,000 m^3 of water is injected with high pressure down the well to induce fractures. The fracturing fluid typically consists of 90-95 % of water, 4.5-9.5% proppant and 0.5% chemical additives such as biocide, surfactant and friction reducers. The generated fractures provide high-permeability conduits for the flow of hydrocarbons through the low-permeability reservoir rock. The fluid volume required for injection is determined based on many factors including type of fluid treatment, number of stages, and the lithology of the targeted formation. There are three types of treatment fluids used for fracturing Montney wells: 1) slickwater, 2) energized fluid, and 3) a combination of both of them. Slickwater treatment is usually used for fracturing brittle heterogeneous rocks and requires large volumes of water to induce large fractures and transport the proppants. On the other hand, energized fluids such as N_2 and $CO_{2\ s}$ solutions, mainly target soft and more ductile rocks and require less amount of water than slickwater treatment (The Scientific Hydraulic Fracturing Review Panel of British Columbia Government. 2019).

After fracturing process, usually the well is shut-in for days or weeks to install completion assemblies. This is followed by the flowback process in which a fraction of the injected water is recovered back at initial time of production. The produced water can be reused after going through different treatments. **Fig 2-3** shows the water usage during the hydraulic fracturing process.
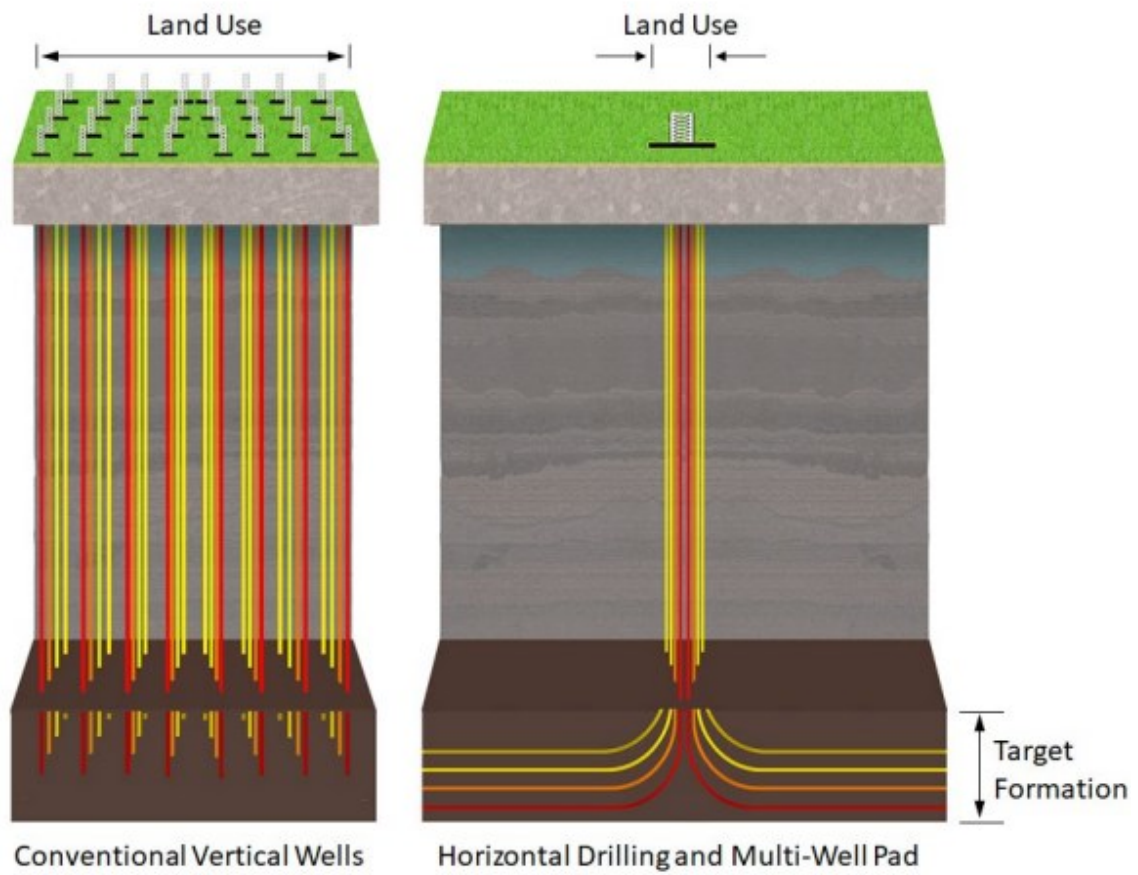
Figure 2-2- The surface area occupied by a horizontal multi-well pad compared to vertical wells with a single pad. It explains that a horizontal multi-well pad occupies less surface are than the vertical wells (The Scientific Hydraulic Fracturing Review Panel of British Columbia Government. 2019).
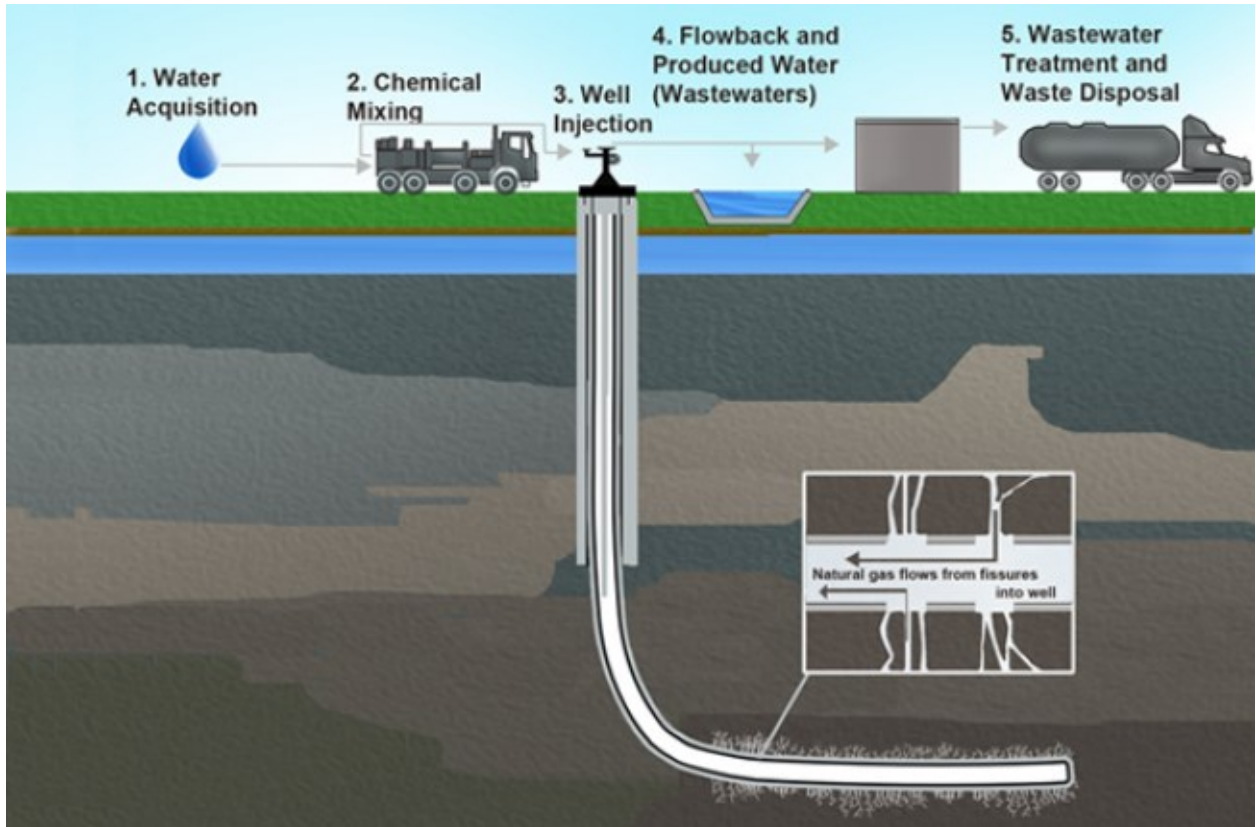
Figure 2-3- Water usage during the hydraulic fracturing process (Burden et al.2016).

2.3 EOR while fracturing

As previously discussed, hydraulic fracturing unlocked the production from the low-permeability unconventional shales and tight oil and gas reservoirs. However, the oil recovered through the hydraulic fracturing is very low, and only between 5-10 % of the Original Oil in Place (OOIP) is recovered during primary production (Habibi et al.2016). In the case of the Montney Formation, the primary oil recovery is not more than 15% of the OOIP (Galas. 2012). Therefore, a huge amount of oil is still unrecovered. Using EOR methods in unconventional resources is necessary to recover the remaining oil. One of the widely used techniques is "EOR while fracturing". In this method, the fracturing fluid is treated by adding chemical additives such as surfactant solutions, allowing the injected fluid to spontaneously imbibe into the matrix and displace more hydrocarbons out (Alvarez and Schechter. 2017). These chemical additives can play an important role in reducing water-oil interfacial tension (IFT), changing the rock wetting affinity, and reducing phase trapping in low-permeability reservoirs. All these factors can lead to enhancement in the spontaneous imbibition of the fracturing fluid into the reservoir matrix, displacement of hydrocarbons from matrix to fractures and consequently higher oil

recovery factor (Austad and Milter.1997, Taylor et al.2009, Nazar et al.2011, Makhanov et al. 2014).

2.4 Surfactants and Microemulsion Principles in Petroleum Engineering

Surfactants (surface-active agent) are widely used in the petroleum industry. Their importance is due to their potential to affect interfacial properties of two immiscible fluids. They are used for many applications in the oil and gas reservoirs. For instance, in liquid-liquid-solid or liquid-gas-solid systems, they are used for wettability alteration of reservoir rocks and increasing oil recovery factor (Schramm. 2000).

Surfactant molecules generally have amphipathic structures, formed from two different groups. In other words, they are composed of a hydrophobic group that has low affinity to solvent (the aqueous phase) and hydrophilic group with high affinity to the solvent. **Fig 2-4** shows the typical structure of the surfactant, where the head is the hydrophilic and the tail is the hydrophobic parts of the molecule. In aqueous solutions, surfactants can generate spherical groups called micelles, with the tails of the surfactants at the center of the sphere, and in touch with the aqueous phase.

When surfactants diffuse in a solvent, the hydrophobic part can change the structure of the solvent and increase the system free energy. The system will react to decrease the free energy by reducing the contact between the hydrophobic part and the solvent. This will lead to expulsion of surfactants to the interface of the solution and exposure to contact with nonpolar air molecules, which leads to the surface-tension reduction of the solvent. The role of hydrophilic parts is to prevent detachment of surfactants from the solvent and formation of a different phase (Rosen and Kunjappu. 2012).

The chain of the hydrophobic group is usually a long hydrocarbon group, while the hydrophilic part consists of ions that can affect the solvent solubility. Surfactants are classified into 4 categories (**Table 2.1**)**,** based on nature of their hydrophobic and hydrophilic parts. In the oil and gas reservoirs,   surfactants are used in combination with other elements and their performance should be evaluated with considering the physicochemical characteristics. Criteria of selecting the type of surfactant for the field applications depend on many factors including costs and. However, to use the proper type of surfactant, their efficiency on the interfacial properties of reservoir fluids, their chemical and physical compatibility with reservoir brine, oil, and rock should be considered (Myers. 2005).
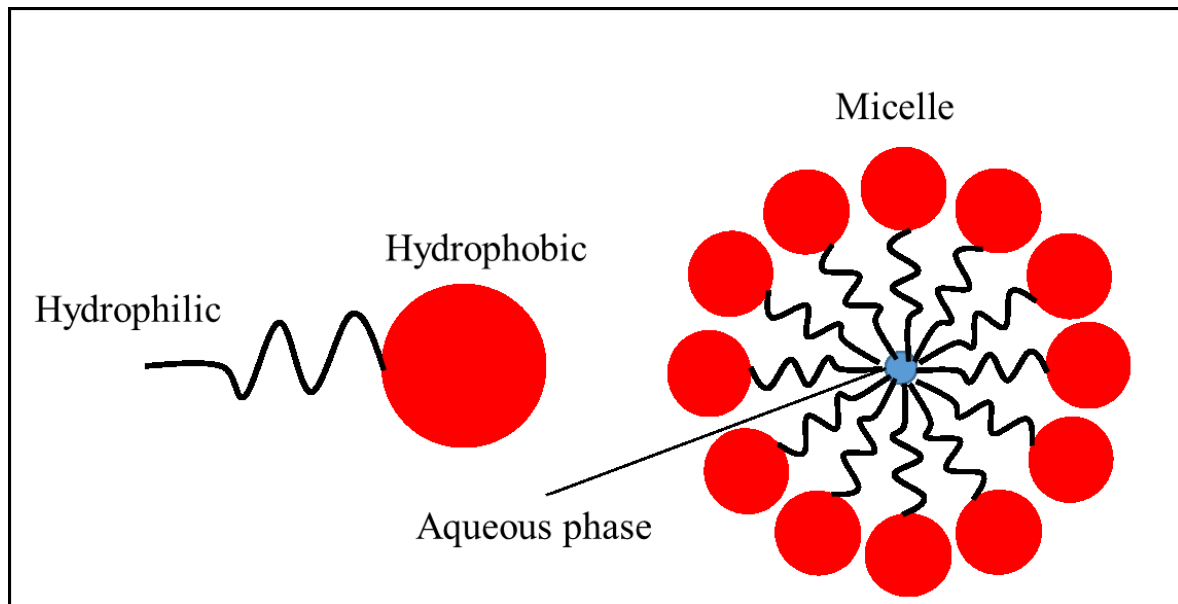
Figure 2-4- The structure of a surfactant molecule that consists of a hydrophilic tail and hydrophobic head. The surfactants in the aqueous phase can form a micelle, where the tail of the molecules is oriented toward the aqueous phase (Figure adapted from Held. 2014).

Microemulsions (ME) are thermodynamically stable, transparent emulsions that consists of hydrocarbon (e.g. Crude oil), water (Fresh or reservoir water), surfactants (e.g. Petroleum sulfonate). In petroleum industry, MEs are widely used due to their high solubilisation in the aqueous phase and their ability to reduce the interfacial tension to ultralow values. The ME properties play an important role in oil recovery during the EOR processe, where microemulsions are used to reduce the interfacial tension between reservoir oil and brine, and mobilize the residual oil left in the reservoir after the primary production. However, one of the limitations of ME is their high cost due to the complex technology required to use it. Nevertheless, the high oil-recovery by using the ME compare to other chemicals, makes it a desirable EOR fluid (Schramm. 1992).

Table 2-1 - Surfactants categories along with example for each category and its corresponding structure (Myers. 2005).

Category	properties	Examples	Structure
Anionic	The hydrophilic part is negatively charged.	Sodium stearate	$CH_3(CH_2)_{16}COO^-\ Na^+$
		Sodium dodecyl sulfate	$CH_3(CH_2)_{11}\ SO_4^-\ Na^+$
Cationic	The hydrophilic part is Positively charged	Laurylamine hydrochloride	$CH_3(CH_2)_{11}\ NH_3^+\ Cl^-$
		Trimethyl dodecylammonium chloride	$C_{12}\ H_{25}\ N^+\ (CH_3)_3\ Cl^-$
Nonionic	The hydrophilic part has no charge, but gains its solubility from the high polar groups.	Polyoxyethylene alcohol	$C_n\ H_{2n+1}(OCH_2CH_2)_n\ OH$
		Alkylphenol ethoxylate	$C_9\ H_{19}—C_6H_4—(OCH_2CH_2)_n\ OH$
Zwitterionic	The hydrophilic part can contain both, negative and positive charge	Dodecyl betaine	$C_{12}\ H_{25}\ N^+\ (CH_3)_2\ CH_2\ COO^-$
		Lauramidopropyl betaine	$C_{11}\ H_{23}\ CONH\ (CH_2)_3\ N^+(CH_3)_2\ CH_2\ COO^-$

2.5 Oil Displacement by Surfactants

In the EOR while fracturing section, we discussed that the oil recovery during the primary production from the tight or shale well is low, and the remaining oil needs to be extracted using EOR techniques. One of the main reasons of the residual oil in reservoir is the capillary forces holding the oil droplets in rock pores. To extract the trapped oil, the EOR fluid should overcome the capillary forces (Clark. 1969, Shah and Schechter. 1977). The Young-Laplace equation presented in Eq. 2.1 describes this force (Washburn. 1921):

$$P_c = \frac{2\ \sigma\ \cos\theta}{r} \qquad (2.1)$$

Where r is the radius of pore in m, P_c is the capillary pressure in Pa, σ is the surface tension in N/m, and θ is the contact angle between the fluid and surface in radian. Using appropriate surfactants in the fracturing water can reduce the IFT of the oil-water to low values, allowing the spontaneous imbibition of the fracturing fluid and oil displacement from matrix into fractures(Rosen et al., 2004). However, the oil-recovery by the spontaneous imbibition is only effective when the reservoir is water-wet. Thus, to expel the oil out from an oil-wet reservoir, wettability alteration of the rock from oil-wet to water-wet state is another important factor along with the interfacial tension to enhance the oil-recovery factor (Golabi et al., 2009).

2.6 Wettability and Interfacial Tension

Wettability is described as the affinity of the rock toward a specific fluid, in the presence of other fluid. In the reservoirs, the wettability of the rock can be classified to three categories: 1) Water-wet rocks where the water mainly occupies the small pores and the middle of the larger pores, 2) oil-wet rocks where the oil occupies the smaller pores and 3) neutral-wet where the rock does not have a tendency to a specific phase. However, the neutral-wettability rocks can be classified into fractional and mixed wettability, where in the fractional-wettability systems a part of the rock minerals have a high affinity toward one phase and the rest of minerals toward another fluid, while in mixed-wettability systems the oil-wet pores can form a path through the small water-wet pores (Alotaibi. 2011, Anderson. 1986, Shanmugam. 2012, McPhee and Zubizarreta. 2015).

Interfacial tension is defined as the adhesion forces between the molecules at the interface of two fluids. According to Eq. 2.1, interfacial tension is an important parameter in determining the capillarity forces in the porous media. Adjusting the interfacial tension by using surfactant solutions can affect the capillary forces and thus enhance the oil mobilization (Amaefule and Handy. 1982, Bahadori. 2016).

2.7 Spontaneous Imbibition of the Fracturing Fluid

Spontaneous imbibition of water is a capillary process resulted from natural wetting affinity of rock for water uptake.. In petroleum reservoirs where the oil is present, when the water contacts the reservoir rock, it can spontaneously imbibe into the rock and displace the oil out. This process is related to the capillary forces which is dominant in the pores of the rock (Schramm. 2009).

The efficiency of surfactants used in the fracturing fluid to enhance the oil recovery, depends on the rate of the spontaneous imbibition in the reservoir rock. In the low-permeability reservoirs, the oil-recovery can be improved by changing the IFT of oil-water system. In a

water-wet reservoir, the capillary forces help in a further spontaneous imbibition of water from fractures into matrix, while in an oil-wet reservoir, the capillary forces act as a resistance force against the spontaneous imbibition of water (Ayirala et al.2006, Ghandi et al. 2019). Based on these facts, many studies suggest that in a water-wet reservoir, it is important not to decrease the oil-water IFT to ultra-low values to have stronger capillary forces and deeper spontaneous imbibition into the reservoir matrix (Mungan. 1964, Milter and Austad. 1996 and 1998). On the other hand in an oil-wet reservoir, reducing the IFT along with wettability alteration to water-wet conditions is crucial to enhance the spontaneous imbibition of fracturing water and thus, improve oil recovery (Sanchez and Hazlett. 1992, Xie et al. 2005, Ayirala et al. 2006, Wu et al. 2008).

2.8 Remedial Solutions for Water Blockage

During hydraulic-fracturing process, a large volume of water is injected to create a large contact area between the horizontal well and the reservoir matrix. Some of the injected water may leak-off into the reservoir matrix (Dehghanpour et al. 2013, Ghanbari and Dehghanpour. 2016). The pore-throat size in the low permeability tight oil and gas reservoirs is typically very small that results in high capillary suction, causing water blockage near matrix-fracture interface and reduction in hydrocarbon mobility (Bennion et al. 1999, Gdanski et al. 2006, Mahadevan et al. 2007, Bahrami et al. 2012).

Different remedial solutions have been proposed to solve this problem. Adding chemical additives to the fracturing fluid is recommended as one of the effective methods to reduce water blockage by lowering interfacial tension between hydrocarbon and water along with changing the rock wettability to more water-wet conditions. Efficient chemical additives can enhance the spontaneous imbibition of the fracturing fluid into the reservoir matrix, resulting in higher oil recovery by counter-current imbibition (Austad and Milter.1997 , Paktinat et al. 2005, Taylor, R. S et al.2009, Nazar, M. F et al.2011, Makhanov, K et al. 2014). Different experimental studies investigated the effect of surfactants on wettability, IFT, and oil-recovery improvement (Dehghanpour et al. 2012, Lan et al. 2014, Habibi et al. 2015, Alvarez and Schechter 2017, Yuan and Dehghanpour 2019, Kewen and Firoozabadi 2000, Levitt et al. 2006, Kumar et al. 2006, Bang et al. 2008). Yarvaci et al. (2018) evaluated the effects of adding surfactant to the fracturing fluid and conducted spontaneous imbibition along with core-flooding experiments on Montney core plugs. They concluded that, adding surfactant to the fracturing water results in two times higher oil recovery compared to a case without adding surfactant. In addition, their core flooding tests showed that, adding surfactant decreases the

pressure drop, suggesting a reduction in phase trapping due to the IFT reduction. Penny et al. (2006) conducted a field-data analysis and experimental study on Barnett shales, and found that adding ME to the fracturing fluid maximizes hydrocarbon recovery by 50% and reduces the formation damage compared to the case without using ME.

As a different mechanism, imbibition of water from fracture into rock matrix during extended shut-in periods may lead to lower water saturation near fracture face and expelling of oil from matrix into fracture (Morrow and Mason 2011, Dehghanpour et al. 2012, Cai et al. 2012, Chen and Mohanty 2015). Many studies have investigated the effect of spontaneous imbibition and extended shut-in time on enhanced hydrocarbon recovery in unconventional reservoirs (Fakcharoenphol et al. 2013, Knudsen and Foss 2013, Xu et al. 2016). Ghanbari and Dehghanpour (2016) conducted a simulation study to understand the effect of shut-in time on gas production from Horn River wells. They found that extended shut-in time can decrease water load recovery but increase gas production. They concluded that water imbibition due to capillary suction increases with extended shut-in time, leading to higher gas recovery through counter-current imbibition.

2.9   Low-salinity Water and Osmosis Pressure as Driving Mechanisms for EOR

Along with the capillary forces, using low-salinity water as the fracturing fluid is another important factor in the spontaneous imbibition of the fracturing fluid into matrix and counter-current oil recovery (Morrow and Buckley. 2011, Fakcharoenphol et al. 2014, Vledder et al. 2010, Austad et al. 2010). Osmotic effect is defined as the flow of water molecules through a semi-permeable membrane from low-salinity side into the high-salinity side, until reaching the equilibrium conditions in salt concentration of both sides (Cath et al. 2011, Li et al. 2013). Xu and Dehghanpour (2014) compared the spontaneous imbibition rates of aqueous fluids with different salinities to investigate the effect of salinity and osmosis pressure on water imbibition. They found that, fluids with low salinity imbibe significantly higher than fluids with higher salinity. In the reservoir, the clay minerals can act as a semi-permeable membrane, allowing water molecules to pass, and restricting the inorganic solutes to pass through them from the low salinity to the high salinity side (Kemper & Rollins. 1966, Malusis et al. 2003, Olsen et al. 1990). Different experimental studies concluded that osmosis pressure is a driving suction

force in addition to capillary pressure, which contributes in the spontaneous imbibition of the fracturing fluid into the matrix and enhances the oil recovery, with the presence of clay minerals in the formation (Binazadeh et al. 2016, Zhou et al. 2016).

Chapter 3

3) Field Observations

This chapter describes the key observations as field production progresses from flowback to post-flowback period.

3.1 Flowback Production

After hydraulic fracturing, the well was put on flowback for 33 days. **Fig.3.1** shows that the well undergoes early single-phase of water production for about 15 days. Oil production starts 4 days after. In the next day, free gas production starts because reservoir pressure is now below bubble point (20 MPa) to allow exsolution of dissolved gas from oil. The well was eventually shut-in for 2 months after flowback. Its load recovery (ratio of cumulative water production to TIV) after flowback is about 48%. This is quite high for 33 days of flowback (Ezulike and Dehghanpour, 2015). However, it could be due to the early single-phase of water production, delayed hydrocarbon breakthrough, long well length (2035 m) and high fractures stages (64 in number).
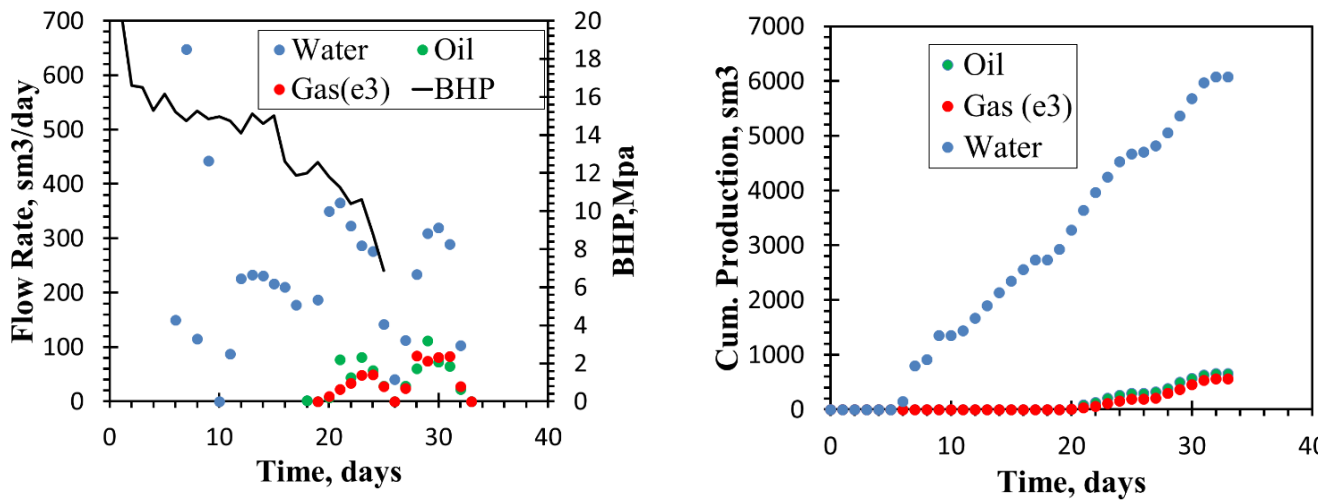
Figure 3-1- Flowback production data. (a) Flow rates and Bottom-hole pressure. (b) Cumulative productions.

3.2   Post-Flowback Production

Here, we present the production flow rates under downhole pressure conditions. We converted the surface flowrate data to downhole by using the measured PVT data and different oil and gas correlations (Beggs and Brill. 1973, Al-Shammasi. 1999, Guo and Ghalambor. 2005). **Fig.2a** shows the post-flow back production of the well, where the well after 5 months of production using the jet pump, was shut-in to complete surface facilities and pipeline constructions. The well remains shut-in for 7 months, and it was reopened for production again. The jet pump was replaced with gas lift to minimize water cut. The volume of injected gas was subtracted from the volume of total produced gas to estimate the gas volume produced from the reservoir. The well was monitored using a bottom-hole pressure gauge. However, the pressure was not recorded during the shut-in period.

3.3   Shut-In Effects on Production

Fig.3.2a shows that before the shut-in period, water, oil and free gas rates decline rapidly along with the bottom-hole pressure depletion. The 7 months of the shut-in significantly affected the instantons oil flow rate after the shut-in, where it jumps from 14 m^3/day before the shut-in, to approximately its initial rate at start of production, 119 m^3/day (750% increase). **Fig.2.b** shows that, in contrast to the oil rate, when the well is reopened, free gas rate decreases from 30 e^3 m^3/day to only 1.43 e^3 m^3/day (95% decrease), before it starts to increase again to values even higher than those at start of the production. To understand this oil and gas behavior we calculated the rate of the gas in solution, in the reservoir. **Fig.2.c** explains that before the shut-in, the gas in solution starts to evolve as the pressure declines. However, during the shut-in the pressure starts to build-up to values even higher than the bubble point pressure, which allows the free gas to dissolve in the oil, and increase the oil volume. This can explain the jump in the gas in solution rate, from 83 m^3/day before the shut-in, to 1453 m^3/day after the shut-in (1650% increase). This spontaneous process can be described as a well Self-Enhanced Oil Recovery (Self-EOR) during the shut-in period, where the dissolved gas helps to enhance the oil-recovery after the shut-in, in response to the pressure build-up. Enhancement of oil permeability after the shut-in can be another effective factor responsible for the increase of the dissolved gas. **Fig.2.d** shows the production-rate ratios of the well. It shows that after the shut-in, the water cut (WCUT) decreases by around 5 time than its value before the shut-in, while oil-water ratio

(OWR) increases after the shut-in 20 times more than its value before the shut-in, suggesting significant rise in oil rate after the shut-in. However, after 38 days of reopening the well, the WCUT gradually returns to almost the same values before the shut-in. Similar to WCUT, the OWR return to its values before the shut-in, but after 65 days of reopening the well. The free gas-oil ratio (GOR) after reopening the well, decreases 5 time than its value before the shut-in, then starts to increase to values even higher than those before the shut-in.

Fig. 3.3 shows the decline curve analysis of free gas and oil in under downhole conditions, before and after the shut-in .The decline curve of the oil production decreases after the shut-in, suggesting enhancement in oil relative permeability after the shut-in. Similarly, the decline rate of the free gas production decreases after the shut-in. This can be explained by gas exsolution after shut-in as bottom-hole pressure quickly falls below bubble-point pressure (20 Mpa) and solution gas becomes free gas, favoring its production over oil and water due to its higher mobility.

The changes in production profile after the shut-in can be due to several possible reasons including pressure buildup, water blockage reduction near the fracture face, counter-current imbibition due to the capillarity and osmotic pressure. **Fig. 2a** shows that bottom-hole pressure increases to around initial reservoir pressure (20 MPa) during the shut-in. The fracturing fluid used in stimulating this well contains microemulsion (ME) additive, which could reduce matrix-fracture skin/damage during the shut-in and improve hydrocarbon production rate. In addition, spontaneous imbibition of the fracturing fluid into reservoir matrix and counter-current imbibition of oil could enhance production rates. The higher salinity of the formation is also an important factor, which can play a big role in the counter-current imbibition due to salinity and osmotic pressure gradients. The investigation of skin/damage reduction near matrix-fracture interface using numerical simulation will be presented in the chapter 5. However, along with the simulation, we conduct experiments to evaluate the oil counter current imbibition and effect of osmosis potential on oil recovery from oil saturated core plugs.
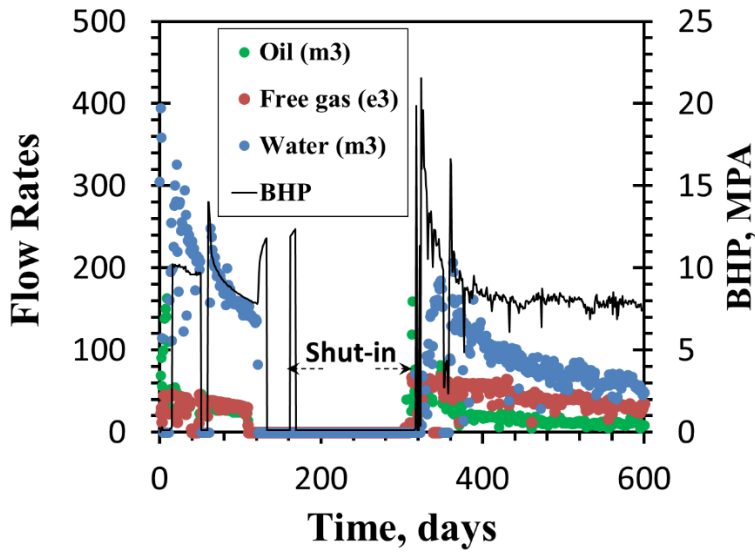
(a)
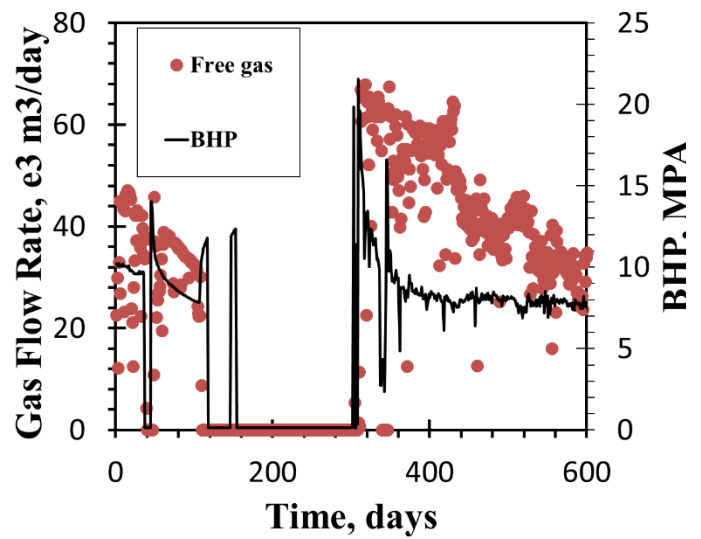
(b)
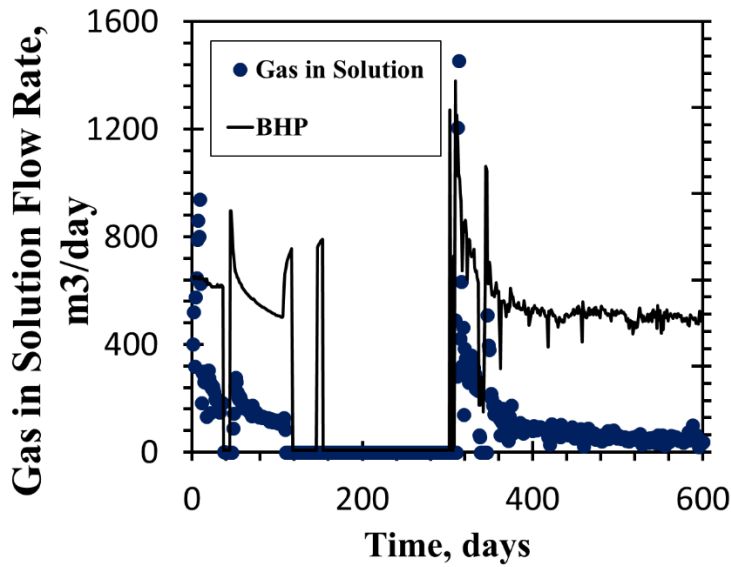
(c)
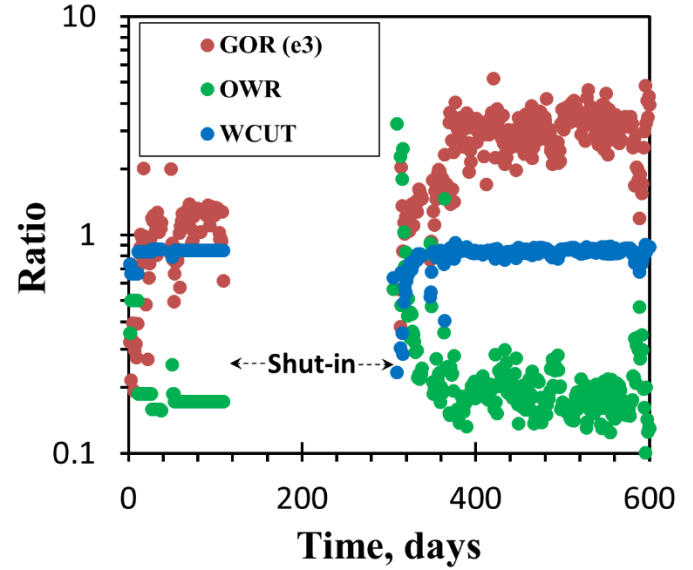
(d)

Figure 3-2- Post-flowback production data under downhole conditions. (a) Flow rates and bottom-hole pressure, (b) Free gas flowrate, (c) Gas in solution, and (d) Profiles of rate ratios at downhole conditions (oil-water ratio (OWR), gas-oil ratio (GOR), and water cut (WCUT).
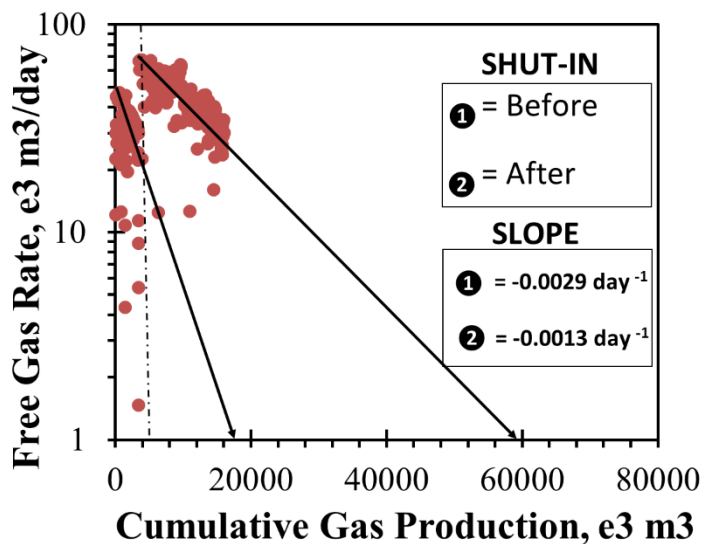
(a)
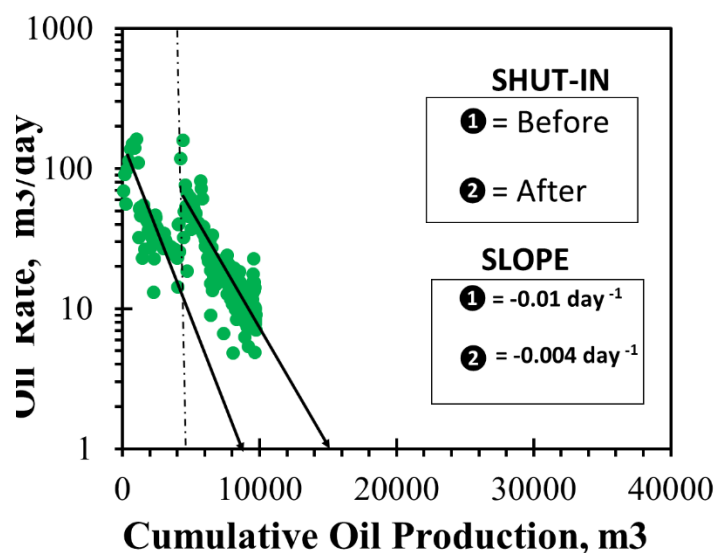
(b)

Figure 3-3- Slopes before and after the shut-in, downhole condition from decline curve analysis. (a) Oil. (b) Gas.

The changes in production profile after the shut-in can be due to several reasons including: 1) pressure build-up, which was discussed in the production data analysis, 2) water blockage reduction near the fracture face, which can enhance the relative permeability of the oil. The fluid used for fracturing this well contains microemulsion (ME) additive, which could reduce matrix-fracture skin/damage during the shut-in and improve hydrocarbon production rate. It is right during the flowback and post-flowback the load recovery rate is high for this well, and does not change after the shut-in, but this can be explained by production of an additional water source, Zone 1. This zone with its mobile water and immobile oil, contributes in the water production through the hydraulic fractures connecting it to Zone 2. The changes in the matrix-fracture skin, before and after the shut-in is discussed in details in Chapter 5. The last possible reason can be 3) counter-current imbibition due to capillary suction, wettability alteration and osmosis. Spontaneous imbibition of the fracturing fluid into reservoir matrix and counter-current imbibition of oil could may lead to an increase in early production rate after the shut-in period. The higher salinity of the formation brine compared with the injected fracturing water can enhance water imbibition into the matrix due to osmosis effect. This will be discussed in details in chapters 6 and 7.

Appendix A-3

Here we show the post-flowback production data for well 1 in surface conditions.
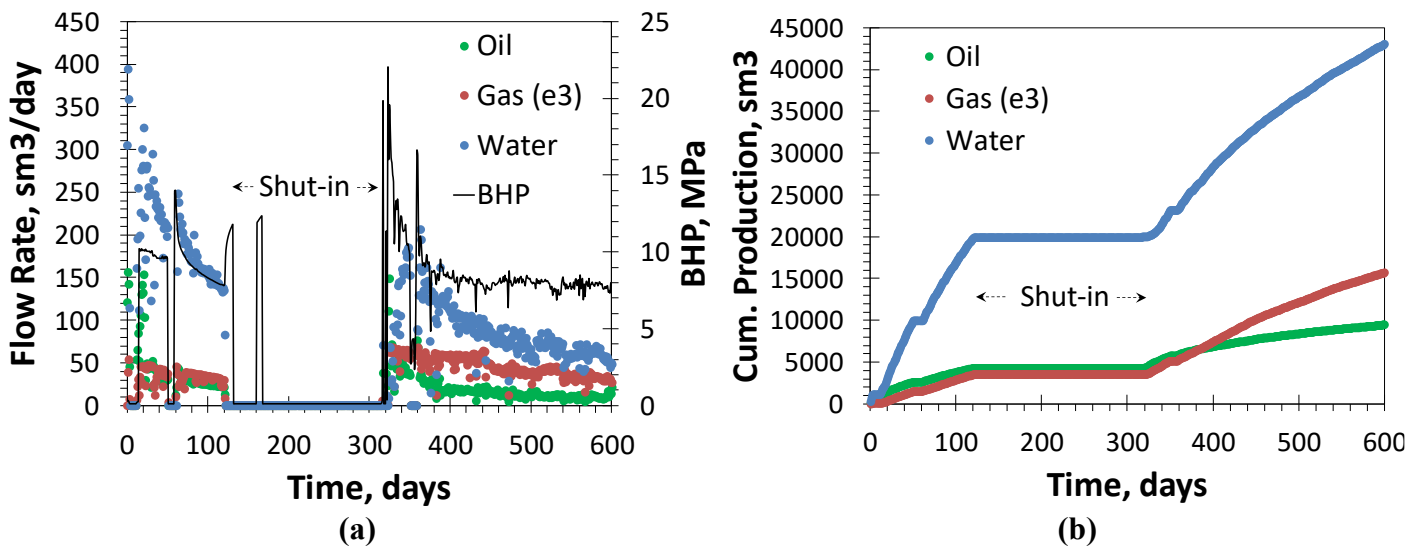
Figure A.1- Post-flowback production data at surface condition. (a) Flow rate and Bottom-hole pressure. (b) Cumulative production
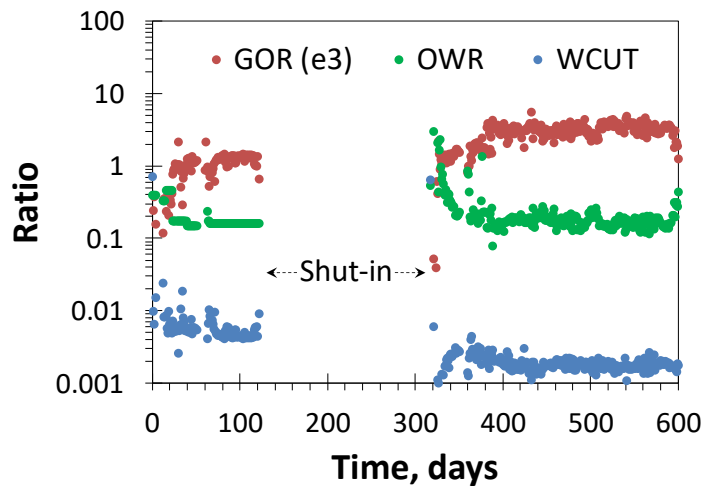
Figure A.2- Profile of rate ratio (oil-water ratio, gas-oil ratio, and water cut).
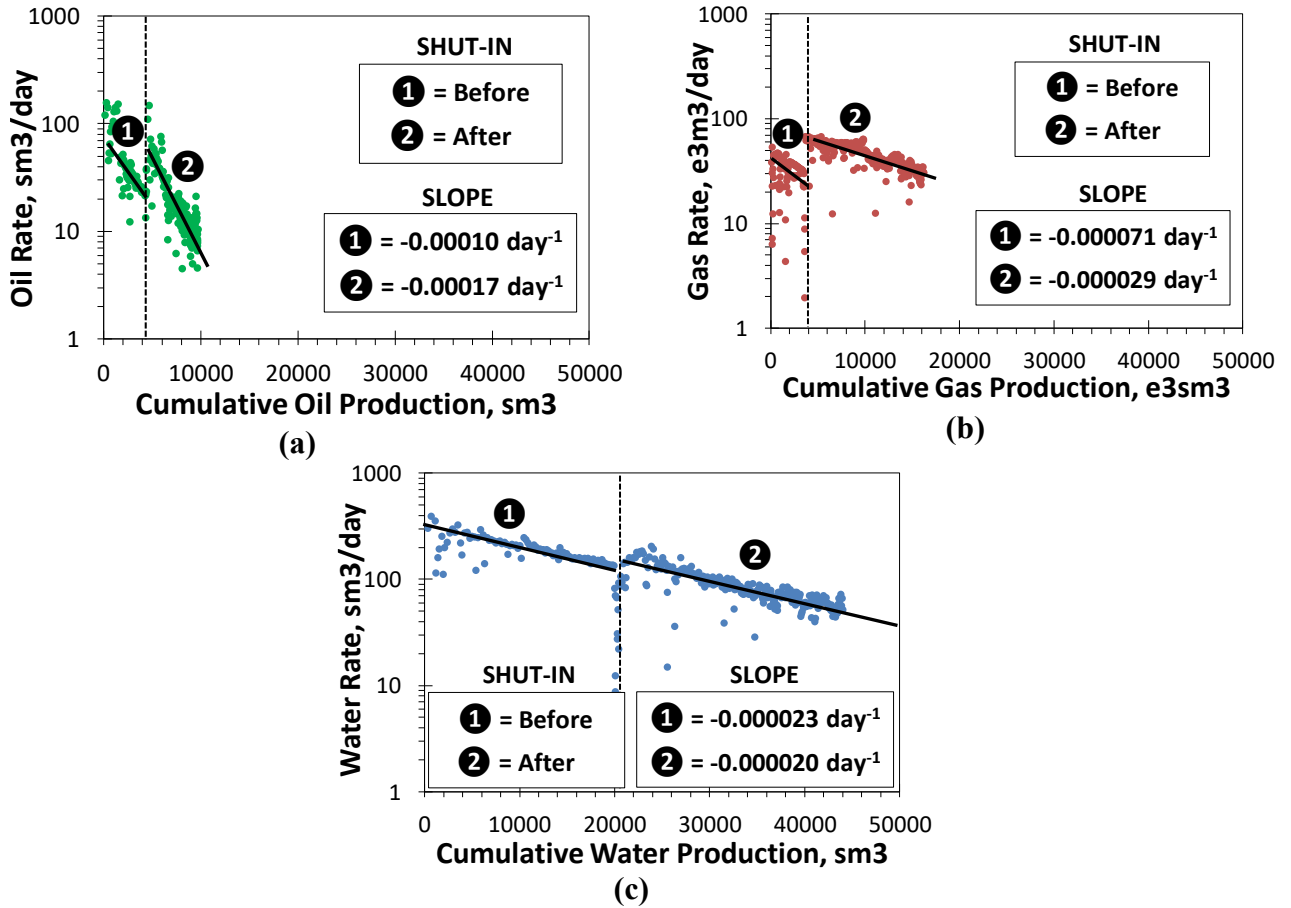
Figure A.3- Slopes before and after the shut-in from Decline curve analysis. (a) Oil. (b) Gas. (c) Water.
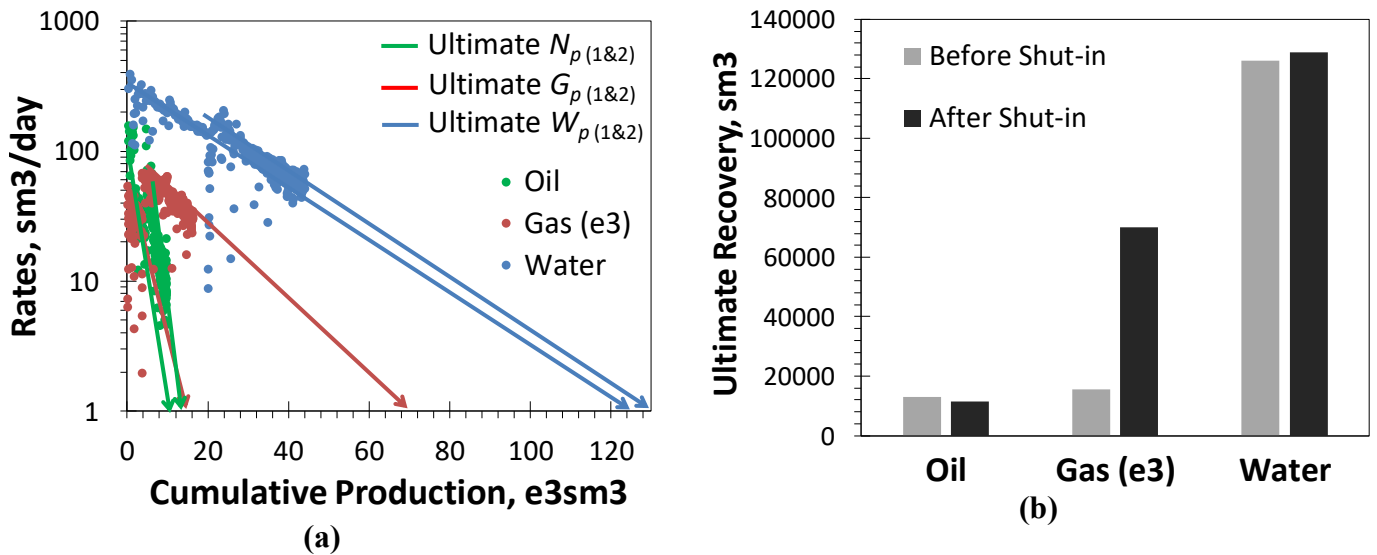
Figure A.4- Estimated ultimate recovery from decline curve analysis for oil, gas and water before & after shut-in.

Chapter 4

4) Petrophysical Properties

In this part of the study, we analyze the petrophysical properties of rock samples from the targeted well along with two adjacent wells drilled in the Montney tight-oil formation. The results of well log data, porosity, permeability, mercury injection capillary pressure (MICP) measurements, SEM analysis and X-ray diffraction (XRD) of the rock samples are presented and discussed in this chapter. It is important to mention that all the following data were measured by commercial companies and laboratories.

4.1 Well Logs

Well logging is used for in-situ well measurements. These measurements are conducted by induced or applied radiation techniques. Important reservoir characteristics such as lithology of the reservoir rock, porosity, and water/hydrocarbon saturations are evaluated by well logging (Peters 2012). **Fig. 4-1** shows the well log data for the three wells, where Well 1 is the targeted one, and the other two are the adjacent wells. The first track (from the left) is the gamma ray (GR) log, that represents the natural radioactivity of the formation. Since GR log can reflect the radioactive elements in organic matter of shales and clay minerals, it is a useful technique to characterize shale beds located in the reservoir. In all the wells, the GR deflects intermediate to the left of the shale base line (75 API) with a uniform shape, with average values ranging from 69.05 to 71.78 API, attributed to less shale content, and more siltstone/sandstone present in the evaluated well (Peters. 2012). Nevertheless, the GR log deflects more to the right side of the shale base line in the interval 2050-2070 m, due to higher shale content. Resistivity log (the middle log), which is used to distinguish between water and hydrocarbon zones and estimate the net-pay thickness of the reservoir. High concentration of the ions in the reservoir brine conducts of the electrical current through it, resulting in lower value of resistivity log in zones with higher brine saturation. On the other hand, the higher value of resistivity log indicates the presence of hydrocarbons due to their poor electrical conductivity. Resistivity logs show higher conductivity in the intervals deeper than 2040 m particularly in Well 2 and Well 3. The last track of the well log data (the right side log), shows the combined density-porosity and neutron-porosity logs. In the density-porosity log, the electron density is calculated based on the number of electrons in the formation. However, electron density is proportional to true bulk-density, which is as well related to rock matrix density, formation

porosity, and fluid contents in the pore system. Thus, the porosity is obtained from the matrix and fluids densities. It should be noted that, in-situ porosity measurements by log data may be different from the laboratory measurements of porosity due to different factors such as 1) the change in the ambient conditions, 2) small size of the core plugs compared to the reservoir size, and 3) the possibility of alteration of petrophysical properties during the coring process (Peters. 2012). For the neutron-porosity log, neutron can detect the hydrogen content present in the formation, thus reflecting the water/hydrocarbon contents in the pores. Neutron logs are used to estimate the liquid-filled porosity, where the high neutron value indicates low porosity and low neutron value is interpreted as high porosity. Gas zones contain less concentration of hydrogen compared to oil and water zones, thus the neutron-porosity will be lower in the zones saturated by gaseous phase than those saturated with oil or water. Since gas density is significantly lower compared to oil and brine densities, gas zones will reflect high density-porosity values. Thus, in a combined density-porosity with neutron-porosity logs, both curves will intersect in the liquid zone, and they will crossover in the gas zone. By analyzing the density-porosity and neutron-porosity logs, we observe that two log data intersect in approximately most of the intervals of the wells, suggesting the presence of a liquid phase. This liquid phase is mostly oil according to the resistivity log. In addition, in intervals between 2058-2070 m along with 2088-2100 m of Well 1, 2062-2072 m of Well 2 and 2014-2020 m of Well 3, the neutron-porosity and density-porosity logs are far apart, indicating the presence of a gas zone. The average porosities from the density-porosity logs are 0.07, 0.05, and 0.04 (v/v fraction) for Wells 1, 2, and 3, respectively. Note that the black dots in the GR log in Fig. 4-1 show the location of the core plugs used for different experiments. Table 4.1 lists the summary of the core plugs used in this study, along with corresponding characterization tests.

Table 4-1- Summary of the core plugs used in the study.

Well number	Core ID	Depth (m)	GR (API)	Resistivity (Ω.m)	Neutron-porosity %	Densit-porosity (%)	MICP measurement	XRD measurement	SEM Images	Used in experiments
1	MTY 1-1	2026.5	82.3	14.09336219	0.093442623	0.107524673	X			X
	MTY 1-2	2044	57.76	25.44216675	0.087978142	0.091222031		X		X
	MTY 1-3	2057	68.96901972	44.17338214	0.053825137	0.067152915	X			
	MTY 1-4	2071	70.03595133	33.41551744	0.067486339	0.050962831	X			X
	MTY 1-5	2073	57.76623785	44.67322803	0.052459016	0.076581269				X
	MTY 1-6	2075	63.10089588	32.36390517	0.045628415	0.066634819	X	X		
	MTY 1-7	2080	76.43754097	44.94290515	0.078415301	0.054650747				
	MTY 1-8	2086.5	72.70328035	48.51916452	0.07431694	0.046576395	X	X		
2	MTY 2-1	2066	68.7295742	115.0417086	0.066492614	0.029229419	X	X	X	
	MTY 2-2	2073	82.92544525	53.57690155	0.024710736	0.015953408	X	X	X	
	MTY 2-3	2091	74.89971541	70.99836315	0.043900895	0.022042368	X	X	X	
	MTY 2-4	2095	80.80377185	34.42213915	0.054744449	0.026204638	X	X	X	
3	MTY 3-1	2084	73.4870312	42.90442174	0.039150946	0.065176368	X	X	X	X
	MTY 3-2	2100	83.99357152	27.61044123	0.058457805	0.06173031	X	X	X	X

(a)

(b)

(c)
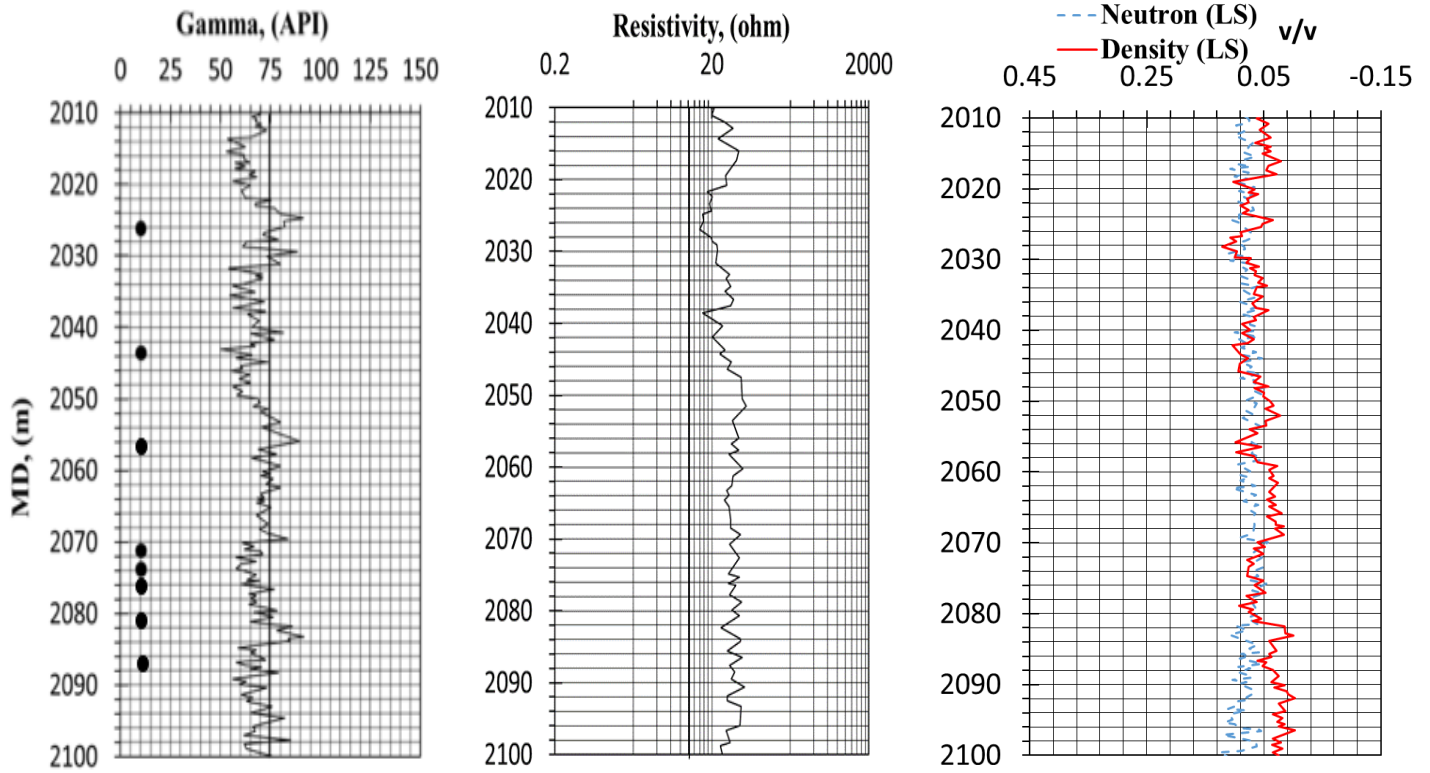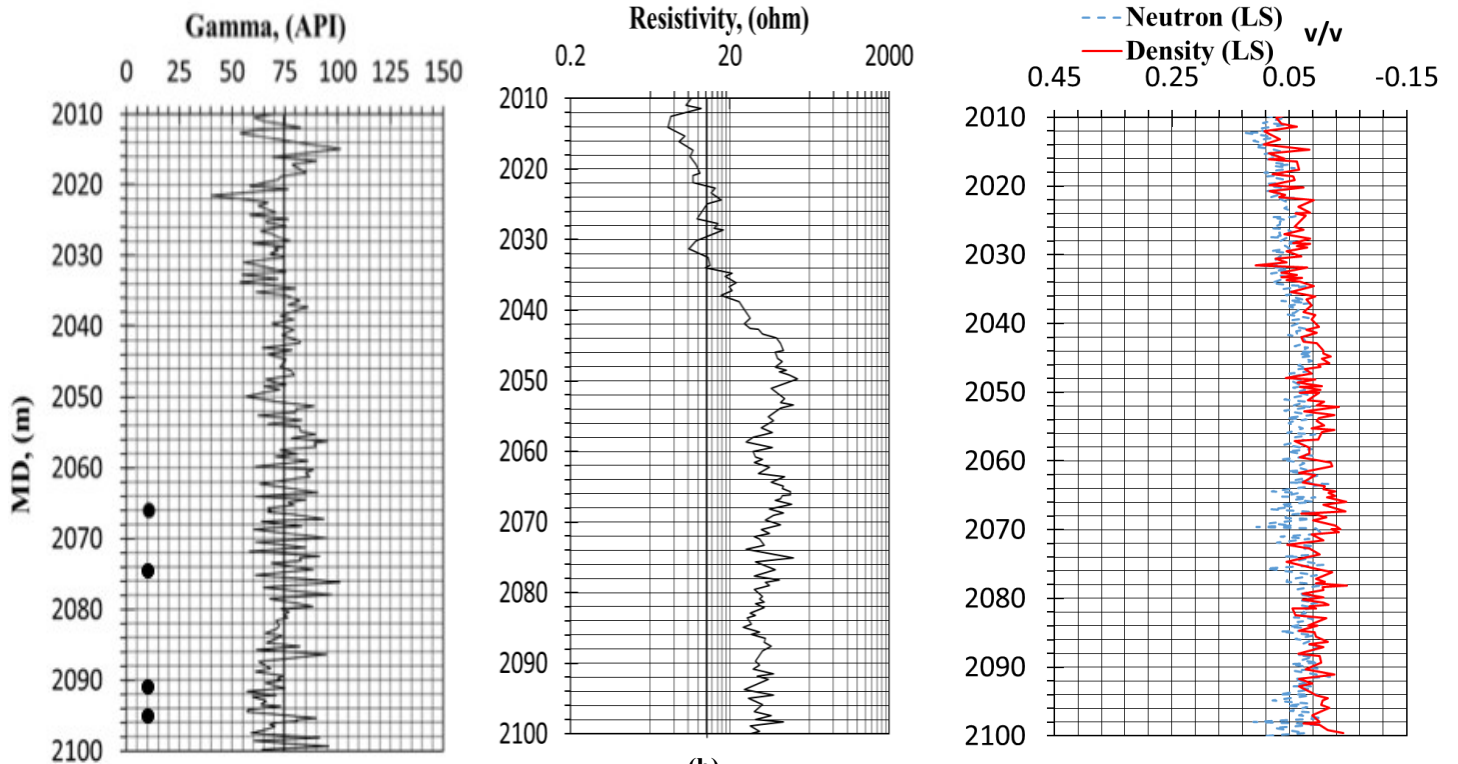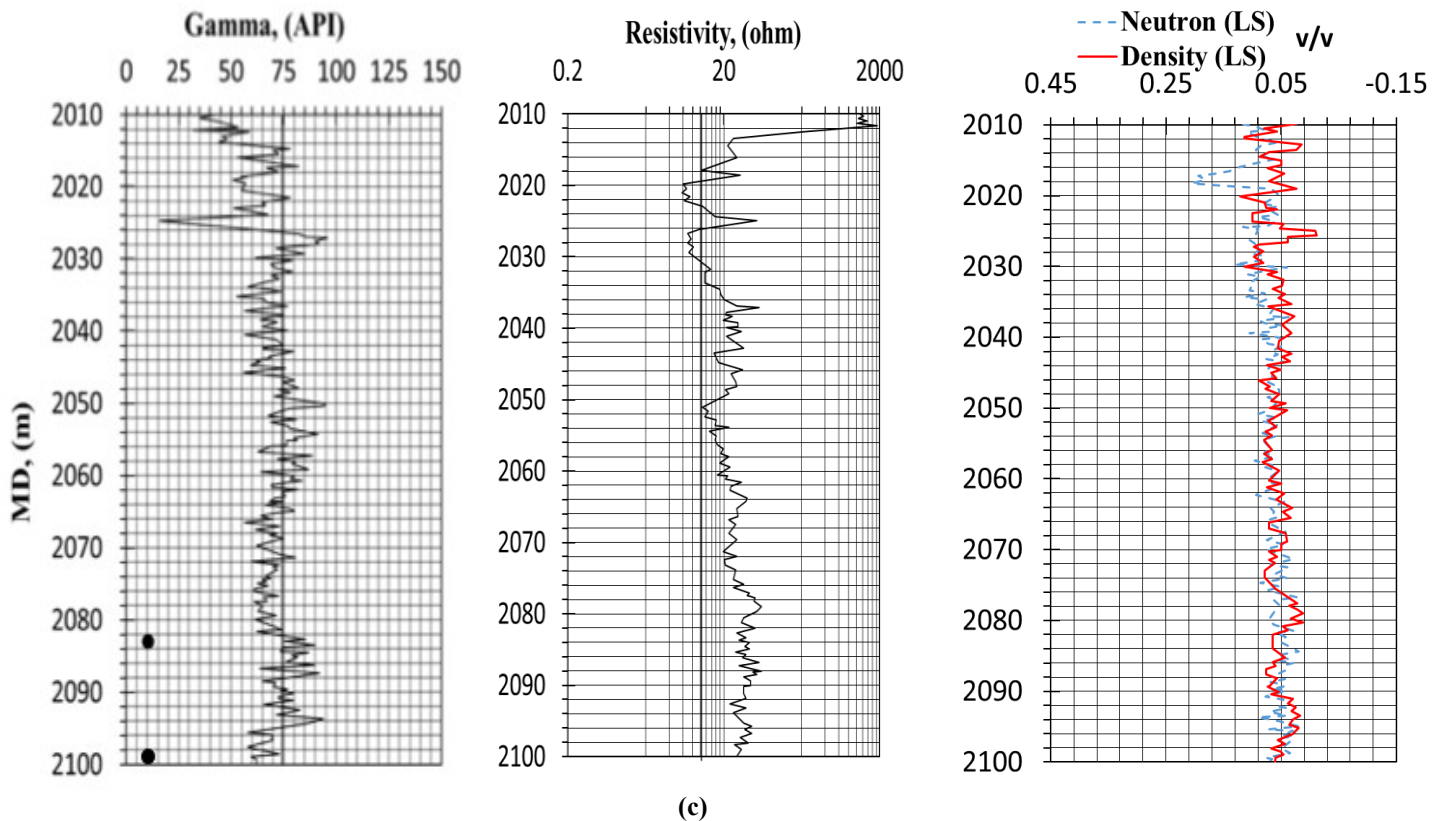
Figure 4-1-Approximate location of the core plugs (black dots) on gamma ray log, resistivity log, and the combined neutron-porosity with density-porosity logs for (a) Well 1, (b) Well 2, and (c) Well 3.

4.2 Porosity and Permeability Measurements

Table 4.2 lists the measured porosity and permeability of the core plugs from the three wells. Porosity was measured using Boyle's law helium porosimetry, after removing the free oil and brine from the core plugs and drying them in the oven. The drying process and porosity measurements were conducted by 1) on intact core plugs and 2) on crushed samples. The measured gas porosities on the core plugs and crushed samples are very similar to each other. The reported porosity values in Table 4.2 are obtained from the crushed-sample measurements. The range of porosity in Well 1, Well 2, and Well 3 is 3.53-11.51%, 2.18-5.23% , and 2.18-5.81 % of bulk volume, respectively. .According to Table 4.2, porosity of core plugs from Well 1 are generally higher than those from Well 2 and Well 3, which is consistence with in-situ porosity measurements presented in the well log section.

Permeability of the core plugs is measured by pulse-decay permeability method. In pulse-decay permeability, the core plug is placed inside a membrane jacket of a modified Hoek cell and tighten between two steel pistons, which allow the helium gas to flow into the core samples. The inlet and outlet pressures of the core plug are recoded with respect to time, and the permeability is measured (Jones.1997).Permeability values reported in Table 4.2 are measured at the initial pressure conditions. Permeability of all the core plugs is in microdarcy range;

indicating an ultra-low permeability relevant to the tight-oil formations. Samples MTY2-2 and MTY1-1 have the highest permeability among all other samples, with permeability of 9.48 and 7.32 µD, respectively.

Figure 4.2 shows the change in porosity and permeability of the core plugs with respect to formation depth. According to these two plots, both permeability and porosity typically have decreasing trends with depth. This observation suggests that the formation is tighter and less porous as the depth increases.

Table 4-2- Petrophysical properties of the core plugs from three Montney wells.

Well number	Core ID	Depth (m)	Permeability, (µD)	Porosity (%BV)
1	MTY 1-1	2026.5	7.32	10.72
	MTY 1-2	2044.0	6.70	7.96
	MTY 1-3	2057.0	6.57	9.03
	MTY 1-4	2071.0	1.22	11.51
	MTY 1-5	2073.0	3.01	6.30
	MTY 1-6	2075.0	0.47	3.53
	MTY 1-7	2080.0	2.59	8.56
	MTY 1-8	2086.5.0	1.64	8.75
2	MTY 2-1	2066.0	3.33	2.18
	MTY 2-2	2073.0	9.48	5.20
	MTY 2-3	2091.0	1.7	5.23
	MTY 2-4	2095.0	0.52	3.12
3	MTY 3-1	2084.0	1.80	4.72
	MTY 3-2	2100.0	3.85	5.81
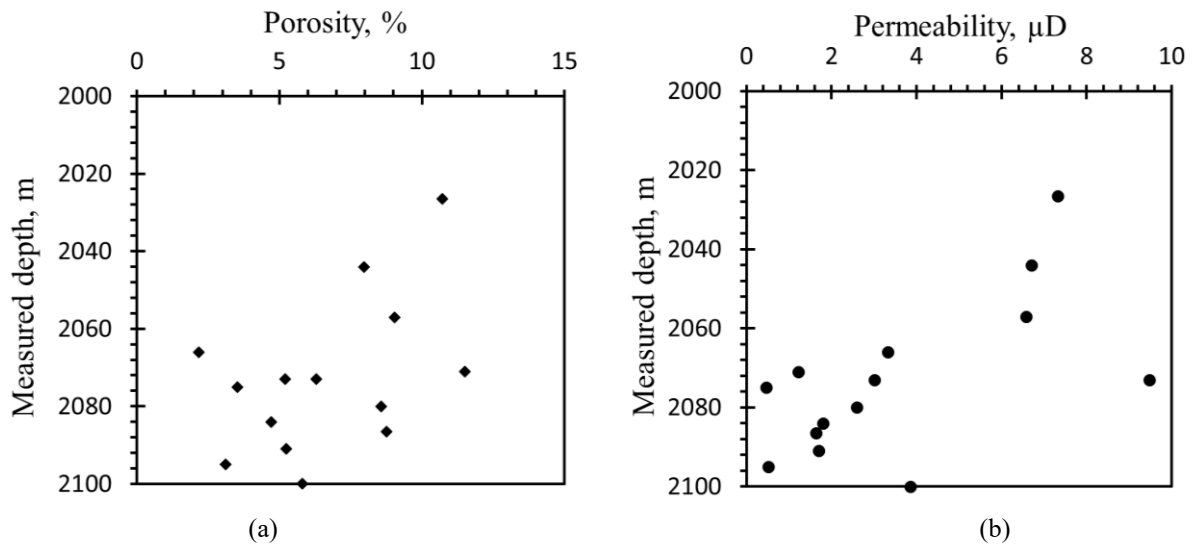
Figure 4-2- The change of the measured (a) porosity, and (b) permeability vs. formation depth.

4.3 X-ray Diffraction

To understand the mineralogy of rock samples, X-ray diffraction (XRD) technique is conducted on samples of the three wells. Table 4.3 lists the mineralogy of the core plugs, obtained from the XRD analysis. It shows that most of the rock structure consists of non-clay minerals (82-97 wt%), where the dominant non-clay minerals are quartz (29-59 wt%) and dolomite (6-22 wt %). clay content ranges between (3-32 wt %) and the highest clay content is observed in well 1 core plugs. The most abundant clays are the mixed layers of illite/mica (0-29 wt%) followed by illite/smectite (0-10 wt %), along with minor amounts of kaolinite (0-2 wt%) and chlorite (0-1wt%), consisting the rest of the clay minerals.

Table 4-3- Mineralogy of the rock samples, obtained from XRD analysis. All the listed values have the unit of wt%.

Well	Sample ID	Core depth (m)	Quartz	K-feldspar	Plagioclase	Dolomite	Pyrite	Fluorapatite	Calcite	Total Non-clay	Illite/Smectite (I/S)	Illite + mica	Kaolinite	Chlorite	Total clay
1	**MTY 1-2**	2044.00	36	13	13	18	2	0	0	**82**	0	18	0	0	**18**
	MTY 1-6	2075.00	29	15	16	6	3	0	0	**68**	0	29	2	0	**32**
	MTY 1-8	2088.00	54	9	13	20	1	0	1	**96**	0	4	0	0	**4**
2	**MTY 2-1**	2066	48	10	11	15	3	1	0	**88**	8	3	0	1	**12**
	MTY 2-2	2073	57	7	11	18	1	1	0	**96**	2	2	0	0	**4**
	MTY 2-3	2091	48	12	12	8	4	0	0	**84**	10	4	0	2	**16**
	MTY 2-4	2095	53	7	9	22	2	2	0	**95**	3	2	0	0	**5**
3	**MTY 3-1**	2084	59	7	11	19	1	0	0	**97**	0	3	0	0	**3**
	MTY 3-2	2100	56	9	10	18	1	1	0	**95**	4	0	0	1	**5**

4.4 MICP and Pore Size Distribution

Mercury injection capillary pressure (MICP) data provides important information about the pore-throat size distribution of rock samples. In this technique, a pressure is applied to force the mercury as the non-wetting phase into the pore space and take the air out. The saturation of mercury is recorded at each pressure step, starting from low pressures corresponding to the large pore-throats, until high pressures corresponding to small pore-throats. (Ausbrooks et al.1999). According to Windland (1972), the pores can be classified based on their size to 1) macropore, 2) mesopore, 3) micropore, 4) nanopores, and 5) picopore. Table 4.4 lists classifications of the pore-throat sizes based on the Windland's work.

Table 4-4- Classification of pore-throat sizes (Windland 1972).

Category	Pore-throat size (μm)
Megaopore	> 10.0
Macropore	2.0 - 10.0
Mesopore	0.5 - 2.0
Micropore	0.1-0.5
Nanopore	< 0.1

To measure the pore-throat size in the MICP test, we assume cylindric pores and use Eq. 4.1 (Washburn 1921):

$$P_c = \frac{2\,\sigma\,\cos\theta}{r} \qquad\qquad (4.1)$$

By rearranging Washburn equation, the pore throat size can be calculated:

$$r = \frac{2\,\sigma\,\cos\theta}{P_c} \qquad\qquad (4.2)$$

However, to calculate the pore throat radius in micron, we can add a conversion factor 0.145 to the equation.

$$r = \frac{2\,\sigma\,\cos\theta \times 0.145}{P_c} \qquad\qquad (4.3)$$

Where r is the radius of pore throats in μm, P_c is the capillary pressure in psi, σ is the surface tension in N/μm, and $\cos\theta$ is the air/mercury contact angle in radian. To calculate the pore-throat sizes by the MICP measurements, the contact angle of air/mercury system at the pore scale along with surface tension of the mercury are considered as 140° and 480 dyne/cm, respectively.

Before starting the MICP tests, all the fluids in the rock samples were extracted with toluene followed by methanol and then dried in the oven at 100 ºC for approximately 24 hours. The extracted solutions were exposed to fluorescence and silver nitrate to make sure that the samples were completely clean.

Fig. 4.3 shows the pore-throat size distribution of all the core plugs, measured by the MICP test. The results show that most of the pore-throat sizes are in the nano-scale range (Table 4.4).. Table 4.5 lists the values of the median pore-throat size of each sample, where the median pore-throat size is described as the pore throat diameter at 50% of mercury injection. According to Table 4.5, the median pore-throat size ranges between 22 to 452 nm. According to Table 4.4 the pore-throat sizes from 100 to 500 nm represent micropore and those smaller than 100 nm, are defined as nanopores. Therefore, all the Montney samples have nanopores, except the core plugs MTY 2-2, MTY 3-1 and MTY 3-2, where the pores are relatively larger.

Fig. 4.4 shows the displacement mercury pressure versus air saturation (wetting-phase saturation). Rock samples MTY 2-1 and MTY 2-4, have different pressure profiles compared to other cores. As listed in Table 4.5, the pore-throat sizes in these rock samples are significantly smaller compared to the other rock samples, thus higher pressures are required for mercury to fill the pores.. In addition, the step curves of MTY 2-1 and MTY 2-4 samples indicate that different displacement pressures are required to fill pores of these two rock samples, due to the poorly-sorted grains. However, the capillary pressure versus air saturation curves are similar and flat for all the other core plugs, indicating larger pores and more uniform pore-throat size distribution.

(a)

(b)

(c)

(d)

(e)

(f)

(g)

(h)

(i)

(j)

(k)
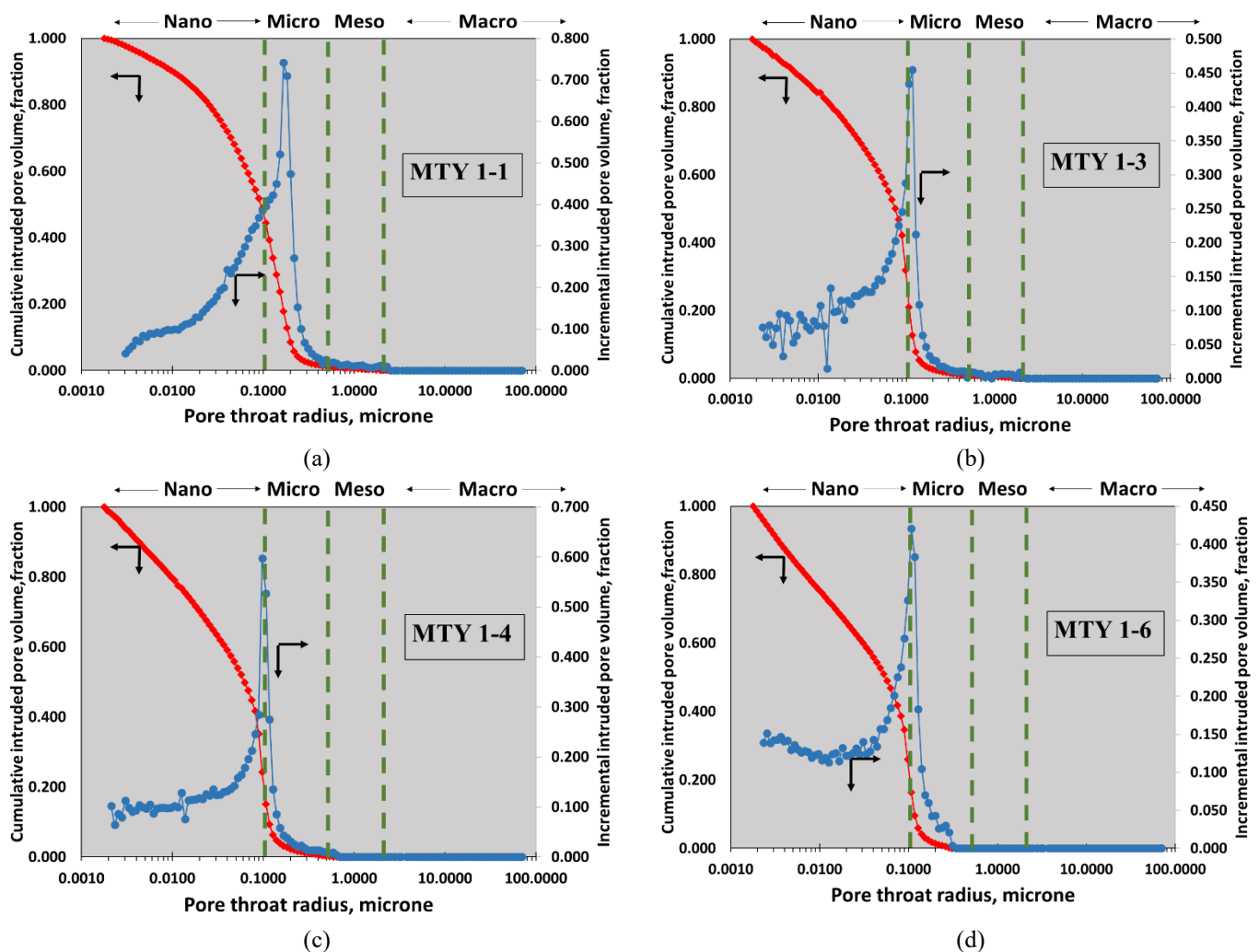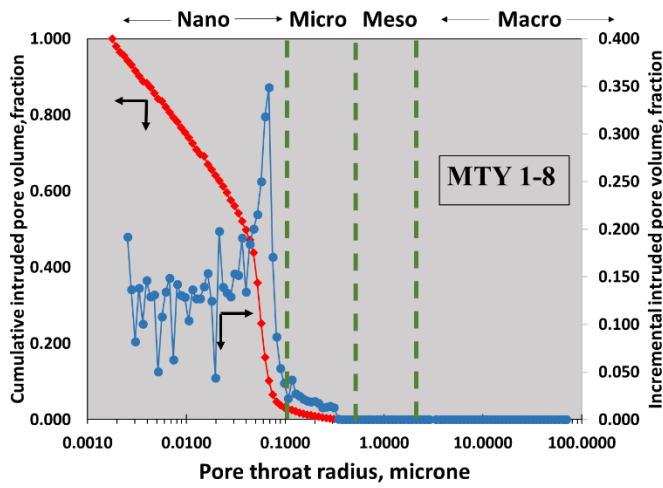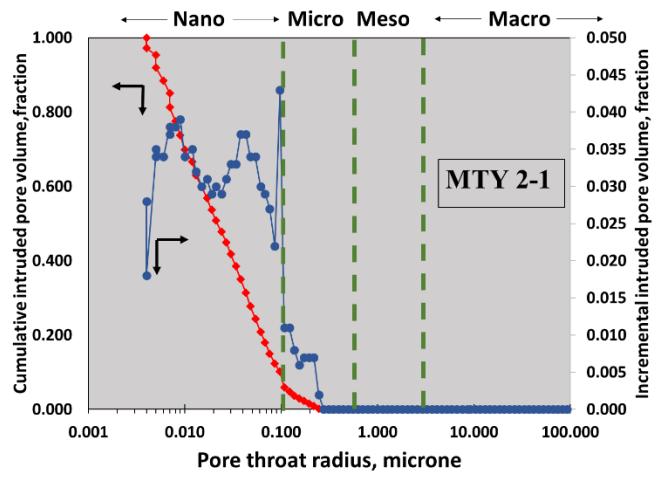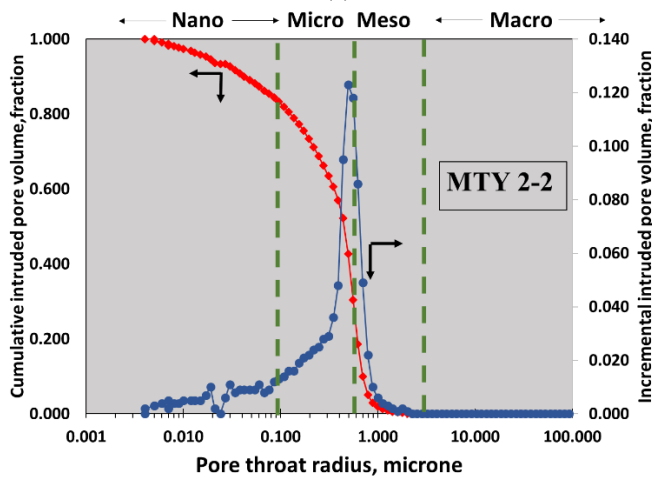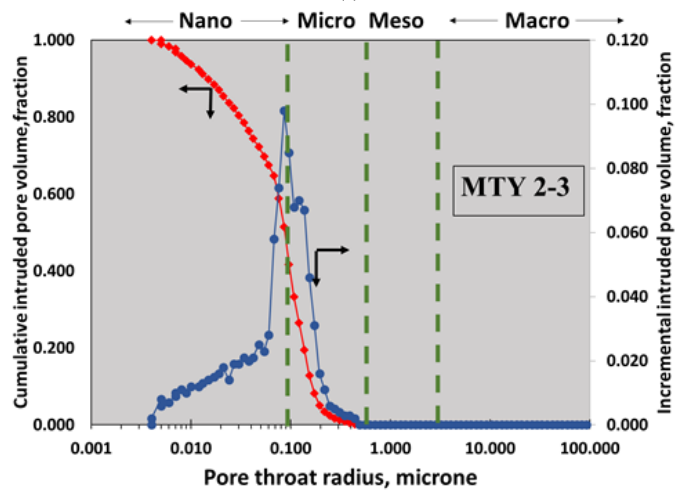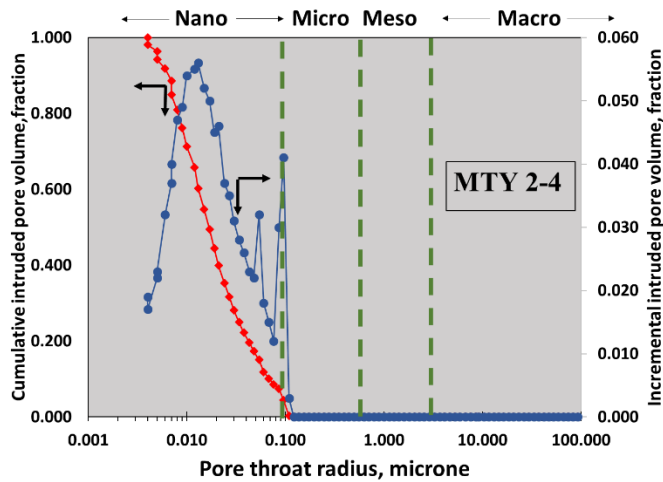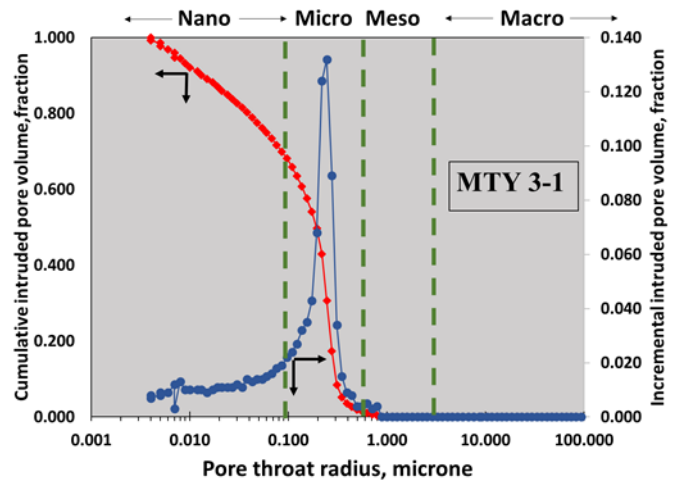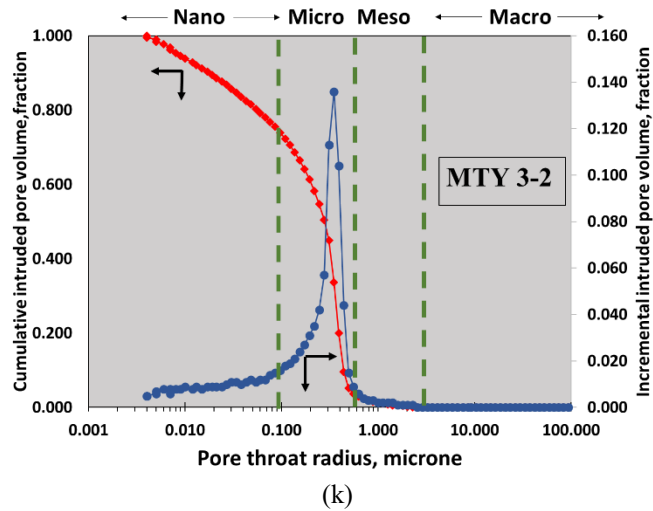
Figure 4-3- Pore size distribution obtained from the mercury injection conducted on the core plugs of the three wells.

Table 4-5- Median pore size distirbution obtained from the MICP test along with category of the pore sizes.

Well Number	Sample ID	Depth (m)	Grain Density (g/cc)	Bulk Density (g/cc)	Median Pore Radius (Nanometer)	Category
1	MTY 1-1	2026.0	2.71	2.45	98	Nanopores
	MTY 1-3	2057.0	2.73	2.54	82	Nanopores
	MTY 1-4	2071.0	2.73	2.56	63	Nanopores
	MTY 1-6	2075.0	2.81	2.63	57	Nanopores
	MTY 1-8	2086.5	2.74	2.62	40	Nanopores
2	MTY 2-1	2066.39	2.72	2.66	22	Nanopores
	MTY 2-2	2073.03	2.68	2.54	452	Micropores
	MTY 2-3	2090.98	2.70	2.57	87	Nanopores
	MTY 2-4	2095.45	2.73	2.65	17	Nanopore
3	MTY 3-1	2083.83	2.70	4.43	193	Micropores
	MTY 3-2	2100.04	2.69	5.06	280	Micropores
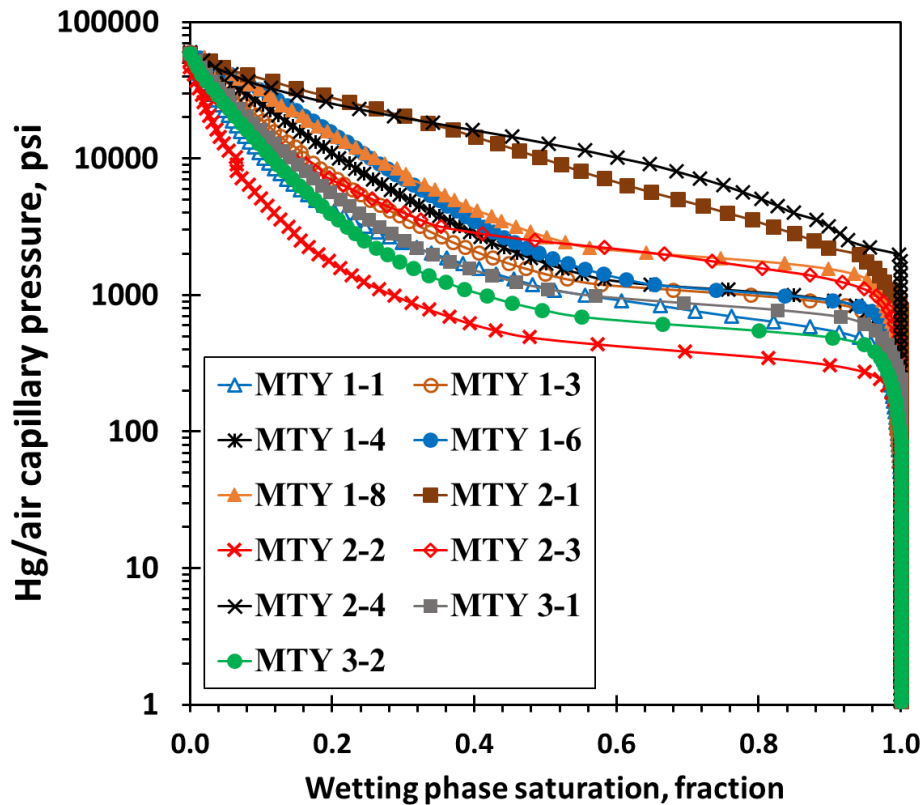
Figure 4-4- Mercury pressure versus air saturation (wetting phase) of the Montney rock samples.

4.5   SEM Images Analysis

Scanning Electron Microscope (SEM) images helps to understand the texture of the rocks, gives an idea about the pores structure along with the size of the pores and defines the minerals present in the rock. SEM is a complementary to the XRD and MICP tests, which can confirm the mineralogy and pore sizes in the rock structure that were discussed in the previous sections, by displaying a visual images of them. Note that, the available SEM images are obtained only from wells 2 and 3.

To conduct SEM, a small, freshly broken piece of each sample is settled on standard SEM mount and coated with platinum/palladium for approximately 1 minute. Then, the samples is imaged using FEL Quanta 650 scanning electron microscope equipped with EDAX energy dispersive X-ray spectrometer (EDX). The obtained SEM images can help to determine the lithotype, interstitial components including clays and cements, pore structure and organic materials.

MTY 2-1 SEM images analysis:

Fig.4.5 shows the SEM images of the sample MTY 2-1. The lithology of this sample is dolomitic siltstone, with framework grains dominantly monocrystalline quartz (q in the figures) and moderate amounts of mica (mi in the figures), a few clayey sedimentary rock fragments (sf in figures). **Fig.4.5.a and 4.5.c** explain that, the framework grains are tight and cemented with minimal porosity. High amount of clays are present in the structure of this sample, including illite (IL in the figures) and mica. Illite coats the framework and has ribbon-like shape (**Fig.4.d**), while mica shows horizontal alignment (**Fig.4.a** the yellow arrows). The carbonate dolomite minerals (do in the figures) are authigenic and common in the matrix. Dolomite along with quartz and potassium feldspar (Kf in the figures), they form cement in some areas. Most of the pores are intergranular pores (red arrows in **Fig.4.b**) associated with mica plates. These pores are completely surrounded by authigenic cements such as dolomite and quartz and partially filled with illite.

MTY 2-2 SEM images analysis:

The lithology of the sample is dolomitic siltstone. The grains in the sample are well sorted and with dominance of quartz with sizes of 40-70 microns across (**Fig.4.6.c**). This confirms the MICP and the XRD observations previously discussed, where this core plug required the lowest mercury displacement pressure .As well, there is minor amount of rock fragments in the rock (the red arrow in **Fig.4.6.c**) and albite (al in the figures) present between the grains. **Fig.4.6.a** displays that, the siltstone has homogeneous, well-cemented and granular texture. The illite in this sample is rare and mica flakes are aligned with the bedding. Dolomite is the common cement in the sample along with the detrital microcrystals quartz cement (the green q in the **Fig.4.6.d**). In the intergranular areas, titanium oxide (yellow arrow in **Fig.4.6.c**) and poor amounts of apatite and pyrite are taking place. The intergranular pores (green arrow in **Fig.4.6.c**) are rare and associated with mica, and most of the intergranular areas are filled with quartz and dolomite cements.
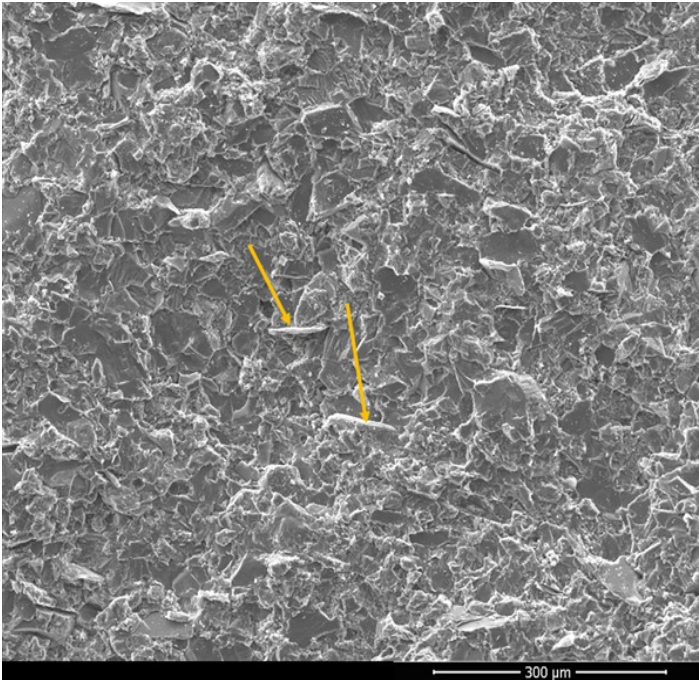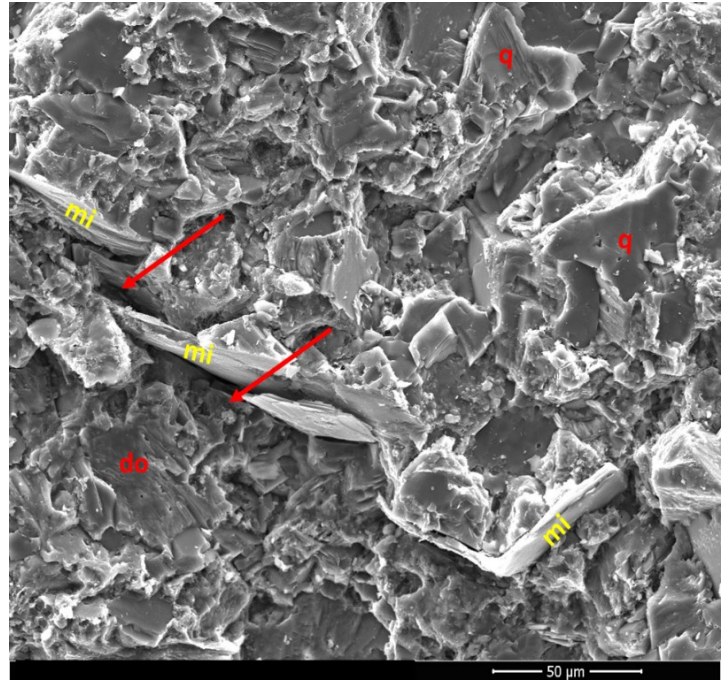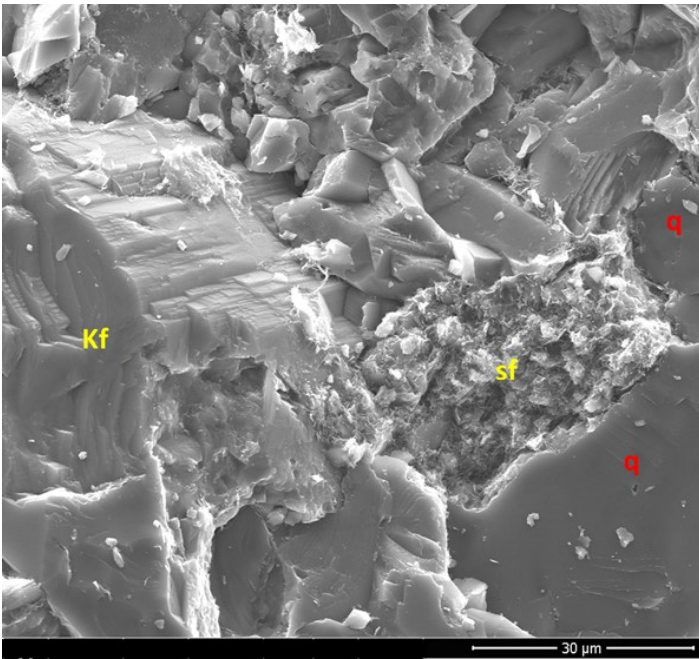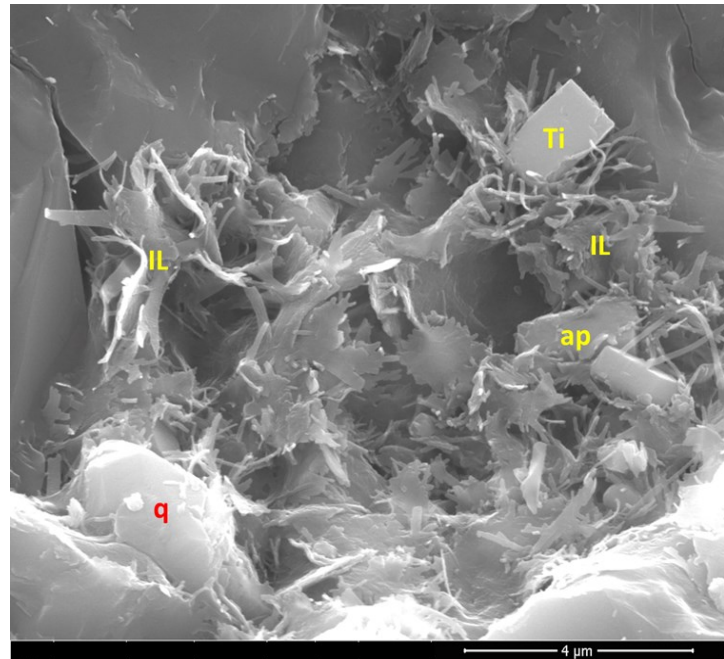
Figure 4-5- Core plug MTY 2-1 SEM images with different dimensions.
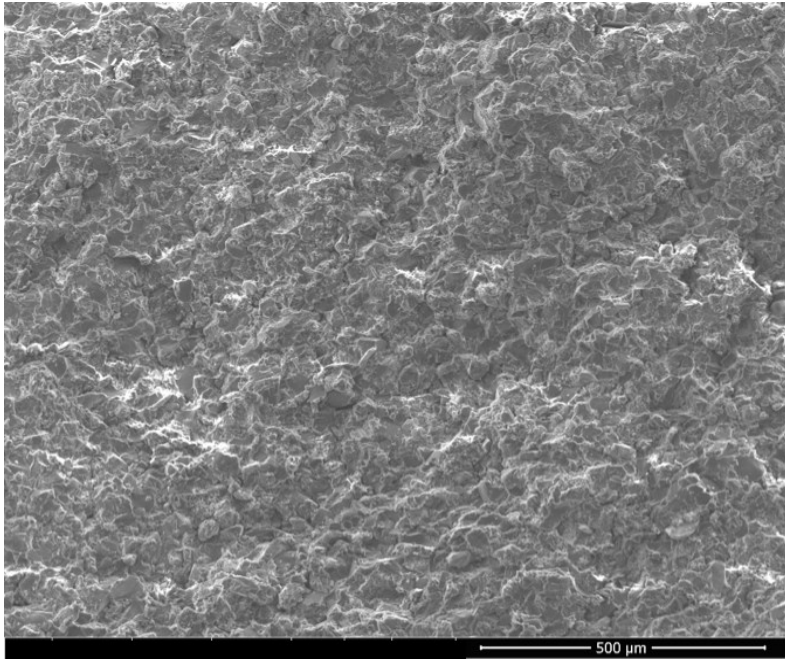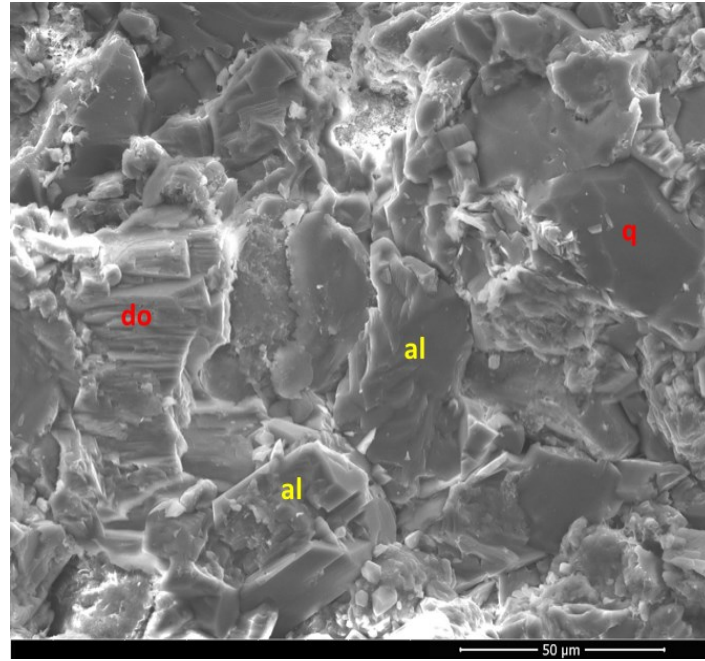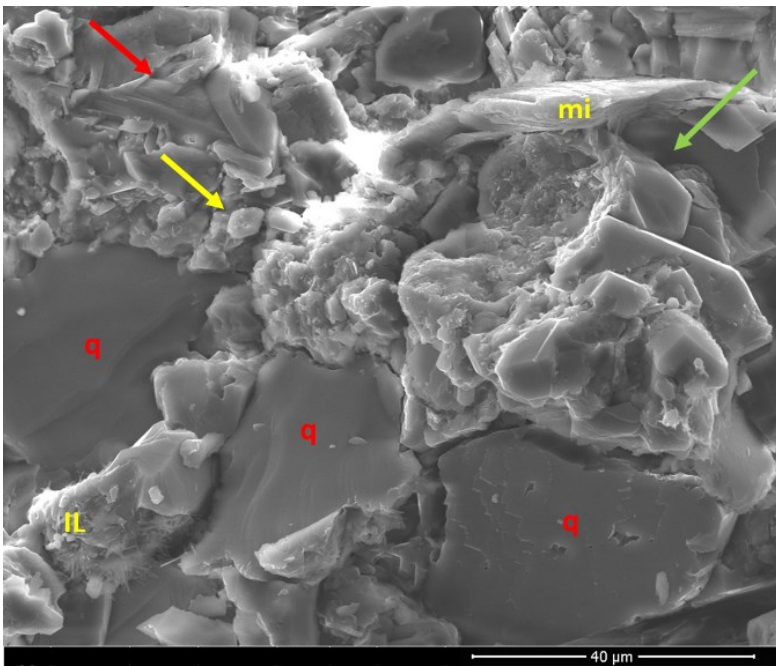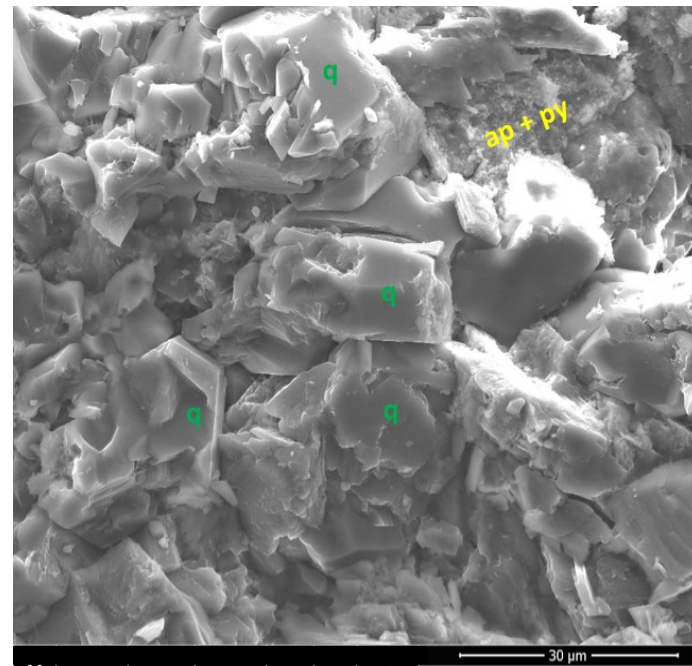
Figure 4-6- Core plug MTY 2-2 SEM images with different dimensions.

MTY 2-3 SEM images analysis:

The lithology of this sample is muddy siltstone, which mainly made of monocrystalline quartz grains with moderate amounts of rock fragments (**Fig.4.7.b**). The grains are unsorted with layered and messy texture (**Fig.4.7.a** and **Fig.4..b**). In **Fig.4.7.b** we observe that, the mica is not aligned with the bedding and it is upturned, which indicates the bioturbation of this rock. Illite and mixed layer of illite-smectite (green arrows in **Fig.4.7.c**) are the most clay minerals, which coat the framework, along with the mica plates. Albite and potassium feldspar, both cements on detrital grains (**Fig.4.7.d**) with minor amounts of detrital microcrystals quartz (green q) and dolomite. The intergranular pores are the dominant pore type, but due to overgrowth of quartz and feldspar cements, they are not very large (yellow arrows in **Fig.4.7.d**). In addition, illite clays, surrounds and partially fills the pores in the sample.

MTY 2-4 SEM images analysis:

Fig.4.8 shows the SEM images of the MTY 2-4 core plug. This dolomitic siltstone is mainly made of monocrystalline quartz with presence of mica plates that are align with the bedding. There is a lot of dolomite minerals present in this rock, which made the texture of this rock, granular to crystalline. Clay minerals are represented by illite and illite-smectite (the green arrows in **Fig.4.8.d**) which are mixed with pyrite and apatite. Mica horizontal plates as well are bulge in the middle of the highly cemented rock as displayed in **Fig.4.8.b**. The abundance and overgrowth of dolomite and quartz makes the sample highly cemented. The intergranular pores are rare and most of them are filled with dolomite. In total, the texture of the sample is very tight and shows a minimal open porosity.
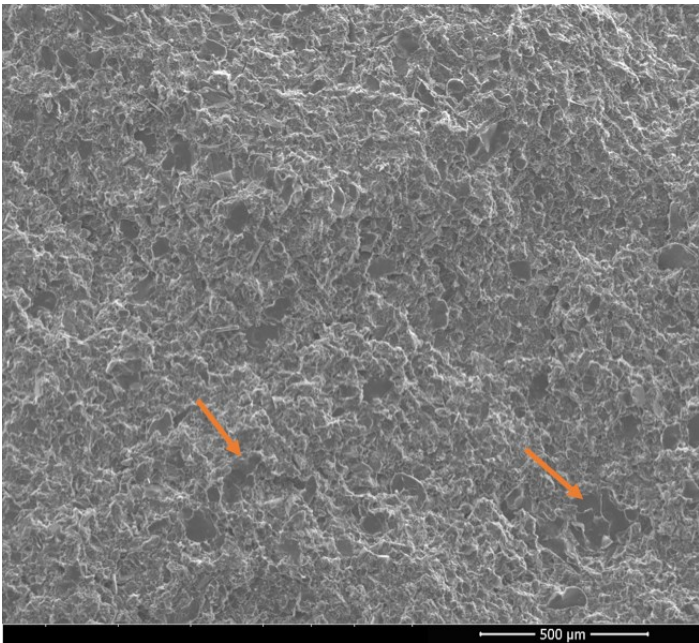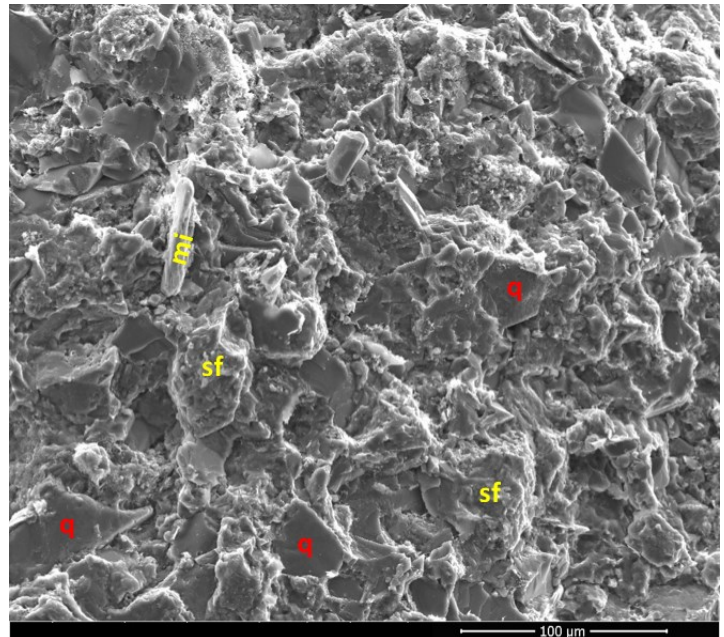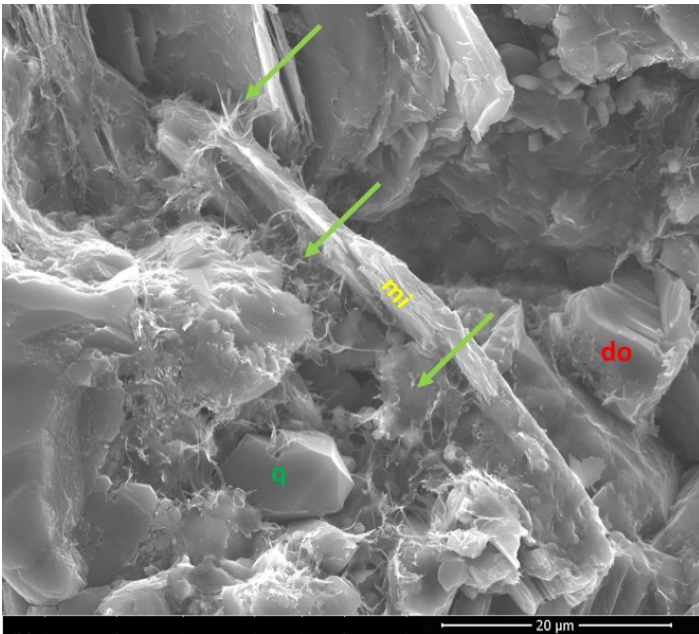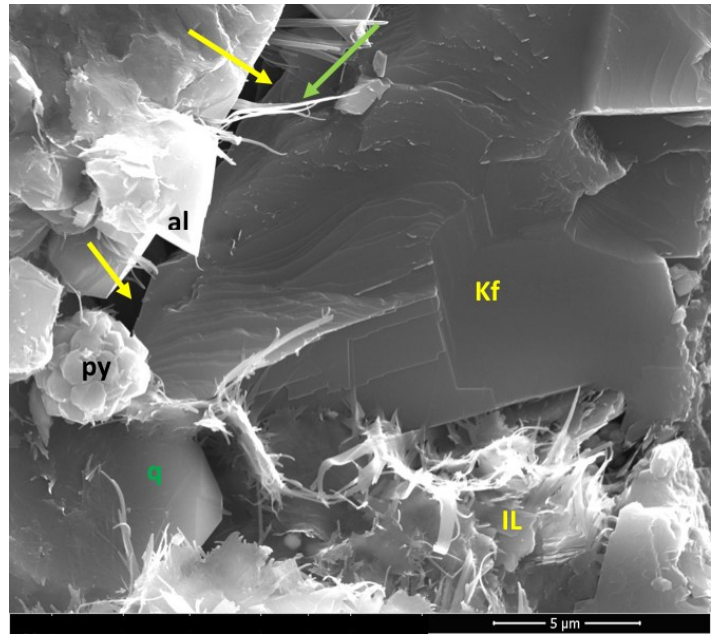
Figure 4-7- Core plug MTY 2-3 SEM images with different dimensions.
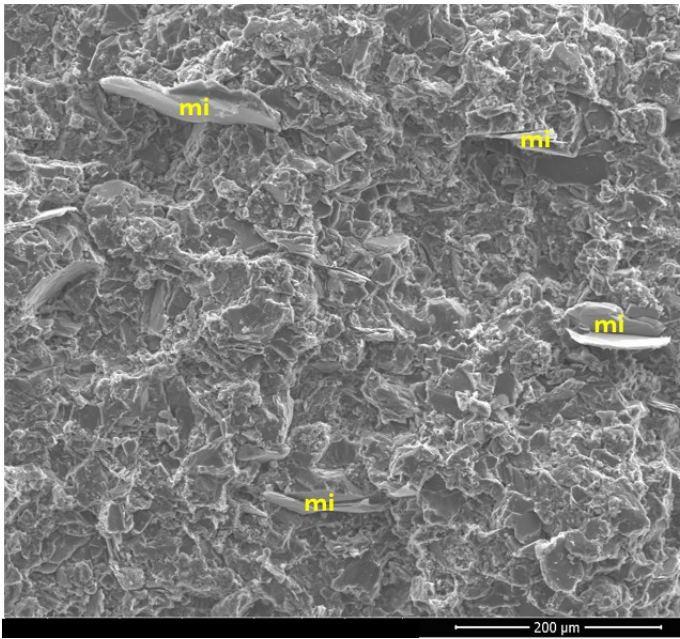
(a)
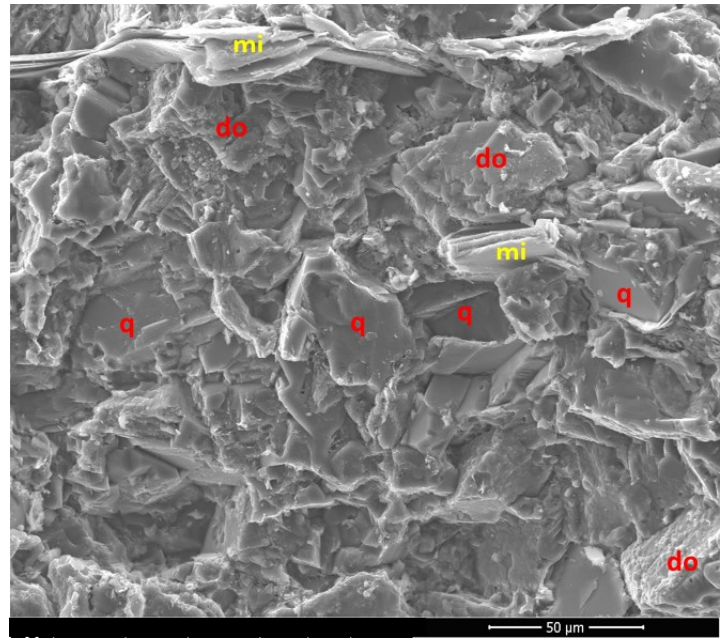
(b)
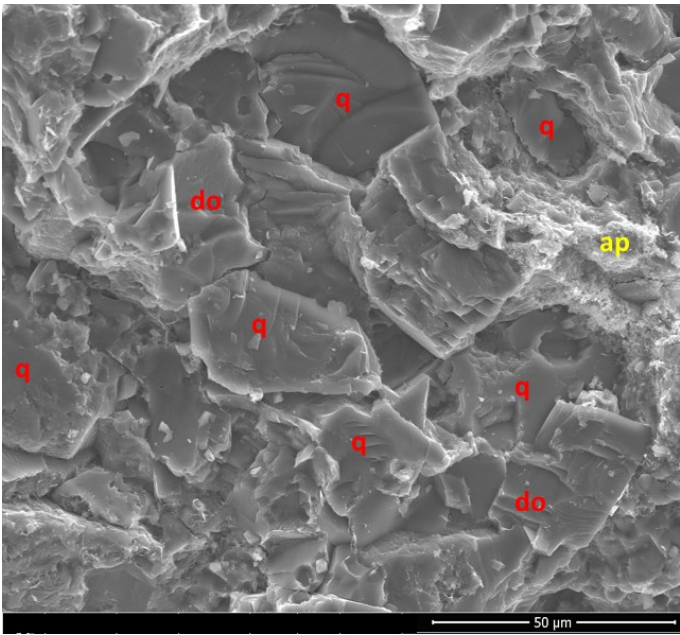
(c)
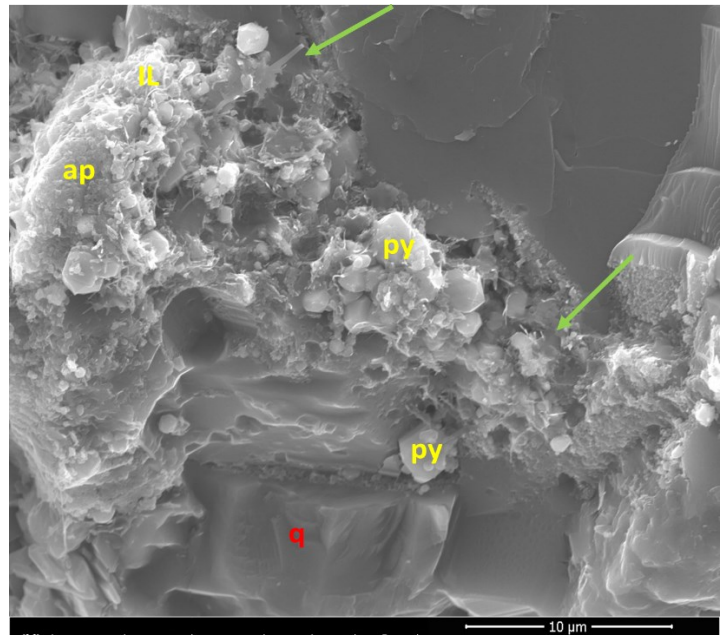
(d)

Figure 4-8- Core plug MTY 2-4 SEM images with different dimensions.

MTY 3-1 SEM images analysis:

The framework grains of this dolomitic siltstone displayed in **Fig.4.9** consisted mainly from quartz with minor amounts of albite and feldspar (Fd in the figures). In total, the texture of this rock is granular to microcrystalline. Illite and mica are the present clays in this rock. Dolomite is observed with minor amounts of pyrite and titanium oxide admixed with apatite. However, the dominant pores are intergranular which surrounded with cements such as dolomite. The pores sizes in this core plug are relatively larger than the other core plugs, and most of the large pores are surrounded by illite.

MTY 3-2 SEM images analysis:

Lithotype of the core plug MTY 3-2 presented in **Fig.4.10** is dolomitic siltstone with abundant quartz grains. The texture of this rock is granular and microcrystalline due to the composition of framework grains with cement. The core contains significantly high amount of illite clays, which they coat the grains and fill most of the pores of the core plug. In addition to illite, rare amounts of chlorite and mica clays are present in this sample. Moreover, the intergranular pores (yellow arrows in **Figs.4.10.b**) are the most common pore type with size less than 10 microns. Along with clays, these intergranular pores are surrounded with cements. Dolomite is the most abundant cement with minor amount of quartz in form of silica cement (red arrows in **Figs.4.10.c** and **4.10.d**) with amounts of barite (ba in the figures).
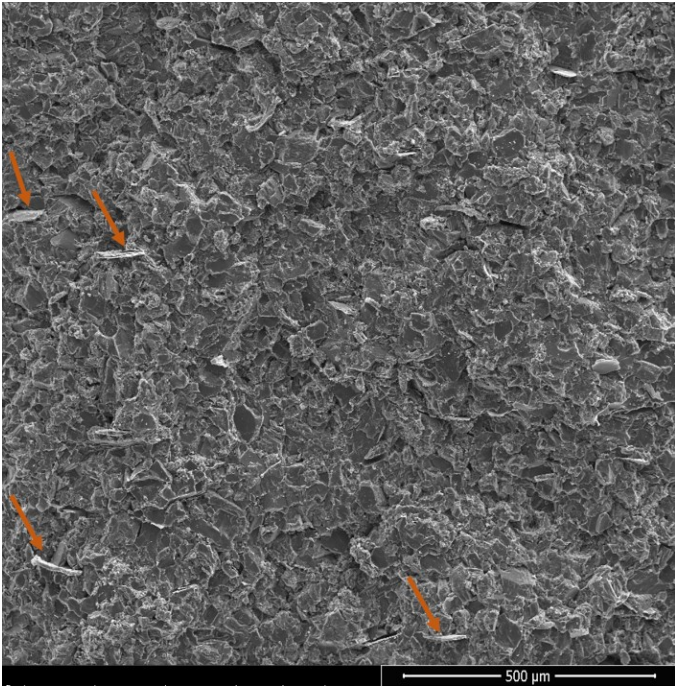
(a)
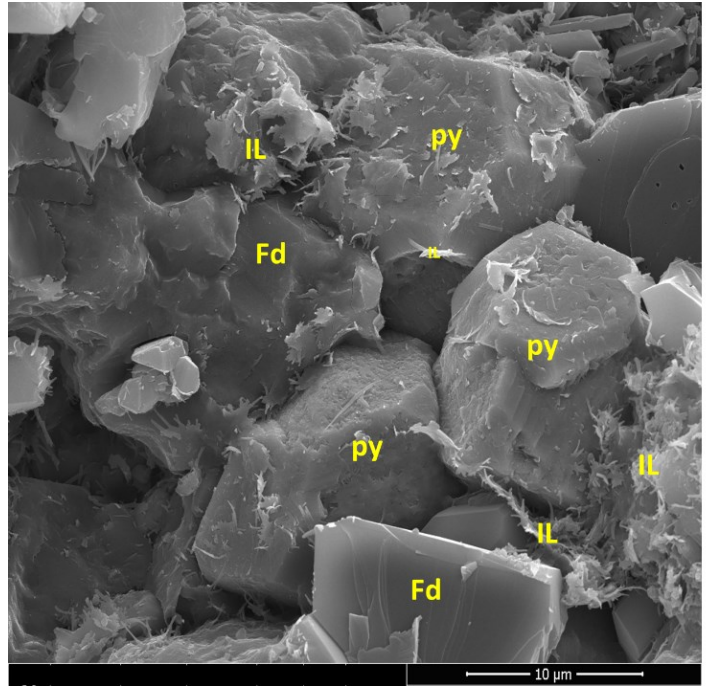
(b)
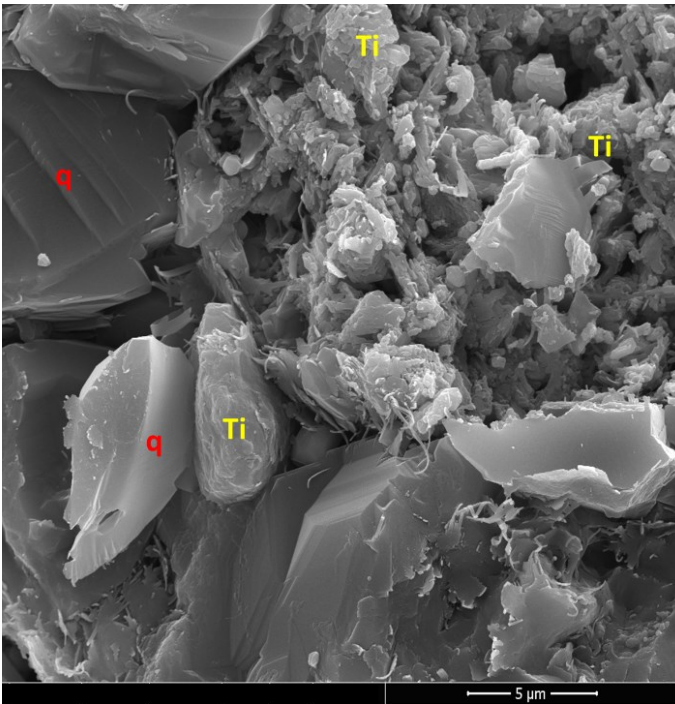
(c)
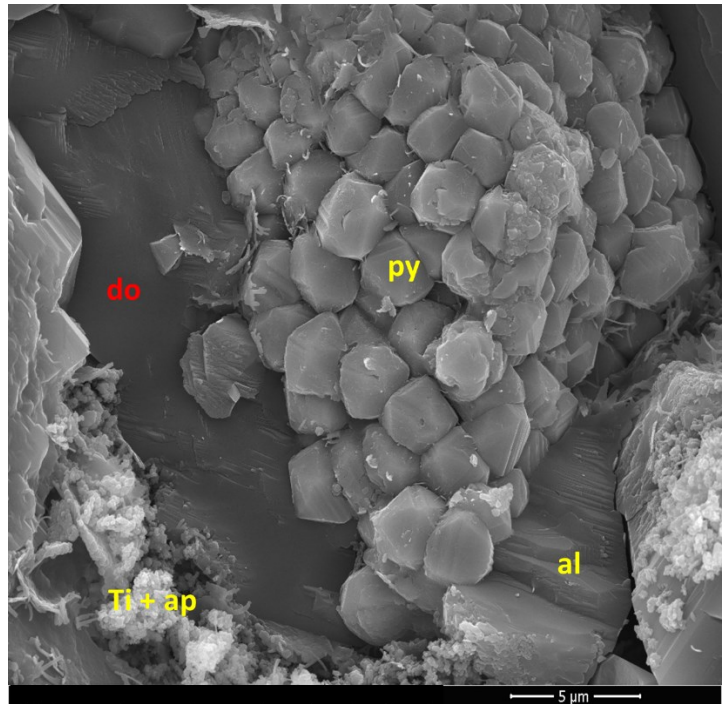
(d)

Figure 4-4-9- Core plug MTY 3-1 SEM images with different dimensions.
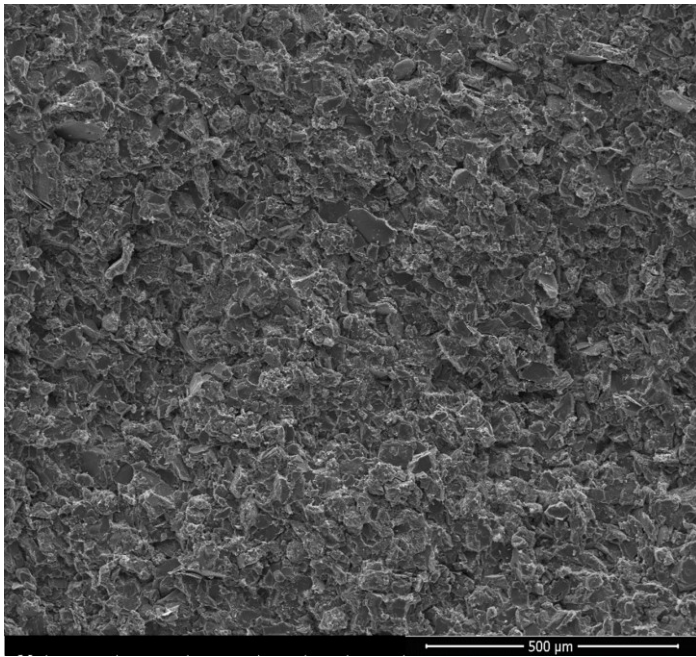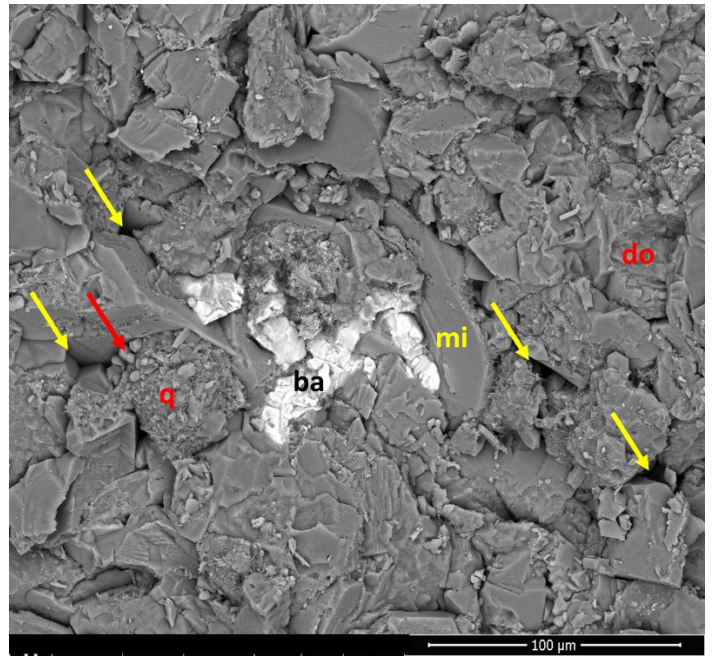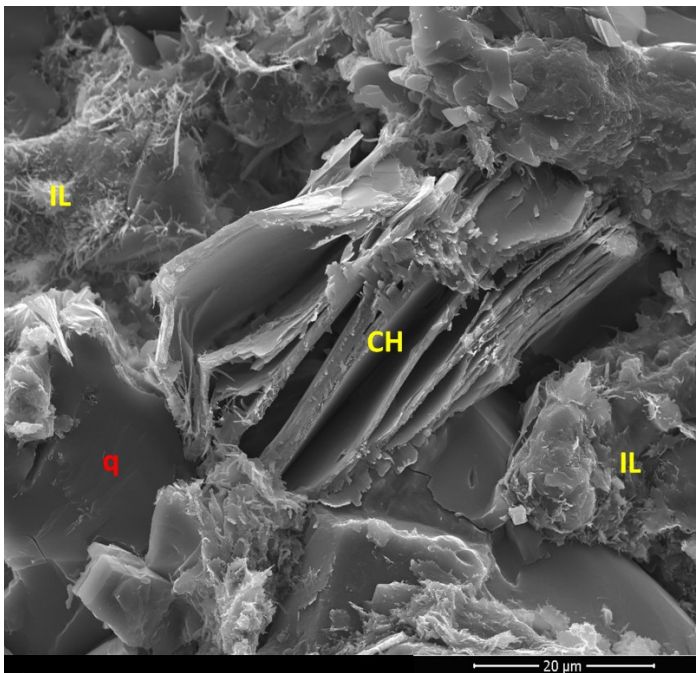
Figure 4-10- Core plug MTY 3-2 SEM images with different dimensions.

Chapter 5

5) Investigating the Effect of The Extended Shut-in Time on the Well Performance

In this chapter, we simulate three-phase production using the actual reservoir geological model and the pressure data measured using downhole gauge, to investigate the reasons behind the enhancement in the oil and gas rates after the shut-in. In addition we perform a sensitivity analysis to determine the optimum shut-in time for this well. The objective functions for determining this optimum shut-in time are net present value (NPV) and cumulative hydrocarbon production

5.1 Reservoir Model Description

The numerical reservoir model was built in CMG-IMEX software by the operating company using the actual reservoir geological model. **Fig.5.1** shows the model comprising over 6 million gridblocks, divided into two zones with 8 layers in zone 1and 69 layers in zone 2. The thickness of the upper and lower zones are 36 m and 128 m, respectively. Tables 5.1 and 5.2 list the geological and fluid properties of the model. The reservoir contains saturated black oil with bubble point pressure of 20 MPa and density of 36.5° API. The initial reservoir pressure is around the bubble point pressure. Oil and gas viscosities at initial reservoir pressure are 2.2 cp and 0.02 cp, respectively. In this homogeneous reservoir, permeability values for zone 1 and zone 2 fall within 0.00098 - 0.73 and 0.00006 - 0.007 mD, respectively. Both zones have an average porosity of 0.06. The initial oil saturation values for zones 1 and 2 are in the range of 0.1 - 0.2 and 0.5 - 0.7, respectively. Although zone 1 has a higher permeability than zone 2 (the target zone), it has immobile oil and mobile water, acting as an additional source for the produced water. A horizontal well with 2035 m length of the horizontal section was drilled in zone 2 and fractured in 65 single-cluster stages with 32 m spacing and average fracture half-length of 25 m.
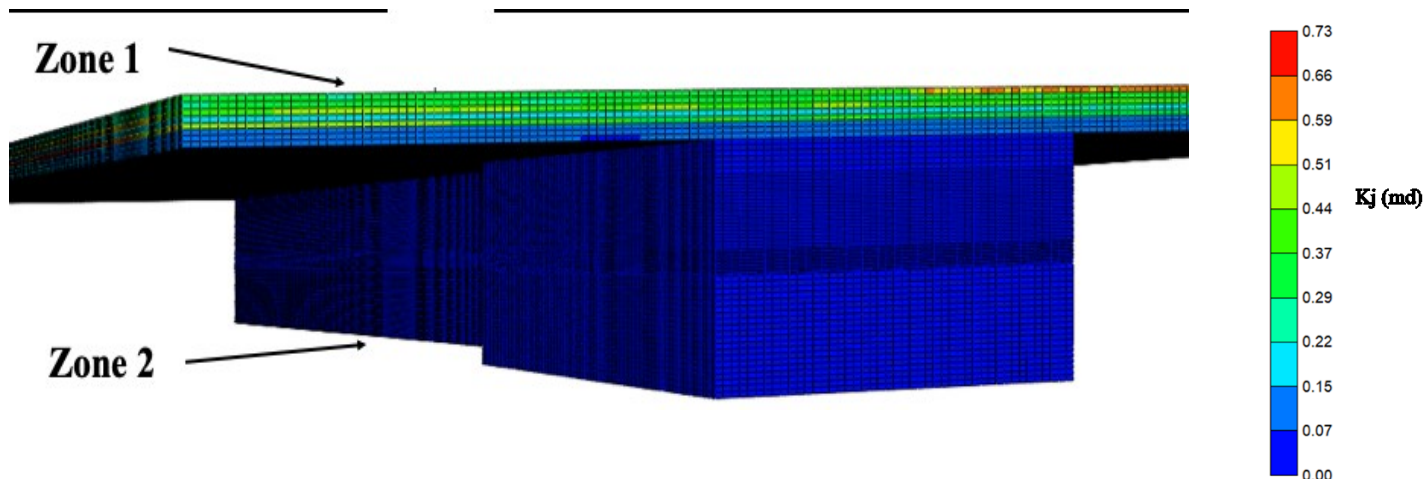
Figure 5-1- The reservoir model for numerical simulation with over 6 million grid blocks. Zone 1 (upper zone) comprises 8 layers and zone 2 (the target zone) comprises 69 layers.

Table 5.1- Geological properties of the reservoir used in the numerical simulator.

Parameter	Value
Number of grid blocks in zone 1	692,200
Number of grid blocks in zone 2	5,559,260
Matrix permeability (Zone 1)	$9.80 \times 10^{-4} – 7.30 \times 10^{-1}$ mD
Matrix permeability (Zone 2)	$6.25 \times 10^{-5} – 7.10 \times 10^{-3}$ mD
Matrix porosity (Zone 1)	0.044 - 0.105
Matrix porosity (Zone 2)	0.019 - 0.100
Fracture Permeability	104 mD

Table 5.2- Reservoir rock and fluid properties used in the numerical simulator.

Property	Value
Bubble point pressure	20 MPa
Rock compressibility	3×10^{-6} kPa^{-1}
Oil density	844.17 kg/m^3
Oil viscosity	2.2 cp
Gas density	0.86 kg/m^3
Gas viscosity	0.02 cp

5.2 Methodology for Production History Match

We run the model using the inputs listed in Tables 5.1 and 5.2. **Fig.5.2** compares the measured and simulated production data before and after the shut-in periods. It shows a mismatch especially for the bottom-hole pressure (BHP) data. The simulated oil and gas rates and bottom-hole pressure before shut-in are higher than the measured data. After the shut-in period, the match between the simulated and measured rates is relatively better. The observed improvement in the hydrocarbon production performance after the shut-in can be explained by enhancement in oil and gas relative permeabilities, possibly due to reduction in water blockage near the fracture face. To test this hypothesis, we attempt to improve the history match before and after the shut-in period by modeling the water blockage using interblock fluid-flow transmissibility multiplier (TM) near the matrix-fracture interface in the simulation model.

5.3 Changing Transmissibility Multiplier

Interblock fluid-flow transmissibility is a factor that controls the fluid flow between two defined grid blocks (Chen 2007). A gridblock's transmissibility can be adjusted by adding a multiplier to the transmissibility formula (Ertekin and Abou-Kassem 2006):

$$T_{lx} = \beta_c \frac{k_x A_x}{\Delta x} \frac{k_{rl}}{\mu_l B_l}$$

(5-1)

Here,

T	= Ttransmissibility of phase l between two gridblocks in the x direction
Subscript l	= Fluid phase, [oil, water or gas]
β_c	= Transmissibility conversion factor
K_x	= Absolute permeability in the x direction, [md]
k_{rl}	= Relative permeability of phase l
A_x	= Cross sectional area normal to the x direction, [ft^2]
μ_l	= Viscosity of phase l, [cp]
B_l	= Formation volume factor of phase l, [m^3/std m^3]
Δx	= Difference along the x direction, [ft]

The derivation of transmissibility for the multiphase flow formulation is demonstrated in **Appendix 5-A**. The CMG-IMEX simulator allows the addition of a multiplier to the interblock transmissibility. The default value of the TM in IMEX is 1, in I and J directions. Using TM < 1 is equivalent to reducing phase relative permeability. Here, we use TM as a tool to change hydrocarbon relative permeability due to possible changes in water saturation near fracture face after the fracturing process and extended shut-in period. Thus, to history match the simulated and field data we follow the bellow steps:

1) Determine the optimum TM values:

We use a stochastic optimization algorithm (Moussa and Awotunde 2018) to obtain the TM values of the interblocks near the matrix-hydraulic fractures interface giving the best match between the measured and simulated data before and after the shut-in. To overcome the non-uniqueness issue associated with stochastic optimization, we split the production data of 605 days into training and validating data sets. In the training stage, we use 465 days of the production history to find the optimum values of TM before and after the shut-in. In total, 110 simulation models are tested, and among all the models in the training stage, we select the best three simulation models according to coefficient of determination (R^2). Next, we use these three models for validating the simulation results using the remaining (unseen) 145 days of production data. We select the model with the highest R^2 in the validation stage, as the model with the optimum TM values that lead to the best matching performance.

2) Match the data before shut-in:

First, we attempt to match the data before the shut-in, since the mismatch between the measured and simulated data is significant in this period. We use the TM values obtained from the optimum model described in step 1 to match the measured data before the shut-in.

3) Use the same TM values applied in step 2 to match the data after shut-in:

If step 2 results in a good history match before the shut-in, then we apply the same TM values to match the data after the shut-in period. The aim of this step is to investigate the change in hydrocarbon relative permeabilities during the extended shut-in period.

4) Achieve the best match after the shut-in by capturing the change in transmissibility:
If step 3 does not result in a good match between the simulated and measured data, we use the
TM values obtained in step 1 to match the production data after the shut-in period.
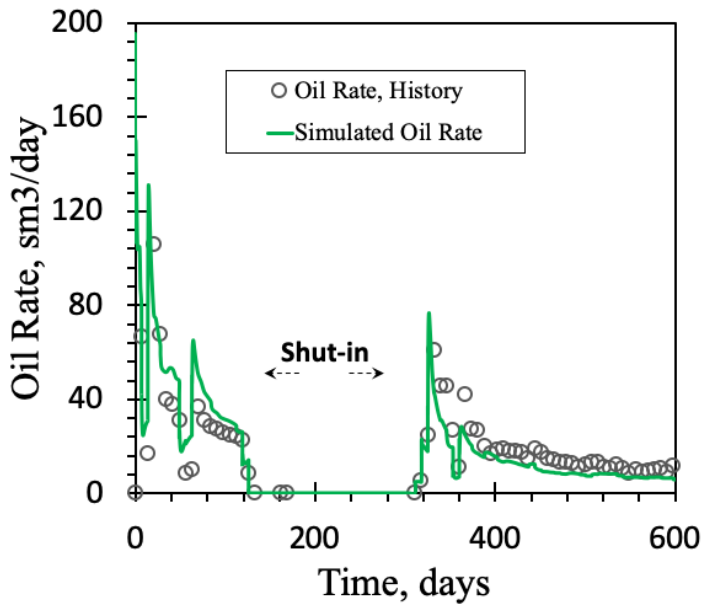
(a)
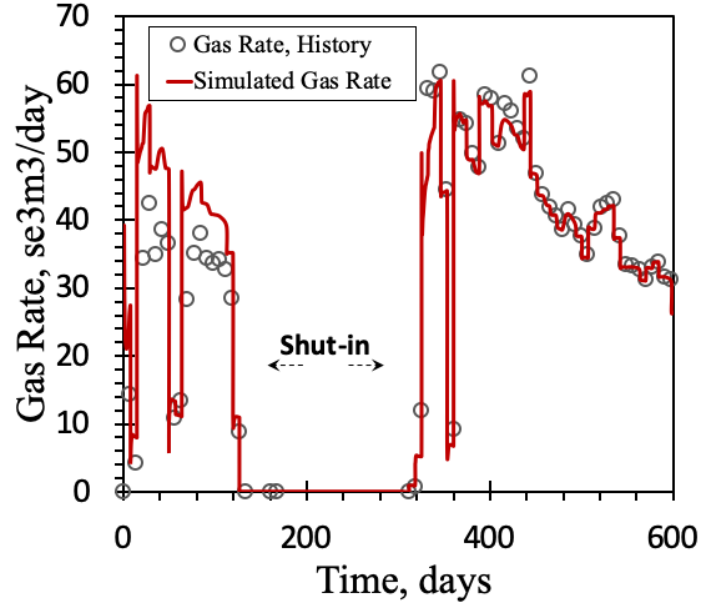
(b)
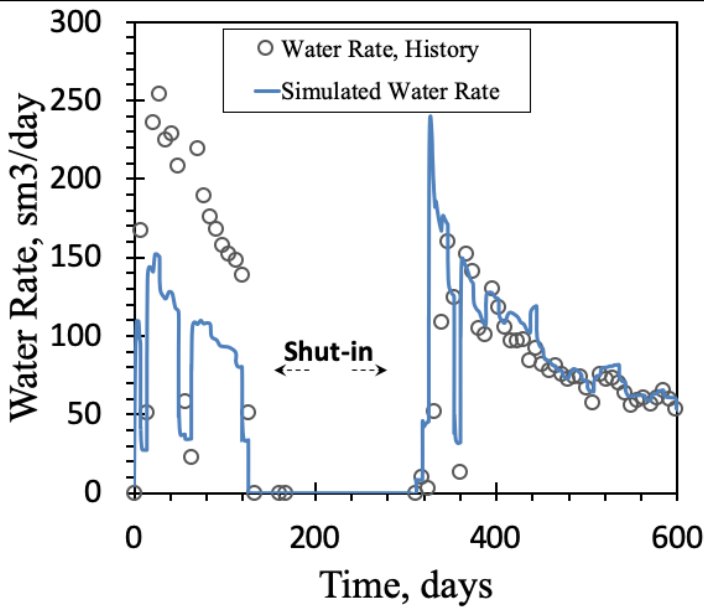
(c)
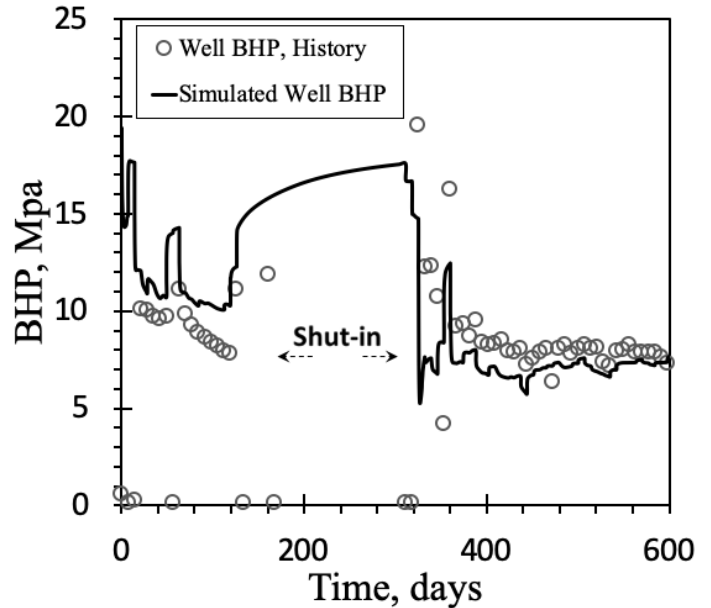
(d)

Figure 5-2- The results of history matching the measured rate pressure data: (a) oil production rate, (b) gas production rate, (c) water production rate, and (d) bottom-hole pressure.

5.4 Production History Match Results

The stochastic optimization algorithm method was used to obtain a simulation model with the best history match. **Fig.5.3** demonstrates that models A, B, and C had the highest values of coefficient of determination (R^2) during the training stage of production data. The same three models were then tested in the validating stage, to obtain the best history match. Model C has the highest R^2 value, suggesting that the best match before and after the shut-in is obtained when the average TM is reduced from 1 (the default TM value) to average of 0.4 before the closing the well and increasing it to average of 2.5 when the well is reopened, as illustrated in **Fig.5.4.**

Using TM = 0.4, improves the match between the simulated and measured field data before the shut-in, but results in a poor history-match after the shut-in period as shown in **Fig.5.5**. It indicates a general improvement in oil and gas relative permeabilities during the shut-in period. To investigate this hypothesis, we use TM=0.4 and TM= 2.5 to simulate the production data before and after the shut-in period, respectively. **Fig.5.6** shows a reasonable match between the measured and simulated data under these conditions. Increasing the average TM from 0.4 to 2.5 suggests reduction in water blockage near fracture face during the shut-in, increasing oil and gas relative permeabilities (which cannot be captured by the capillary-pressure and relative-permeability models used in the simulator).
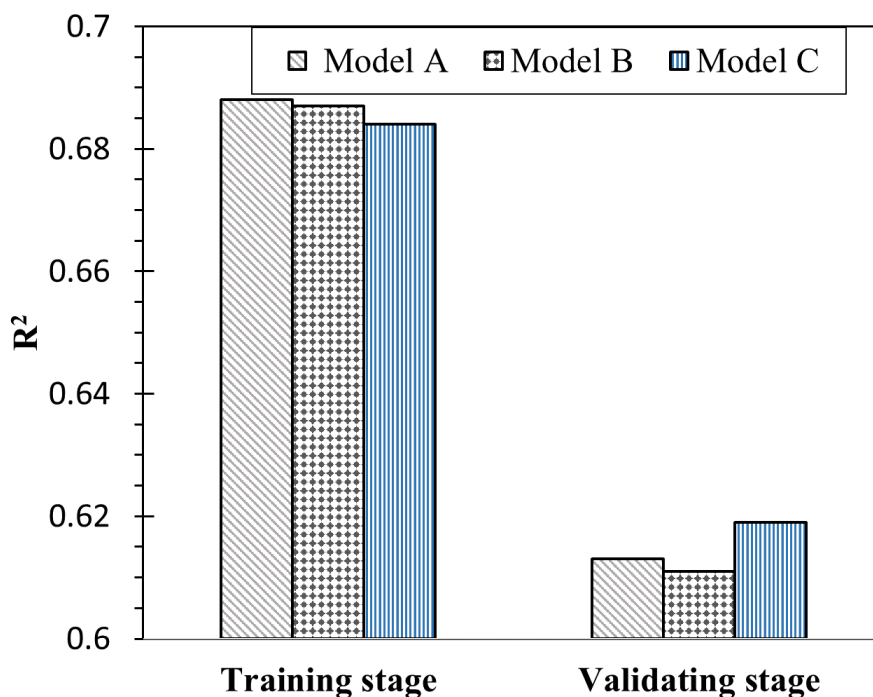
Figure 5-3- The best 3 models obtained from training and validating the simulation outputs with the field history rates and pressure. Model C is defined as the optimum model with the highest R^2 in the validating stage.
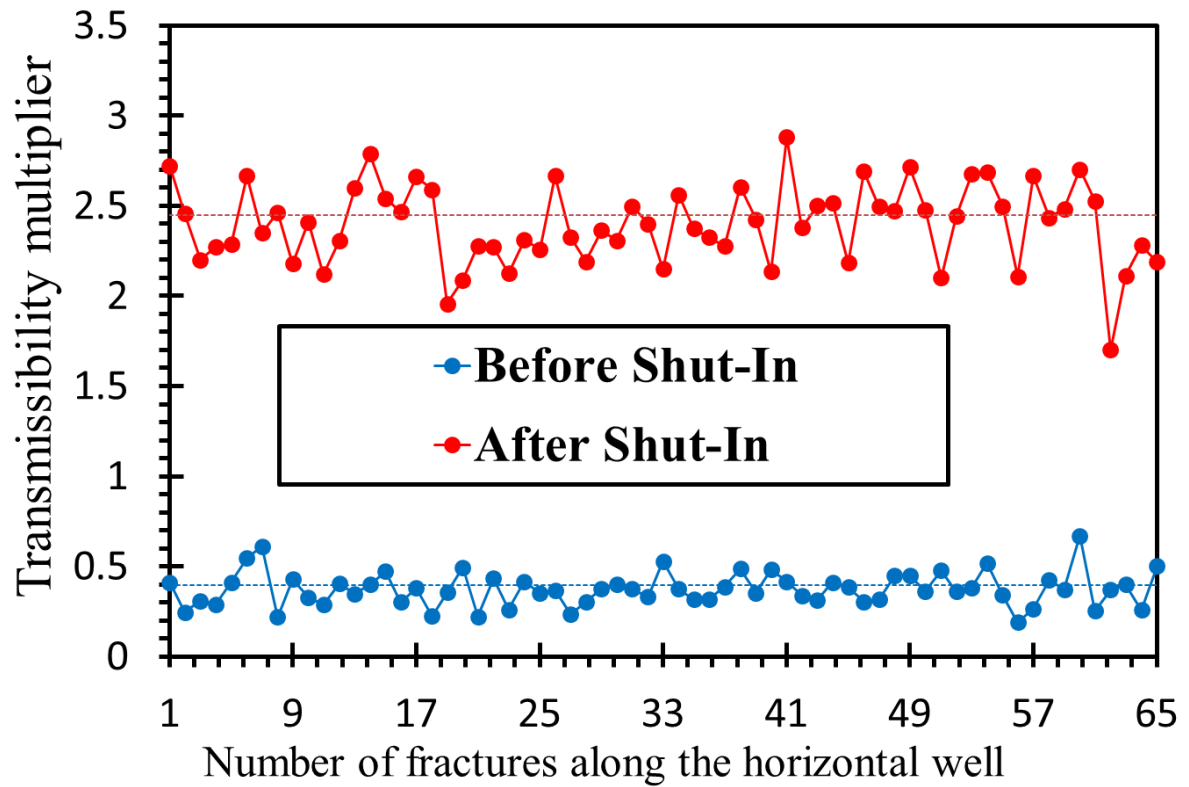
Figure 5-4- The change in TM in the 65 fractures grid block during the shut-in obtained from model C. The transmissibility multiplier values in the fractures increases from average of 0.4 before the shut-in to 2.5 after the shut-in.
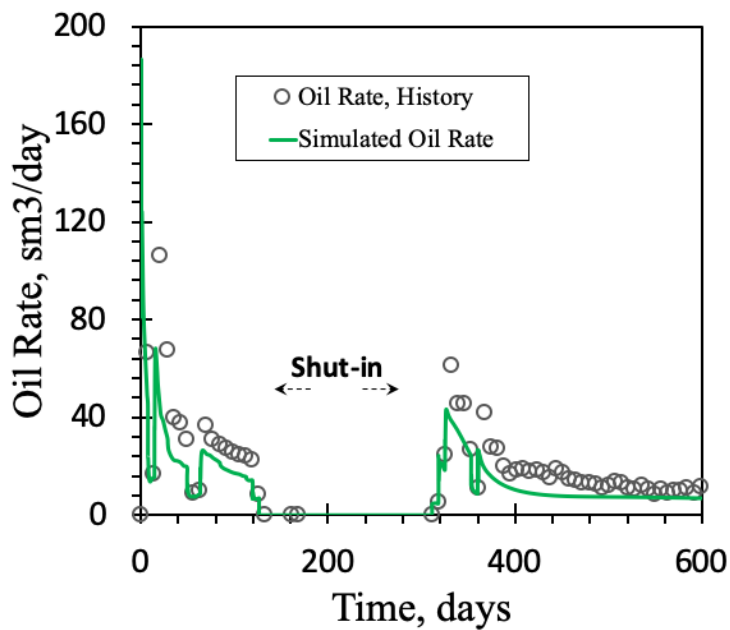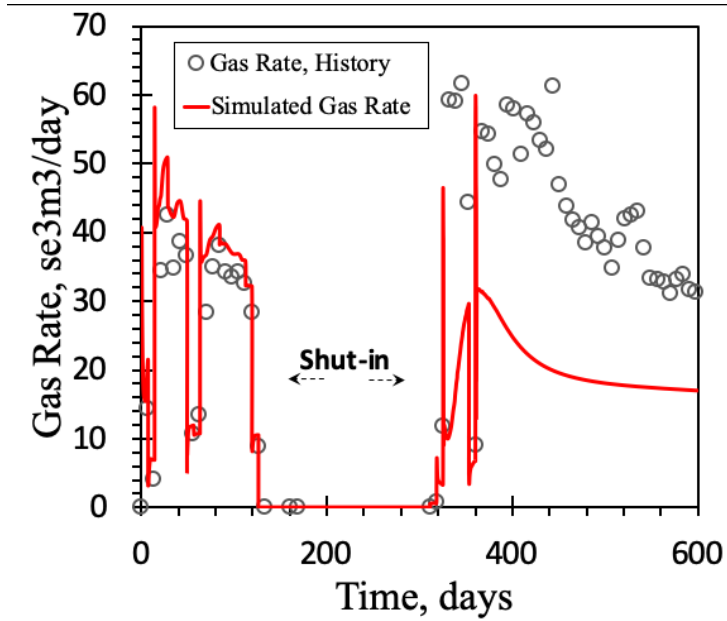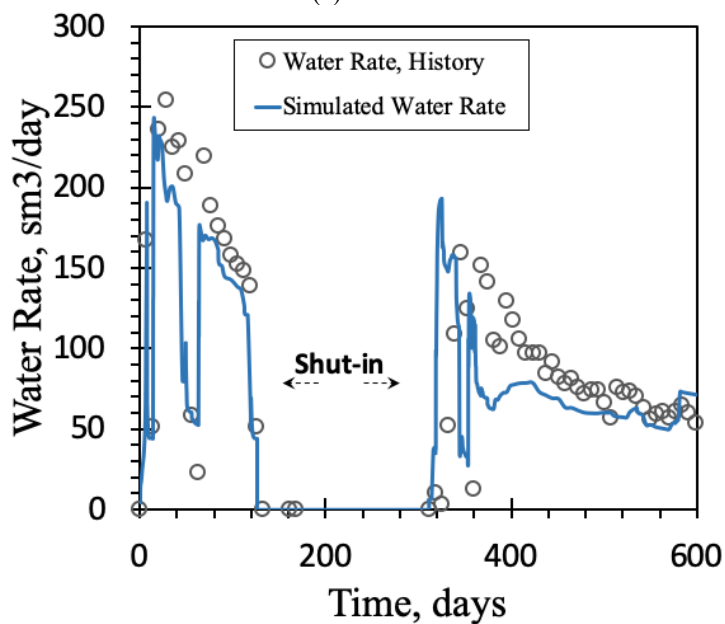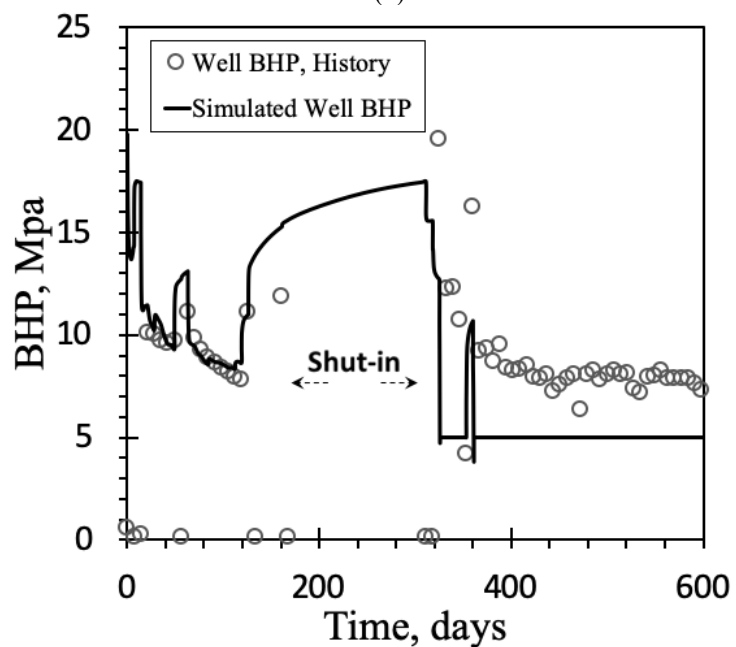
Figure 5-5- Steps 2 and 3 simulation results of history matching the well's field data, for: (a) oil production rate, (b) gas production rate, (c) water production rate, and (d) well bottom-hole pressure.
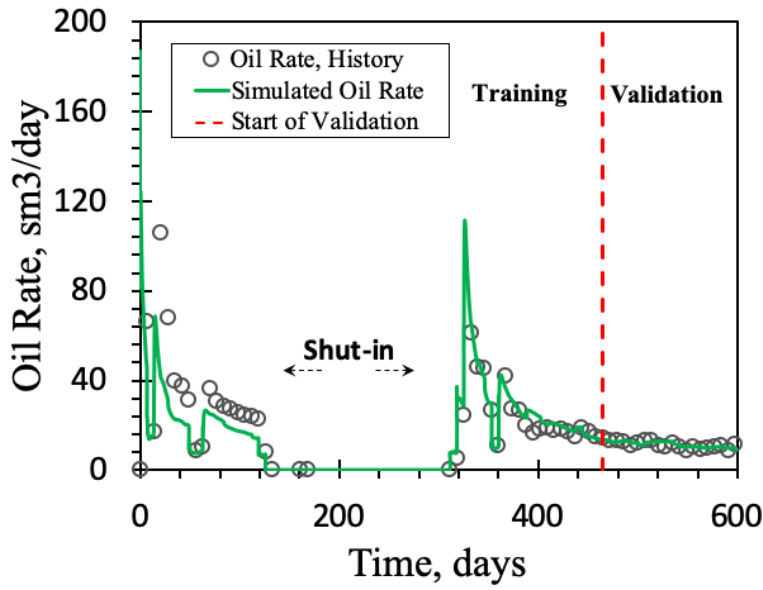
(a)
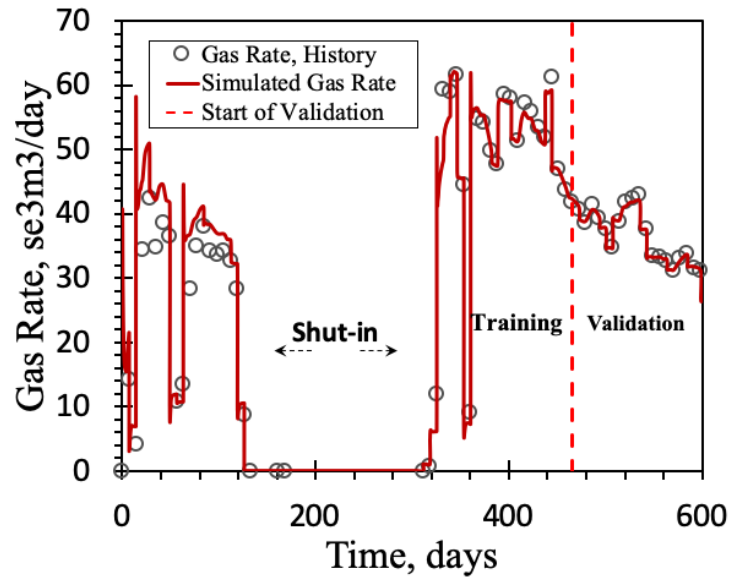
(b)
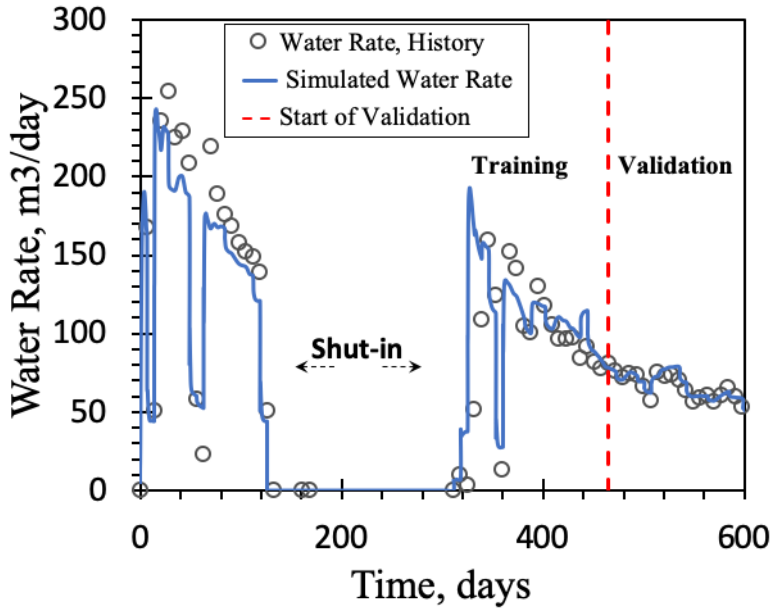
(c)
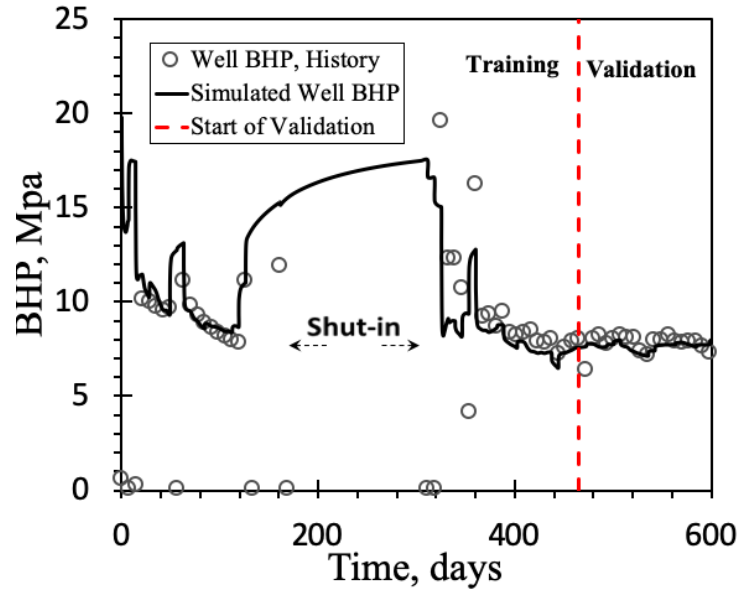
(d)

Figure 5-6- Step 4 simulation results of history matching the well's field data, using transmissibility multipliers obtained from Model C, where 0.4 is the transmissibility multiplier before shut-in and increases to 2.5 for after the shut-in, It shows: (a) oil production rate, (b) gas production rate, (c) water production rate, and (d) well bottom-hole pressure.

5.5 Determining the Optimum Shut-in Time

Here, the objective is to develop an algorithm to determine the optimum shut-in time from the simulation model and field data. We assume that the optimum shut-in time gives the maximum cumulative hydrocarbon production and Net Present Value (NPV). The challenge is that determining the TM after each shut-in period requires history matching field data with similar shut-in (which is unavailable). To solve this problem, we initially need to find a relationship between the well behavior during the shut-in and TM. In the optimum history matched model, we observed that during the shut-in, the average S_w decreases in the fractures with time. This S_w reduction corresponds to enhancement of the hydrocarbon relative permeability in the fractures. Moreover, according to Eq.5-1, the relative permeability is proportional to the transmissibility, thus reduction of S_w leads to improvement in the transmissibility of the fractures. Therefore, since the S_w declines linearly along the shut-in time as illustrated in **Fig.5.7a,** we assume the TM will increase similarly. To determine the TM values after the shut-in for different soaking time scenarios, we use linear interpolation as shown in **Fig.5.7b**

We run 5 different scenarios (0, 2, 4, 8 and 10 months of shut-in), to determine the optimum shut-in time for this well. The determined objective functions for each scenario are cumulative hydrocarbon production and NPV. However, to determine NPV for each shut-in scenario, we assume 10% yearly discount rate, oil price of 70$/bbl and 0.10$/m^3 for gas.
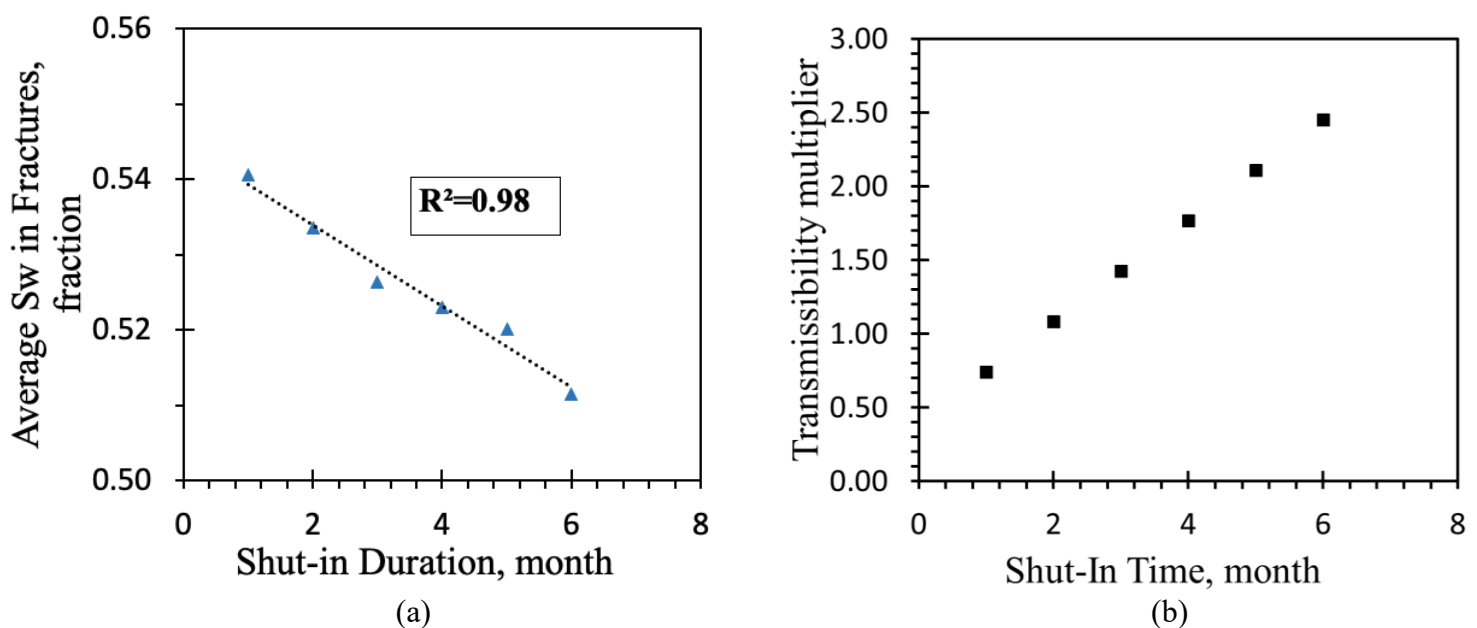
Figure 5-7- Assumption for sensitivity analysis: (a) Average water saturation in the fractures, obtained from model C, decreases linearly overtime during the well shut-in (b) Calculated transmissibility multiplier for each shut-in period, increases linearly as the average water saturation.

5.5.1 Sensitivity Analysis for Finding the Optimum Shutting Time

Fig.5.8 shows the simulation results for different well shut-in scenarios. Each figure contains an inset showing the final data value from each shut-in scenario, to illustrate the cumulative effect of extended shut-in. **Fig.5.8a** demonstrates that extending the shut-in time increases oil production until it plateaus when the well is closed between 6-8 months. However, well shut-in more than 8 months, results in reduction of the cumulative oil production. **Fig.5.8b** explains that closing the well for 2 months will result in lower cumulative gas production compared to the case without a shut-in. However, extending the shut-in time for 4 months will increase the cumulative gas production to higher rates than the no shut-in and the 2 months scenario. Nevertheless, extending the soaking time over 4 months, will bring the cumulative gas production to values even lower than the case without the shut-in. Since the optimum shut-in time varies in the cumulative produced oil and gas cases, we use the NPV obtained from the oil and gas selling prices, as the key function to assign the best shut-in scenario. **Fig.5.8c** shows that NPV gradually increases as soaking time is extended. The optimum shut-in scenario to obtain the highest NPV is determined as 6 months. Extending the shut-in for 8 months will reduce the NPV to a value equal to that obtained from the 4 months of shut-in. Moreover, 10 months of shut-in leads to even lower NPV than a scenario without a shut-in.
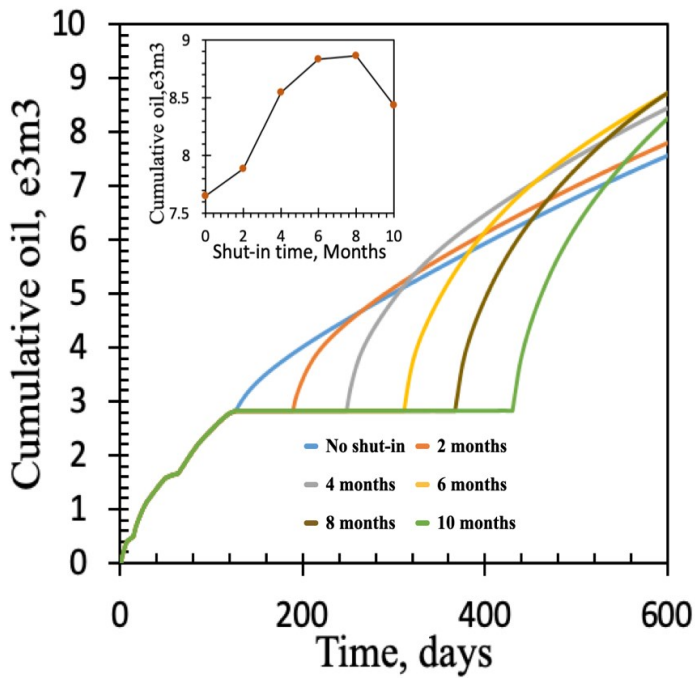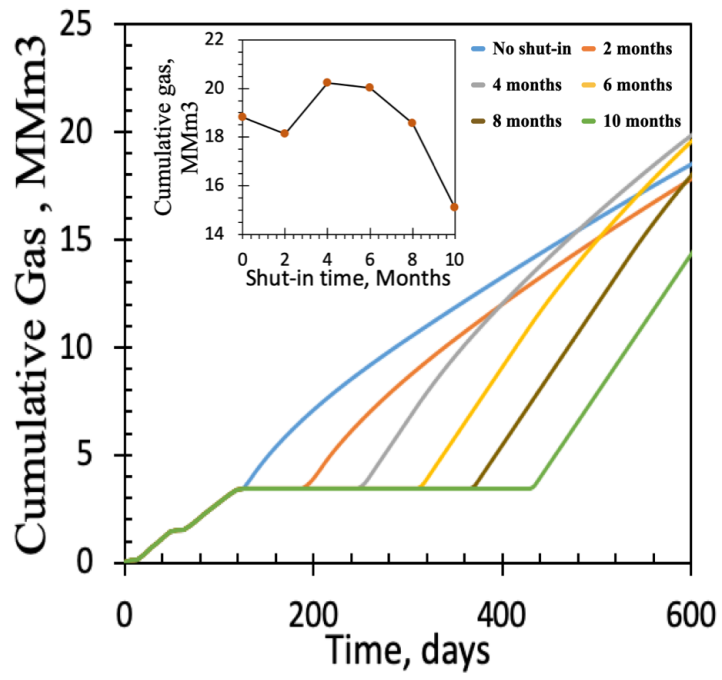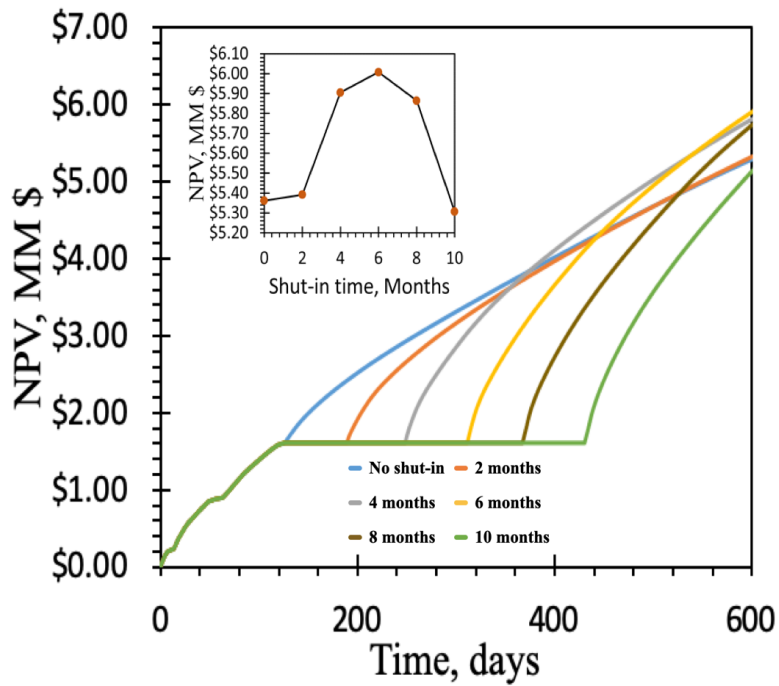
Figure 5-8- Effect of different shut-in times scenarios on: (a) cumulative oil production, (b) cumulative gas production, and (c) net present value of the net cash flow obtained from the total production in each scenario. Insets represent the final values for each corresponding plot after 600 simulation days.

Chapter 6

6) Roles of Microemulsion and Salinity in Oil-recovery: Laboratory Experiments

In this chapter, we conduct experiments to evaluate the oil counter current imbibition and effect of osmosis potential on oil recovery from oil saturated core plugs. We will run the spontaneous imbibition tests in 4 different scenarios to investigate the effects of ME solution and salinity on oil recovery. In addition, we will measure interfacial tension (IFT) and contact angle for well 1-core plugs.

6.1 Materials

6.1.1 Core properties

To conduct spontaneous imbibition oil-recovery tests, six core plugs were collected from wells 1 and 3, drilled in the Montney Formation. The depth of four core plugs from well 1 ranges from 2026 To 2073 m while that of two core plugs from well 3 ranges from 2083 to 2099 m. Table6.1 lists the physical and petrophysical properties of the core plugs collected from both wells. More details about the core plugs are presented in chapter 4.

Permeability in these core plugs changes from 1.80 to 7.32 μd. Core plug MTY 1-1 has the highest absolute permeability (7.32 μd) among all the core plugs. The significant change in permeability and porosity between core plug MTY 1-3 and MTY 1-4 , indicates high heterogeneity in the reservoir. These core plugs are mainly composed of siltstone and clay minerals.

6.2 Fluid properties

We use crude oil sample produced from well 1 in all tests. It is a light oil (36.5° API) with viscosity and surface tension of 4.97 cP and 24 mN/m, respectively at room temperature and pressure. We use synthetic brine because the produced water is a mixture of fracturing fluid and formation brine. Also, the presence of some additives in the produced reservoir water during flowback operations may effects the results. Salinity, density, viscosity and surface tension of the synthetic brine is 130,000 ppm,1.089 g/cm^3, 1.10 cP and 68 mN/m, respectively at room temperature and pressure.

6.2.1 Microemulsion properties

We use a customized complex nano-fluid (CnF) sample to conduct the experiments. To prepare the ME solution, we add the CnF product to the aqueous phase of 1cm3/L concentration. This environmental-friendly additive comprises non-ionic surfactants and solvent (citrus terpenes, 10-50 wt %). The range of specific gravity of this product is 0.904-0.964 and is thermodynamically stable. The viscosity and surface tension of the ME are 0.98 cP and 30 mN/m respectively.

Table 6-1- Petrophysical properties of wells 1 and 2 of Montney formation. . ***Permeability is from pulse decay method.**

Well	Sample ID	Depth,(m)	Diameter, (cm)	Length,(cm)	*Permeability,(µd)	Porosity, (%)	Bulk density, (g/cm³)
	MTY 1-1	2026	2.33	1.88	7.32	10.72	2.45
Well 1	MTY 1-2	2044	2.33	1.67	6.70	7.96	2.56
(Target well)	MTY 1-3	2071	2.33	1.99	1.22	11.51	2.44
	MTY 1-4	2073	2.33	1.83	3.01	6.30	2.56
Well 3	MTY 3-1	2084	3.81	6	1.80	5.10	2.57
	MTY 3-2	2100	3.81	6	3.85	6.18	2.53

6.3 Methodology

Imbibition oil-recovery tests:

As previously discussed, one of the possible reasons of the hydrocarbon enhancement after the shut-in, is the counter-current imbibition due to wettability alteration, capillary suction, and osmosis. To further investigate the effect of these factors on the imbibition oil-recovery, we considered three test scenarios. In Scenario 1, we performed the tests using four oil-saturated side-wall core plugs immersed in the tap water and the ME solution. This is to investigate if adding ME to tap water, which affects the interfacial tensions (IFT) and wettability, can enhance the spontaneous imbibition of the aqueous phase into the plugs to improve the oil recovery. In Scenario 2, we repeat the previous Scenario to compare the oil-recovery factor of the same core plugs, but this time in absence of the initial salt in the core pore network. Prior

to describing the experimental procedure for these two cases, we describe the procedure for saturating the core plugs with oil:

- Place core plugs in an oven at 60 ºC for 24 hours to dry fluids left in the core plugs before measuring the weight of the dry plugs.
- Place core plugs in a high-pressure accumulator filled with the oil and increase accumulator pressure to 3550 kPa using a pulse-free pump connected to the bottom of the accumulator.
- Soak the core plugs inside the accumulator at 3550 kPa for 24 hours.
- Measure weight change of the core plugs after 24 hours.
- Increase the applied pressure to 20785 kPa in 3550 kPa steps and measure the weight change at each step, leave the cores in the accumulator for 24 hours at each pressure step. Stop the saturating process at 20785 kPa to prevent creation of induced fractures.

Scenario 1: Investigating the effect of capillary pressure

To understand how capillary pressure affects the oil recovery factor from the oil-saturated core plugs, we immersed these plugs in the imbibition cells filled with the tap water and the ME solution prepared in tap water. This is to investigate if adding ME solution in tap water can enhance spontaneous imbibition of aqueous phase into the plugs to improve oil displacement. We used the four sidewall core plugs collected from well 1, placing them in imbibition cells filled with tap water (reference case) and ME solution prepared in tap water. We used two core plugs for the tap water and two other core plugs for the ME solution since the core plugs have small pore volumes (Table 6.2). The produced oil volume accumulated at the top of the imbibition cells due to buoyancy. This accumulation was periodically measured using a graduated tube with 0.02 cm^3 accuracy.

In the next step, to check the repeatability of the oil recovery results and to make sure that the results are independent of petrophysical properties, we repeated the imbibition tests using these core plugs. Here is the procedure for preparing the core plugs for repeating the imbibition tests as follows:

- Clean the core plugs with toluene and methanol using a Soxhlet extractor. The detailed procedure is presented elsewhere (Gant and Anderson, 1988).
- Place the core plugs in the oven at 90ºC for 48 hours to make sure there is no solvent left in the core plugs.
- Saturate them with the oil by following the saturation procedure mentioned earlier.

To perform the imbibition test, place two core plugs in the imbibition cells filled with tap water. These core plugs were immersed in the ME solution in the previous step. Place two other core plugs (immersed in the tap water in the previous step) in the ME solution.

Scenario 2: Investigating the effect of osmotic pressure

To understand how osmotic pressure affects the oil recovery factor from the core plugs, we followed a procedure to make the core plugs saturated with salts. Here is the procedure for preparing the core plugs for running the experiments in this scenario as follows:

- Clean the core plugs as mentioned in scenario 1.
- Follow the saturation procedure. Instead of oil, fill the accumulator with the high saline reservoir brine and saturate the core plugs with brine.
- Place the brine saturated core plugs in the oven at $90^{\circ}C$ for 7 days to make sure water completely evaporated and just salts left in the pore space.
- Place the salt-saturated core plugs in the accumulator filled with the oil and follow the saturation process.

Scenario 3: Investigating effect of low salinity water on oil recovery

To furthermore investigate the effect of salinity on the oil-recovery, we conduct another scenario of imbibition oil-recovery test on core plugs of another well (well2). This well is drilled into Montney Formation and it is near to the target well (well1). The reasons behind using core plugs from a different well, rather than the target well (well 1) is that, the core plugs from well 2 are larger in volume and contain larger pore volume compare to the target well core plugs, and the available SEM images of these core plugs, helps in analyzing the results. We use the two core plugs from well 2 to soak them with tap water and synthetic brine. Table 3 shows the pore volume and soaking fluid used for each core plug. We saturated the core plugs with oil only by following the same procedure in previous scenarios, and then placed each of them in a different imbibition cell filled a soaking fluids.

Table 6-2- Core plugs pore volume and soaking fluids used in scenarios 1 and 2.

Well	Sample ID	Pore volume, cm³	Soaking fluid
Well 1	MTY1-1	0.85	ME-tap water
	MTY1-2	0.56	ME-tap water
	MTY1-3	0.97	Tap water
	MTY1-4	0.49	Tap water
Well 3	MTY 3-1	3.48	Synthetic brine
	MTY 3-2	2.56	Tap water

6.4 IFT measurement

To calculate the capillary pressure, we need to measure the interfacial tension (IFT) between the aqueous and oleic phases. We measured IFT between (i) tap water and the reservoir oil sample (reference case), (ii) ME solution and the reservoir oil sample, and iii) synthetic brine and reservoir oil sample using a spinning drop tensiometer (SDT, Krüss, Germany). We used the ADVANCE ^{TM} software to analyze the shape of the oil droplet spinning in the capillary tube and to calculate the IFT value. The Vonnegut equation is used for calculating low IFT values:

$$\sigma = \frac{(\rho_1 - \rho_2)\omega^2 \mathcal{R}^3}{4} \tag{6.1}$$

where σ is interfacial tension (mN/m) , ρ_1 is density of aqueous phase (kg/m³), ρ_2 is density of oleic phase (kg/m³), ω is angular velocity (radians/s) and R is radius of the spinning oil droplet (m). IFT values were recorded every 60 seconds until constant values were reached. Each IFT measurement was repeated three times and the mean value was reported.

6.5   Contact angle measurement

To investigate how the ME additive affects the rock-fluid interactions, we performed liquid-liquid contact angle measurements using end-pieces of the core plugs, tap water, the ME solution and the oil sample. Attention Theta (Biolin Scientific) instrument was used to investigate wettability of the core plugs. This instrument has Navistar lens (1984×1264-pixel resolution, max 3009 FPS) and an LED light source. To remove dirt and mitigate the effect of surface roughness on contact angle measurements, surface of the end-pieces was polished by 440 and 600 grit sandpapers. We performed two types of liquid-liquid contact angle measurements. In type 1, we saturated the end-pieces of the core plugs with oil by immersing them in the oil for 14 days; then immersed the oil-saturated end-pieces into a cell filled with the aqueous phase (tap water or ME solution). We injected oil droplets from bottom of the sample using a J-shape needle and monitor the droplet change in presence of tap water and ME solution. In type 2, we immersed the oil-saturated end-pieces in the reservoir brine (60 cc); then injected the oil droplets from the bottom of the cell, and finally injected the ME solution (30 cc) into the cell. We monitor the oil droplet during the ME solution injection to make sure that the oil droplets did not disappear. We monitored the changed of the contact angle of the oil droplets for 48 hours. This test was repeated three times and the average values are reported.

6.6   Results and discussions

Scenario 1: Investigating the effect of capillary pressure

Fig.6.1a and b show closer looks at the surface of the oil-saturated core plugs immersed in the tap water and the ME solution prepared in the tap water after 6 hours. The oil droplets are expelled from the core plug immersed in the ME solution while no oil expulsion was observed from the core plug immersed in the tap water after 6 hours. **Fig.6.2a** shows the oil-recovery profiles for the imbibition tests performed with tap water and ME solution. The oil recovery factor for the core plugs immersed in the ME solution is almost 12% of the original oil in place after 6 hours. Then, the oil recovery factor gradually increases to 24% after 25 days of the imbibition test and remains constant. The oil recovery factor for the reference case (tap water) slowly increases and plateaus to around 2% after 3 days. Therefore, one may conclude that the imbibition potential of the ME solution is 12 times higher than that of the tap water.
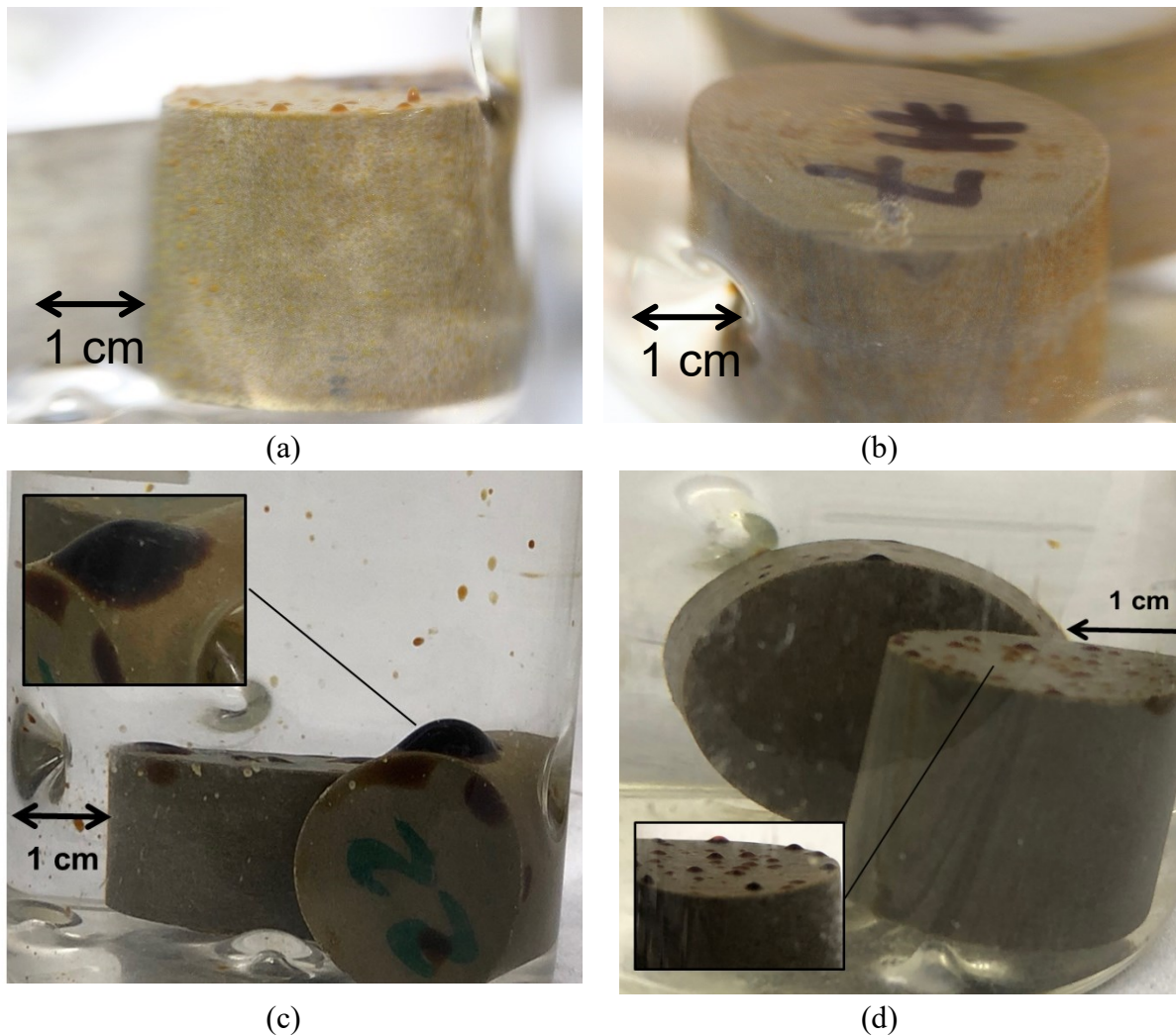
Figure 6-1- A closer look at, scenario 1 (a, core plugs immersed in the ME solution prepared in tap water , and (b) in tap water (reference case). Scenario 2, oil droplets expelled from the core plugs immersed in the (c) tap water and (b) ME solution after 20 hours. Note salt completely precipitated in the core plugs used in scenario 2.

In the next step, we placed two core plugs (were already immersed in the tap water) in the imbibition cells filled with the ME solution after cleaning and restoring the initial oil saturation conditions. Similarly, the next two core plugs (were already immersed in the ME solution) were placed in the tap water. The purpose of this step is to investigate the repeatability of the oil recovery results. There was negligible oil production in both imbibition cells after 14 days. The results of this test was the same after repeating the test twice. The main different between the first and second steps of the imbibition test was the initial conditions of the core plugs. In this step, we performed the test on as-received core plugs and did not clean them with solvents. However, in the second step, we cleaned them to make sure there is no fluid trapped or salts precipitated in the core plugs. The difference on the initial conditions of the core plugs may affect the results of imbibition oil- recovery tests. Since the crude oil used in this study is light, we do not expect to have heavy oil components precipitation on the pore walls. To investigate

66

the effect of precipitated salts on generating the osmotic pressure, we studied the second scenario for the imbibition test.

It might be possible to remove the salts precipitated in the pore space since we cleaned the core plugs in the second step of scenario 1. The salinity difference in and out of the core plugs dictates the magnitude of the osmotic pressure. When the salinity difference reduces the osmotic pressure generated in the high-saline side decreases. We hypothesize that removing salts precipitated on the pore walls results in reduction in the osmotic pressure. Therefore, we did not observe any significant oil displacement because the osmotic pressure as a driving force for the aqueous phase imbibition into the core plug reduced.

Scenario 2: Investigating the effect of osmotic pressure

Fig.6.1c and d show a closer looks at the oil droplets expelled out of the oil-saturated core plugs immersed in the tap water and the ME solution after 20 hours. The size of oil droplets expelled from the core plugs immersed in the tap water are 2.5 times larger than those expelled from the core plugs immersed in the ME solution. However, the large oil droplets in the tap water test did not detach from the outer surface of the core plugs while the oil droplets recovered from the core plugs immersed in the ME solution easily detached from the outer surface of the core plugs. This is due to the force balance acting on the oil droplets attached to the surface. If the buoyancy force dominates the interfacial tension between the solid surface and the oil sample (γso), the oil droplets can detach from the surface while if γso is dominant, oil droplets become large and attach to the surface until the buoyancy force overcomes γso. Evaluating the wetting affinity of the rock surface in presence of different fluids can be an indication of the rock-fluid interactions. We will present the CA results in next section. **Fig.6.2b** shows the oil recovery profiles for the imbibition tests performed in Scenario 2. It demonstrate that, after 300 hours of the soaking the core plugs, the oil-recovery from the core plugs immersed in the tap water reached the equilibrium with only 5% recovery of the original oil in place, while the at this time the oil-recovery from the core plugs immersed in ME solution reached 14% and was still recovering. After 40 days of the test, 34% of the original oil is recovered from the core plugs soaked with ME solution and remains constant.

Scenario 3: Investigating the effect of low-salinity water on oil recovery:

After 24 hours, the oil droplets appeared on the surface of the core plug immersed in the tap water, while no oil droplets was observed on the surface of the core plug immersed in the synthetic brine. **Fig.6.2c** shows production profile for scenario 3 spontaneous imbibition oil-

recovery. It demonstrate that, first, only 7% of the original oil in place is produced for the core plug immersed in the synthetic brine and the oil-recovery reaches the plateau after 300 hours of the test. Second, the oil recovery factor for the core plug immersed in tap water is 15% of the original oil in place after 1400 hours and reached the plateau after 300 hours of the test.

The imbibition oil-recovery results from the three scenarios show that:

(i)   Using ME solution as the soaking can enhance the oil-recovery.

(ii)   We observed no oil-recovery from the core plugs immersed in the tap water and either from the core plugs immersed in the ME solution, when we repeated the scenario 1 after cleaning the cores from the precipitated salt. In scenario 2, after saturating the cores with salt, we observed 34% and 5% of oil-recovery when the core plugs immersed in ME solution and tap water, respectively. The results indicated that, there is a strong relation between the oil recovery factor and the salinity different between the imbibing fluid and salts precipitated in the pore space.

(iii)   The ME solution prepared in tap water could imbibe into the oil-saturated core plugs with precipitated salts up to 34% of the oil in place while that could imbibe into the oil-saturated core plugs without the precipitated salts up to 24%. This suggests that the osmotic pressure can be an additional driving force for delivering the MEs into the narrow pores. Yes, more analysis is required to quantify the extent of osmotic pressure on improving oil displacement from narrow oil-saturated pores. In the next chapter we will present the quantification analysis of osmotic pressure.

(iv)   The results obtained from scenario 3 demonstrate that, oil-recovery factor is twice higher when we use low salinity fracturing fluid(tap water) compare to the high salinity fluid (synthetic brine).
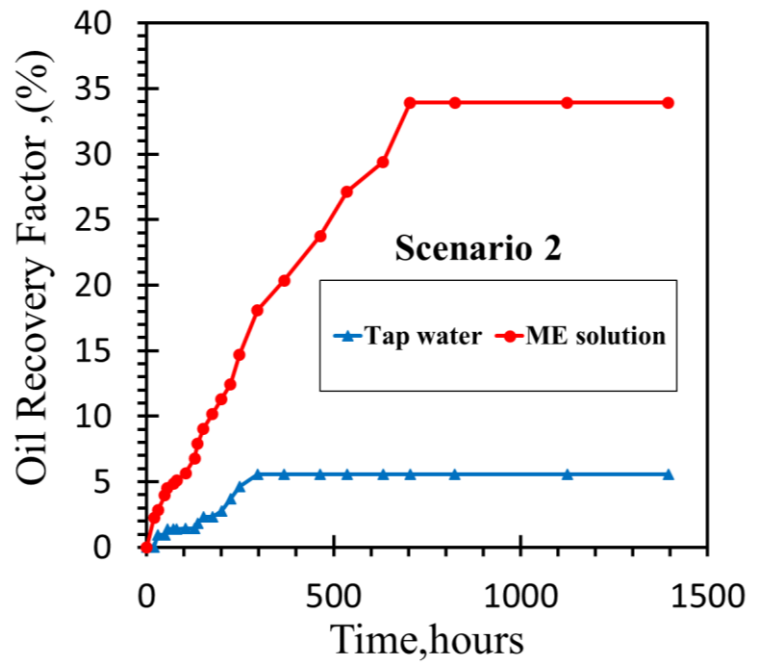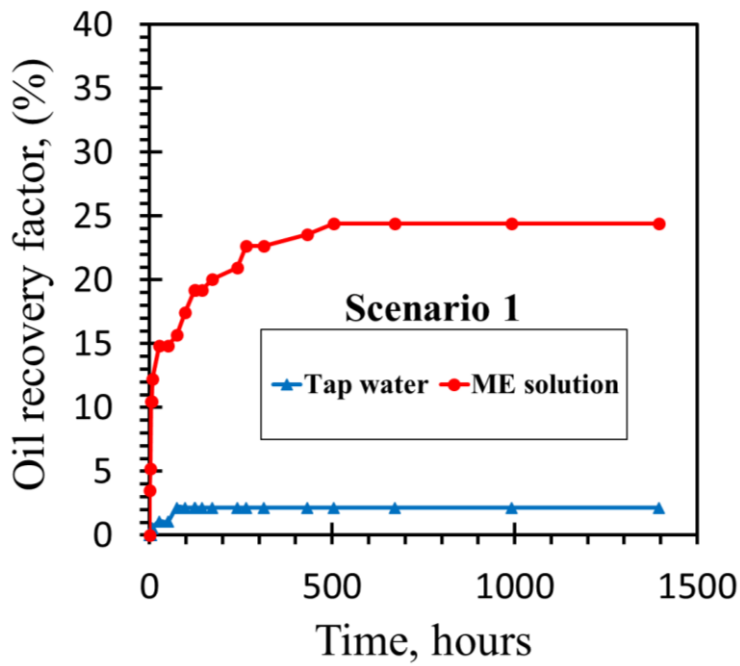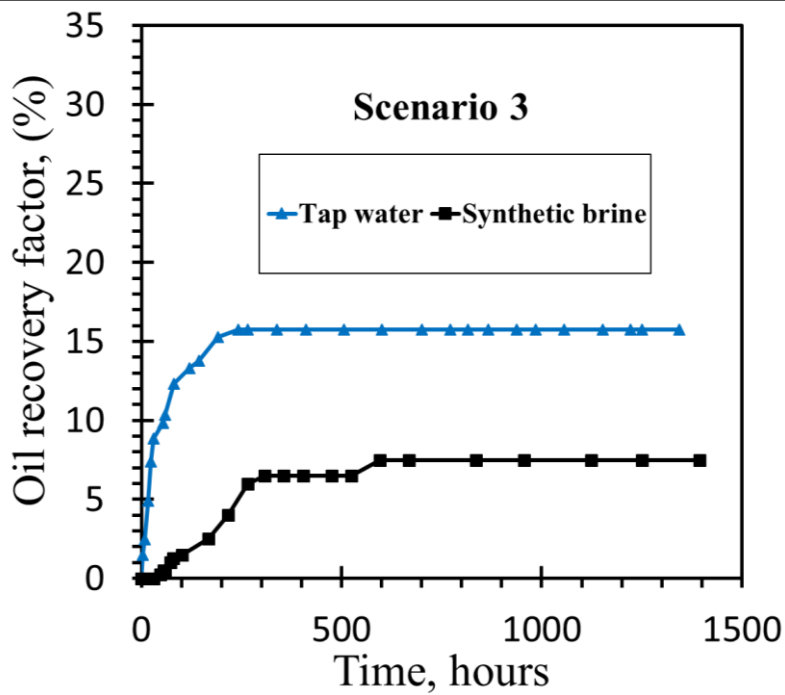
Figure 6-2- imbibition oil-recovery profiles for: (a) Scenario 1 where the oil recovery from core plugs immersed in ME solution is 12 times higher than that for the core plugs immersed in tap water. (b) Scenario 2, where 34% of the oil recovered from the core plugs immersed in the ME solution while only 5% of oil recovered from tap water. (c) Scenario 3, where 15% of the total oil in the place recovered from the core plug immersed in tap water, compare to only 7%, of oil-recovery when the core plugs immersed in synthetic brine.

6.7 IFT measurements

The equilibrium IFT values for the oil-tap water, oil-ME mixtures and oil-synthetic brine are 8.57±0.44 mN/m, 0.55±0.33 mN/m and 1.25±0.02, respectively. Although IFT value for the oil-ME mixture is 15 times less than that for the oil-tap water mixture and 7 times for the oil-synthetic brine it cannot explain the rapid imbibition of the ME solution in the core plug by capillary suction, compared with the tap water and synthetic brine. However, the IFT value for oil-ME mixture is not within the ultra-low range (IFT > 0.1 mN/m); thus, we expect sufficient capillary suction for imbibition of ME solution into the oil-saturated core plugs. Wettability is another factor controlling the capillary suction as a driving force for spontaneous imbibition. Therefore, we compare the wetting behavior of ME solution and tap water in the contact angle measurements.

6.8 Contact Angle Measurement Results

Liquid-Liquid Contact Angle Measurement Type 1:

Fig.6.3a, b and c, show equilibrated oil droplets on oil-saturated end-pieces when the aqueous phases are synthetic brine, tap water and ME solution, respectively. The equilibrated oil contact angle when the end-piece immersed in synthetic brine and tap water, is lower than that for the tap water case. The mean values of oil contact angles for synthetic brine and tap water are 46.14±1.34 and 53.98±5.25, respectively. On the other hand, the equilibrated oil contact angle in presence of ME solution is 59.71±4.20. The oil droplet shows less affinity to imbibe into the end-piece in presence of ME solution, compare to its higher affinity in presence of synthetic brine and tap water. However, the liquid-liquid result still showing an oil-wet behavior ($\theta_{oil} <$ 80) when the ME solution is the aqueous phase, and this does not explain the increased oil recovery factor during the spontaneous imbibition oil-recovery test.

Liquid-Liquid Contact Angle measurement Type 2:

Fig.6.4 shows the oil droplet contact angle changes during the type 2 contact angle experiment. At the start of the experiment, the oil contact angle showed an oil-wet behavior for the end-piece, with mean equilibrium value of 76±2.25 **(Fig.6.4a).** We started to inject the ME solution into the brine filled cell, and as **Fig.6.4b** shows, the contact angle decreased to 66.67±3.66, indicating more oil-wet behavior. **Fig 6.4c and d** show the contact angle of the oil droplet after 24 and 48 hours respectively. The figures demonstrate that, the contact angle slightly increased

to 70.82±2.81 after 24 hours, and the end-piece still shows high affinity to the oil droplet, however the end-piece affinity interestingly changed from oil-wet to significantly water-wet after 48 hours, with equilibrium value of 108.72±6.82. In total the contact angle results confirms the wettability alteration of the reservoir rock from oil-wet to water-wet, and it can explain the higher oil recovery when the chemical additives are used in the fracturing fluid, even though they reduce the IFT between the oil and the fracturing fluid.

(a)

(b)

(c)
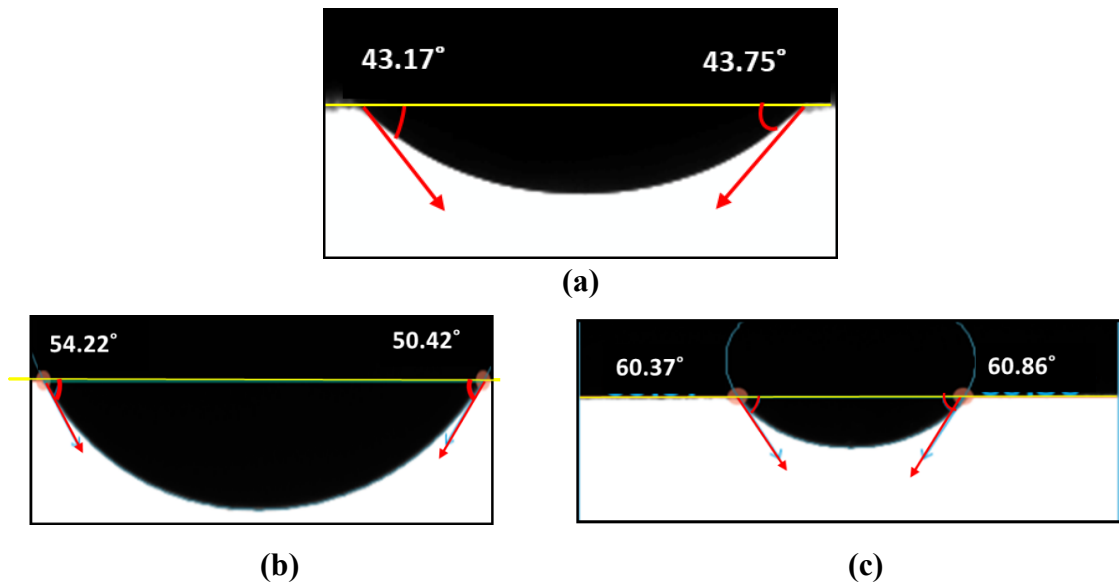
Figure 6-3- Type 1 liquid-liquid contact angle measurements of oil droplet on oil-saturated end-piece of Montney core plug immersed in (a) synthetic brine, (b) tap water, and (c) ME solution.

(a)   **(b)**

(c)   **(d)**
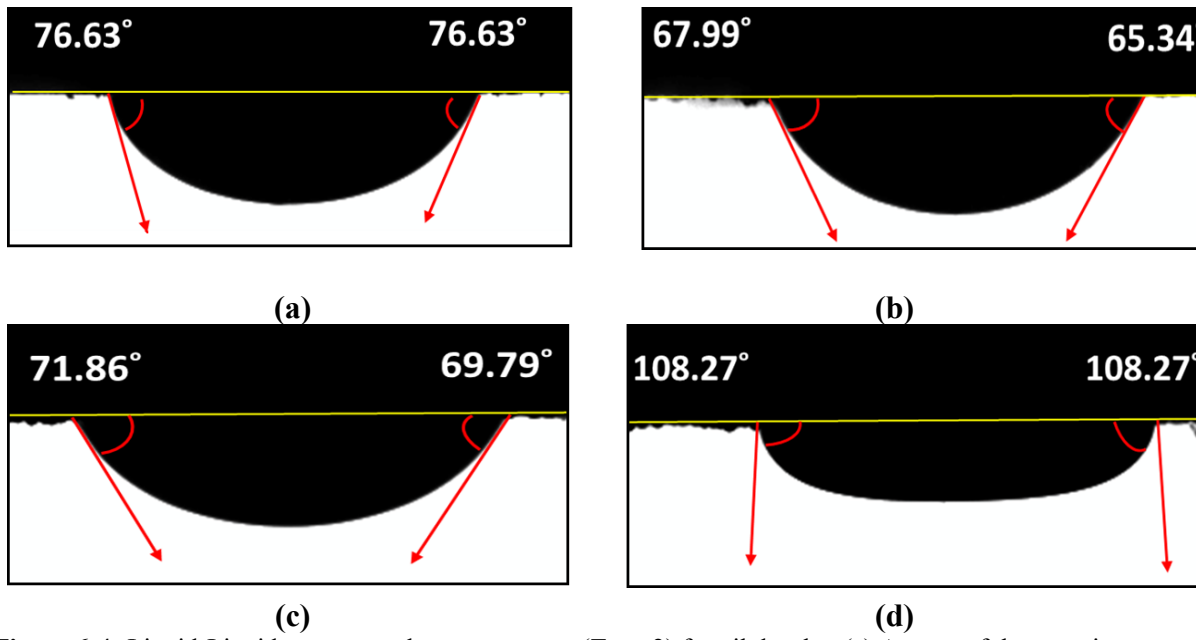
Figure 6-4- Liquid-Liquid contact angle measurement (Type 2) for oil droplet: (a) At start of the experiment where the aqueous phase is synthetic brine only. (b) 30 minutes after adding the ME solution. (c) After 24 hours of the experiment in presence of synthetic brine and ME solution as aqueous phase. (d) After 48 hours of the experiment, where the aqueous phase is synthetic brine and ME solution.

Chapter 7

7) Capillary Pressure and Osmotic Pressure as Driving Forces

In the previous chapter, the experimental results led to two important outcomes that require further discussions: i) The low IFT between ME-oil do not explain the high oil-recovery due to capillary pressure, ii) No oil-recovery observed when the salt inside the core plugs is washed. These observations indicate that, there is another driving force rather than the capillary pressure, responsible for the oil-recovery by the counter-current imbibition in the fluid-matrix interface. In tight rocks reservoirs, we find macropores and micropores with micron and nanometer ranges respectively. Most of the micropores are surrounded by clay minerals such as illite, and they contain bound water, which can be replaced only with high entry pressure. Clays act as a semipermeable membrane between the micropores and the water flowing along with salt rejection properties (Fritz. 1986, Saarenketo. 1998, Schmid et al. 2014).When different micropores separated by clays have water of different salinities flowing them, water from the lower salinity pores will flow into those with higher salinity through the clays. This phenomenon is called chemical osmosis. The driving force in chemical osmosis is the difference of chemical potential of the water on both sides of the membrane. The membrane can be ideal or non-ideal, where if only the water is allowed to move through, it is ideal membrane and when in addition to water, salt diffuses in opposite direction of the water flux, it is non-ideal membrane (Fritz. 1986, Kooi et al. 2003). **Fig.7.1** explains the mechanisms of the osmosis, where only the water moves from the low salinity side of an ideal semi-permeable membrane to the high salinity side. However, this movement of water, creates an external pressure on the higher salinity side. This pressure is defined as the osmotic pressure.

To understand the effects of capillary pressure and osmosis on the oil-recovery from the sidewall core plugs of well 1, initially we calculate the capillary pressure created by tap water and by ME solution, second we calculate the osmotic pressure resulted from the synthetic brine used in the experiments.
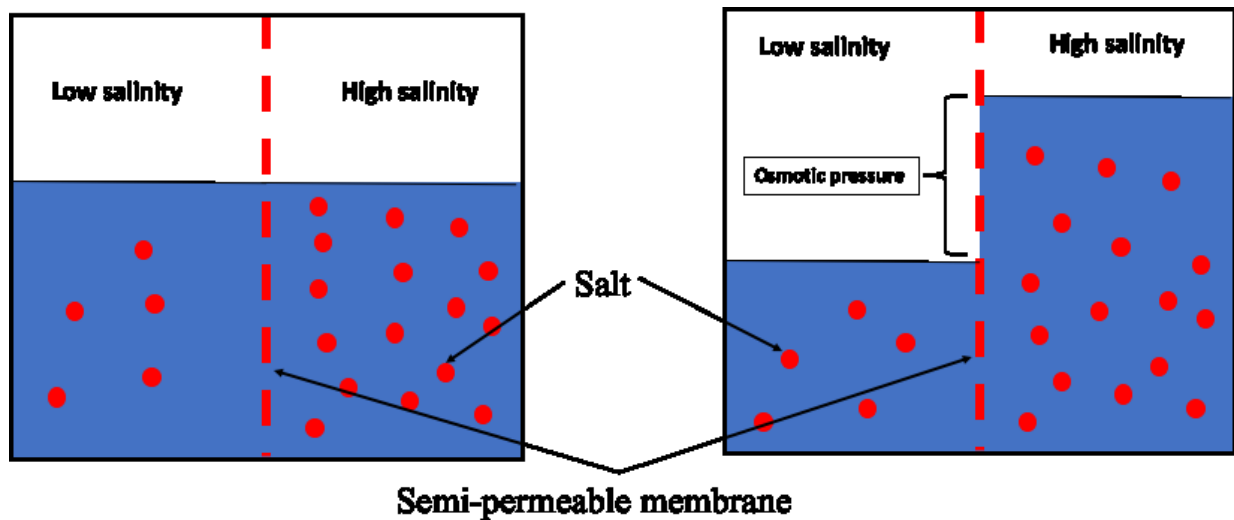
Figure 7-1-Osmosis mechanism through an ideal semi-permeable membrane. The fluid moves from the low salinity side of the membrane to the high salinity one, creating an extra force on the high salinity side. This force is called osmotic pressure

Calculation of Capillary Pressure

Here we calculate the capillary pressure for an idealized capillary tube. We assume that, the pore-throat size ranges from 1 to 250 nm in all core plugs. This assumption is made based on the pore-throat size distribution obtained from the MICP tests (Appendix D), where most of the pore-throats of these core plugs fall in this range. The IFT and contact-angle values used in capillary-pressure calculations are obtained from experimental results presented before (tap water contact angle obtained from type 1, and the ME solution from type 2 contact angle measurements). **Fig.7.2** shows the calculated capillary pressure versus pore-throat size, for tap water-oil and ME solution-oil systems. However, the results indicate that, the capillary is insufficient to be the only driving mechanism for the oil-recovery during the spontaneous imbibition of the fluids. Therefore, the quantification of osmotic pressure, which in the experimental observations is determined to be an important factor for the oil-recovery, should be analyzed to understand its contribution in the oil-recovery process.

.
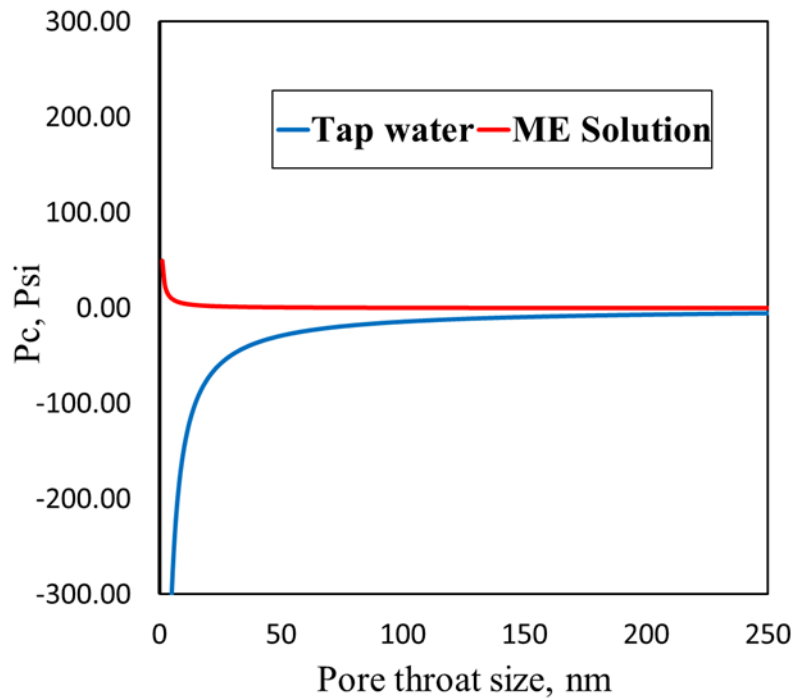
Figure 7-2- Calculated capillary pressure versus pore-throat size, for tap water-oil and ME solution-oil systems.

Calculation of Osmotic Pressure

In order to calculate the osmotic pressure during the spontaneous imbibition oil-recovery of the well 1 sidewall core plugs , we require to analyze the composition of the synthetic brine was used to saturate the core plugs in the experiments. Table 7.1 list the amount of the different salts used to prepare the synthetic brine. The total salinity of the synthetic brine is 134,688 ppm, which is equivalent to the salinity of the reservoir brine.

Table 7-1- Ions concentration in the synthetic brine

Ions	conc. (ppm)
Na	49750
K	1220
Ca	1120
Mg	596
Cl	81379
SO4	623
Total	134,688

However, to calculate the osmotic pressure we use an equation derived from the thermodynamic Gibbs energy equation (Kuhn et al.2009):

$$\Pi = -\frac{RT}{V_{m,s}} \ln a_s \tag{7.1}$$

Where Π is the osmotic pressure, R is the ideal gas constant, T is the temperature in Kelvin, $V_{m,s}$ is the molar volume of the solvent and a_s is the activity of the solvent which is obtained from:

$$a_s = x_i \cdot \gamma_i \tag{7.2}$$

Where x_i is the mole fraction of the solvent and γ_i is the solvent activity coefficient. The derivation of osmotic pressure and solvent activity is presented in Appendix 7-A. The activity coefficient for the ideal solutions is $\gamma_i = 1$, and for the real solutions is less than 1. To calculate the synthetic brine activity, we assume it as an ideal solution, and its proportional only with its mole fraction. However, we correct the final osmotic pressure value by considering a 50% of the non-ideality for the synthetic brine. Nevertheless, we analysed the change in the osmotic pressure when the brine is diluted by the factor of 10. Table 7.2 lists the obtained osmotic pressure for the different salinities, assuming temperature of 25°C.

Table 7.2- The results of osmotic pressure of the base case brine salinity and the diluted brine.

Salinity (ppm)	a_s	Π (psi)
134,688 (Base case)	0.89	1,185.82
13000	0.96	121.38
1300	0.98	12.20
130	0.99	1.22

Fig.7.3a shows the change of osmotic pressure with the salinity. It demonstrates that, the osmotic pressure increases linearly with the salinity. **Fig.7.3b** displays the solvent activity of the solvent with the corresponding salinity. It explains that, the activity is higher in the diluted solutions. **Fig.7.3.c** presents the effect of the temperature on the osmotic pressure in the base case. It explains that, osmotic pressure increases linearly with the temperature.

By comparing the osmotic pressure (1,185 psi) with the capillary pressures, one may conclude that osmotic pressure is playing a crucial role in the oil-recovery mechanism along with the capillary forces. In fact, osmosis and capillary forces are complementing each other in the spontaneous imbibition oil-recovery mechanism.
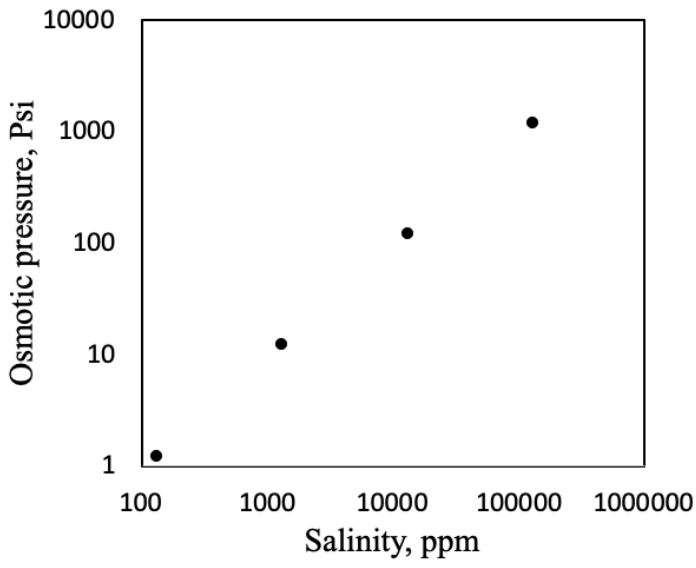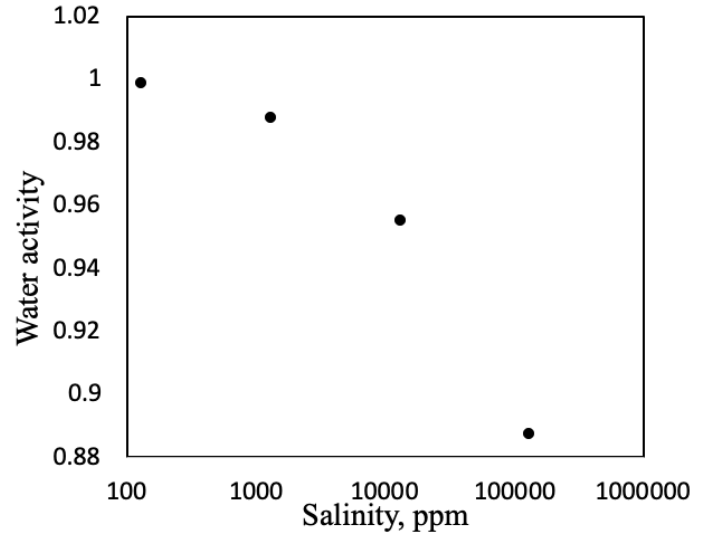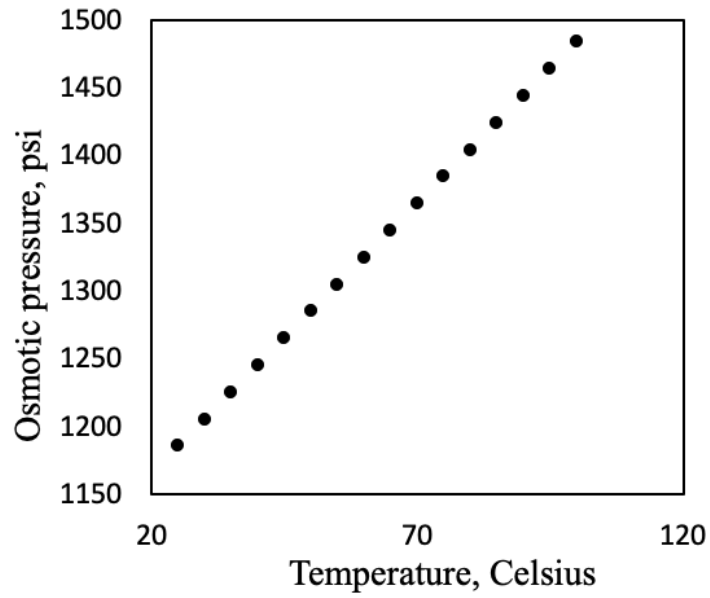
Figure 7-3- This figure shows: (a) salinity effect on the osmotic pressure, (b) water activity change with the salinity and (c) temperature effect on the osmotic pressure of the base case.

78

Appendix 7-A

The well-known Gibbs energy is defined as (Kuhn et al.2009):

$$G = H - TS \tag{7-A.1}$$

Where G is the Gibbs free energy (J), H is the enthalpy (J), T is the temperature (K) and S is entropy (J/K). By combining first and second laws of thermodynamics, Gibbs energy for a closed system can be written as:

$$dG = -SdT + Vdp \tag{7-A.2}$$

Where V is volume (m³) and P is the pressure (Pa). In an isothermal system where T is constant, the change in Gibbs energy is related to pressure and volume. Thus:

$$\Delta G = \int_{G_1}^{G_2} dG = \int_{P_1}^{P_2} VdP \tag{7-A.3}$$

The relation described in eq.3, can be used to define the Gibbs Energy for the ideal gasses:

$$\Delta G_{ideal\ gas} = \int_{P_1}^{P_2} V_{ideal} dP = \int_{P_1}^{P_2} \frac{nRT}{P} dP = nRT.\ln\frac{P_2}{P_1} \tag{7-A.4}$$

Thus, we define an ideal gas as a substance whose Gibbs Energy is given by:

$$G = G^{\ominus} + nRT.\ln\frac{P}{P^{\ominus}} \tag{7-A.5}$$

Where $G^{\ominus}$ is the Gibbs energy under standard conditions and $P^{\ominus}$ is a reference pressure. However, integration of the equ.4 for real gases is more complicated, since volume is more dependent to the pressure. To solve this problem, the *fugacity* as the partial pressure of an ideal gas, is used instead of pressure for real gasses. If we compress a gas from a pressure P_0 to a pressure P, we can write the change in Gibbs energy as:

$$G = G^{\ominus} + nRT.\ln\frac{f}{f^{\ominus}}$$

(7-A.6)

Where f is the fugacity and $f^{\ominus}$ is the *fugacity at standard state*.

The *fugacity* can be calculated by:

$$f = \emptyset.P$$

(7-A.7)

Where $\emptyset$ is the fugacity coefficient, which is a function of pressure and temperature.

For a chemical system, the partial molar change of the Gibbs energy is very important. This partial molar change in the Gibbs energy is defined as chemical potential. At constant temperature and pressure:

$$dG_{AB} = \mu_A dn_A + \mu_B dn_B$$

(7-A.8)

Where:

$$\mu_A = \left(\frac{\partial G}{\partial n_A}\right)_{T,P,n_B}, \mu_B = \left(\frac{\partial G}{\partial n_B}\right)_{T,P,n_A}$$

(7-A.9)

Are the partial molar Gibbs energy, that is chemical potential. The partial molar volume of a solution depends on the composition of the solution, n_A/n_B, not on the amount of the species. If we prepare a solution by adding n_A/n_B in small steps and fixed ratios, then the total Gibbs energy for an ideal solution is given by:

$$G_{AB} = \mu_A.n_A + \mu_B.n_B$$

(7-A.10)

Taking differential of eq.10:

$$dG_{AB} = d(n_A\,\mu_A + n_B\,\mu_B) = dn_A.\,\mu_A + d\mu_A.\,n_A + dn_B.\,\mu_B + d\mu_B.\,n_B$$

(7-A.11)

Combining eq. 8 and 11:

$$n_A\,d\mu_A + n_B\,d\mu_B = 0$$

(7-A.12)

The relation described in eq.11 is called Gibbs-Duhem equation. The Gibbs-Duhem equation can be used for arbitrary number of components. In general it described as:

$$\sum_i n_i \, d\mu_i = 0 \qquad \text{(7-A.13)}$$

Where n_i is the amount of component i and μ_i is the chemical potential of component i. Since:

$$\mu = \left(\frac{\partial G}{\partial n}\right) \qquad \text{(7-A.14)}$$

Eq.2 can be written as:

$$d\mu = -SdT + Vdp \qquad \text{(7-A.15)}$$

Also for ideally diluted solution, we use the ideal gas equation describe in eq.5.Knowing that, the chemical potential is identical with the molar Gibbs energy, the following equation can be obtained:

$$\mu = \left(\frac{\partial G}{\partial n}\right)_{T,P} = \frac{G}{n} = G^{\ominus}{}_m + RT.\ln\frac{P}{P^{\ominus}} \qquad \text{(7-A.16)}$$

Thus, for Ideally diluted solution we find that:

$$\mu = \mu^{\ominus} + RT.\ln\frac{P}{P^{\ominus}} \qquad \text{(7-A.17)}$$

With $\mu^{\ominus} = G^{\ominus}{}_m$

Where $G^{\ominus}{}_m$ is the partial molar Gibbs energy at standard pressure, and $\mu^{\ominus}$ is the chemical potential at standard pressure.

For the real solutions, similarly to real gas equation, we define *fugacity* to have the same relationship to chemical potential as the partial pressure of an ideal gas:

$$\mu = \mu^{\ominus} + RT.\ln \frac{f_i}{f^{\ominus}{}_i}$$

(7-A.18)

Assume the *fugacity* of pure species i is the same as its fugacity in a mixture in an ideal solution, Thus:

$$f_i = x_i f^{\ominus}{}_i$$

(7-A.19)

In the solutions we use the term activity, as an alternative of fugacity, rewriting eq.18 :

$$\mu = \mu^{\ominus} + RT.\ln a$$

(7-A.20)

Defining a as:

$$a = x.\gamma$$

(7-A.21)

a is the activity of the solvent, x is the molar fraction of the solvent and γ is the activity coefficient, where In the case of an ideal solution, the γ=1

Osmotic pressure

Consider a pure solvent under the standard pressure $P^{\ominus}$, and its in equilibrium with a solvent in a solution under a pressure $P^{\ominus}+ P^*$, where P^* is the osmotic pressure (Π). At equilibrium:

$$\mu_{s,pure} = \mu_{s,solution} \tag{7-A.22}$$

The chemical potential in both solution described as:

$$\mu_{s,pure} = \mu_{s,pure}^{\ominus} \tag{7-A.23}$$

$$\mu_{s,solution} = \mu_{s,solution}^{*} + RT \ln a_s$$

Where the superscript * is used for a solvent in the solution which is under a different pressure. Then, from equ.1 and 2 we have:

$$\mu_{s,pure}^{\ominus} - \mu_{s,solution}^{*} = RT \ln a_s \tag{7-A.24}$$

The difference in the chemical potentials condition can be written as:

$$\mu_{s,pure}^{\ominus} - - \mu_{s,solution}^{*} = \int_{P^{\ominus}+\Pi}^{P^{\ominus}} \left(\frac{\partial \mu_{s,pure}^{\ominus}}{\partial P} \right)_T dP = \int_{P^{\ominus}+\Pi}^{P^{\ominus}} V_{m,s}^{\ominus} dP \tag{7-A.25}$$

Where $V_{m,s}^{\ominus}$ is the molar volume of the solution under the standard state. However, if we assume the liquid in the solution as incompressible fluid, then: $V_{m,s}^{\ominus} = V_{m,s}$, thus:

$$\int_{P^{\ominus}+\Pi}^{P^{\ominus}} V_{m,s}^{\ominus} dP = V_{ms} \left(P^{\ominus} - P^{\ominus} - \Pi \right) = - V_{ms} . \Pi \tag{7-A.26}$$

Combining eq.5 and eq. 3 :

$$- V_{ms} \cdot \Pi = RT \ln a_s \qquad \text{(7-A.27)}$$

And by rearranging eq.6:

$$\Pi = -\frac{RT}{V_{ms}} \ln a_s \qquad \text{(7-A.28)}$$

Which is the osmotic pressure equation for the real solutions.

Chapter 8

8) Conclusions and Recommendations

8.1 Overview

The objective of this study is to investigate how shutting a horizontal well completed in the Montney Formation and fractured using water containing a ME additive, affects hydrocarbon production. To evaluate the

- Initially in <u>Chapter 3</u>, we presented the production data of the well, before and after the shut-in. Field data show significant increased production rates of oil and gas rates after the shut-in period. The decline curve analysis conducted on the production data of the well shows that, after the shut-in period, the decline rate of oil and gas decrease, suggesting a rise in the cumulative oil and gas production rate. The production changes after the shut-in can be due to several possible reasons including pressure buildup, water blockage reduction near the fracture face, and counter-current imbibition due to capillarity and osmotic pressure. But before investigating these hypothesis, first we need to analyze the reservoir rock.

- In Chapter 4, we analyzed the petrophysical properties of the target well, along with two other adjacent wells. The logs of the wells indicate presence of the silt-stone in the reservoir rock and higher chances of extracting hydrocarbon in the depths between 2040-2100 m. However, permeability and porosity measurements of the core plugs shows that, the reservoir permeability is ultra-low with average of 3.29 μd. Nevertheless, the XR-D results showed that, the reservoir is very heterogeneous, and the reservoir rock contains high amount of clays, which can play an important role in the rock-fluid interactions. At the end, the MICP measurements of the core plugs showed that, most of the pores in are nanopores, and the almost all the core plugs have a uniform sorted grains.

- We simulated the production data before and after an extended shut-in period of the well, to investigate the changes in it during the shut-in time in Chapter 5. We were able to match the production data by changing the transmissibility multiplier for the fractures

interblocks. This change mimics phase trapping in the model and simulates the reduction in hydrocarbon relative permeability due to water blockage. Reducing the transmissibility value leads to a good match before the shut-in. However, applying the same transmissibility value for after the shut-in results in a poor match in this period, indicating a general improvement in oil and gas mobilities during the shut-in period. The best history match before and after the shut-in periods is obtained when the transmissibility multiplier before shut-in is increased 6.5 times after the shut-in. This suggests enhancement in oil and gas relative permeabilities due to water saturation reduction around the fractures during the shut-in. At the end, the sensitivity analysis results suggest that 6 months of shut-in is optimal for maximizing hydrocarbon production and economic profit for this well. However, closing the well for over 6 months negatively affects its performance and NPV.

- We conduct experiments to evaluate the oil counter current imbibition and effect of osmosis potential on oil recovery from oil saturated core plugs, in Chapter 6. Spontaneous imbibition scenario 1, conducted on the target well show 24% oil-recovery factor with water containing microemulsion as the soaking fluid, compared with 2% oil-recovery factor with tap water, indicating enhancement in spontaneous imbibition and reduction of water blockage near fracture face. However, reversing scenario 1 of the spontaneous imbibition oil- recovery test resulted in no oil recovery from both tap water and microemulsion solution, suggesting that cleaning the core plugs while preparing them to reuse, lead to reduce the salinity in the core plugs pores. Saturating the cores with the synthetic brine and drying them before saturating them with reservoir oil for spontaneous imbibition oil recovery (scenario 2) leads to 35% oil-recovery factor using microemulsion-water mixture as soaking fluid. This is higher than the 5% oil-recovery factor from using tap water as soaking fluid. It confirms i) the initial results obtained from scenario 1, and ii) osmotic pressure play important role in the counter-current imbibition.

- In Chapter 7, we calculated the capillary and osmotic pressures of the core plugs used in the experiment, to determine the contribution of both forces in the spontaneous imbibition oil-recovery mechanism. The results demonstrate that, osmotic pressure is playing a crucial role in the oil-recovery mechanism and can be as high as 1,185.82 psi during the spontaneous imbibition mechanism.

8.2 Key Findings:

The key findings in this research can be summarized as:

- Extending the well shut-in time plays an important role on reducing the water saturation around the fractures, due to the further spontaneous imbibition of the water from the fracture into the matrix.
- Contact angle measurements in reservoir condition method, is a better and more reliable representative of the wettability alteration in the liquid-liquid measurement.

- The simulation and laboratory experiments are consisted with each other, suggesting enhancement of oil-recovery due to the extended shut-in time and using ME additives.

- osmosis and capillary forces are complementing each other in the spontaneous imbibition oil-recovery mechanism, in a way that without salinity in the rock matrix, there would be no oil recovery by capillary imbibition.

- Combined analysis from field data, simulation results and laboratory experiment suggest that, using ME in the fracturing fluid, reduces the IFT between oil and the fracturing fluid, alters the rock wettability from oil-wet to water-wet, which helps to reduce the water blockage near the fracture face and capillary suction of the fracturing fluid. However, osmotic pressure is a crucial driving force for the improved oil-recovery by counter-current imbibition.

8.3   Recommendations

To better understanding the rock-fluid interaction in the future studies, it is recommended:

- To Conduct the spontaneous imbibition oil-recovery test under the reservoir condition. This is can be done by designing an Amott-cell which can be under high pressure and temperature. This will give more accurate results by simulating the real reservoir conditions.

- The osmotic pressure needs more studies to understand its important role in oil-recovery mechanism. This is can be done by modeling different reservoir simulations, considering the osmotic pressure as an important driving force and going into the details of the ions and solvent interaction, in the reservoir.

- The liquid-liquid contact angle measurements do not mimic the real reservoir condition. The current method can be modified by designing a cell which allows the interactions between the reservoir-fluids and the reservoir-rock for sufficient time, before starting adding the injected fluid.

Bibliography

Alotaibi, M. B., Nasralla, R. A., & Nasr-El-Din, H. A. (2011). Wettability studies using low-salinity water in sandstone reservoirs. SPE Reservoir Evaluation & Engineering, 14(06), 713-725.

Al-Shammasi, A. A. (1999, January 1). Bubble Point Pressure and Oil Formation Volume Factor Correlations. Society of Petroleum Engineers. doi:10.2118/53185-MS

Alvarez, J. O., & Schechter, D. S. (2017, February 1). Wettability Alteration and Spontaneous Imbibition in Unconventional Liquid Reservoirs by Surfactant Additives. Society of Petroleum Engineers. doi:10.2118/177057-PA

Amaefule, J. O., & Handy, L. L. (1982, June 1). The Effect of Interfacial Tensions on Relative Oil/Water Permeabilities of Consolidated Porous Media. Society of Petroleum Engineers. doi:10.2118/9783-PA

Anderson, W. G. (1986, October 1). Wettability Literature Survey- Part 1: Rock/Oil/Brine Interactions and the Effects of Core Handling on Wettability. Society of Petroleum Engineers. doi:10.2118/13932-PA

Austad, T., & Milter, J. (1997, January). Spontaneous imbibition of water into low permeable chalk at different wettabilities using surfactants. In International Symposium on Oilfield Chemistry. Society of Petroleum Engineers.

Austad, T., Rezaeidoust, A., & Puntervold, T. (2010, January 1). Chemical Mechanism of Low Salinity Water Flooding in Sandstone Reservoirs. Society of Petroleum Engineers. doi:10.2118/129767-MS

Ausbrooks, R., Hurley, N. F., May, A., & Neese, D. G. (1999, January). Pore-size distributions in vuggy carbonates from core images, NMR, and capillary pressure. In SPE annual technical conference and exhibition. Society of Petroleum Engineers.

Austad, T., & Milter, J. (1997, January 1). Spontaneous Imbibition of Water Into Low Permeable Chalk at Different Wettabilities Using Surfactants. Society of Petroleum Engineers. doi:10.2118/37236-MS

Ayirala, S. C., Vijapurapu, C. S., & Rao, D. N. (2006). Beneficial effects of wettability altering surfactants in oil-wet fractured reservoirs. Journal of petroleum science and engineering, 52(1-4), 261-274.

Bahadori, A. (2016). Fluid phase behavior for conventional and unconventional oil and gas reservoirs. Gulf Professional Publishing.

Bahrami, H., Rezaee, R., & Clennell, B. (2012). Water blocking damage in hydraulically fractured tight sand gas reservoirs: An example from Perth Basin, Western Australia. Journal of Petroleum Science and Engineering, 88, 100-106.

Bang, V. S. S., Yuan, C., Pope, G. A., Sharma, M. M., Baran, J. R., Skildum, J., & Linnemeyer, H. C. (2008, January 1). Improving Productivity of Hydraulically Fractured Gas Condensate Wells by Chemical Treatment. Offshore Technology Conference. doi:10.4043/19599-MS.

Beggs DHU, Brill JPU (1973) A study of two-phase flow in inclined pipes. J Pet Technol 25:607–617

Bennion, D. B., Thomas, F. B., &Bietz, R. F. (1996, January). Low permeability gas reservoirs: problems, opportunities and solutions for drilling, completion, stimulation and production. In SPE Gas Technology Symposium. Society of Petroleum Engineers.

Bennion, D. B., Thomas, F. B., Bietz, R. F., & Bennion, D. W. (1999, August 1). Remediation of Water And Hydrocarbon Phase Trapping Problems In Low Permeability Gas Reservoirs. Petroleum Society of Canada. doi:10.2118/99-08-01.

Bera, A., & Mandal, A. (2015). Microemulsions: a novel approach to enhanced oil recovery: a review. Journal of Petroleum Exploration and Production Technology, 5(3), 255-268.

Bertoncello, A., Wallace, J., Blyton, C., Honarpour, M., & Kabir, C. S. (2014, February). Imbibition and water blockage in unconventional reservoirs: well management implications during flowback and early production. In SPE/EAGE European Unconventional Resources Conference and Exhibition (Vol. 2014, No. 1, pp. cp-399). European Association of Geoscientists & Engineers.

Binazadeh, M., Xu, M., Zolfaghari, A., & Dehghanpour, H. (2016). Effect of electrostatic interactions on water uptake of gas shales: the interplay of solution ionic strength and electrostatic double layer. Energy & Fuels, 30(2), 992-1001.

Brodie, J., & Jerauld, G. (2014, April 12). Impact of Salt Diffusion on Low-Salinity Enhanced Oil Recovery. Society of Petroleum Engineers. doi:10.2118/169097-MS

Burden, S., Fleming, M. M., Frithsen, J., Hills, L., Klewicki, K., & Knightes, C. D. (2016). Hydraulic fracturing for oil and gas: Impacts from the hydraulic fracturing water cycle on drinking water resources in the United States. Washington, DC: US EPA.

Cai, J., Hu, X., Standnes, D. C., & You, L. (2012). An analytical model for spontaneous imbibition in fractal porous media including gravity. Colloids and Surfaces A: Physicochemical and Engineering Aspects, 414, 228-233.

Cath, T. Y., Childress, A. E., & Elimelech, M. (2006). Forward osmosis: principles, applications, and recent developments. Journal of membrane science, 281(1-2), 70-87.

Chen, Z. (2007). Reservoir simulation: mathematical techniques in oil recovery (Vol. 77). Siam.

Chen, P., & Mohanty, K. K. (2015, April 13). Surfactant-Enhanced Oil Recovery from Fractured Oil-wet Carbonates: Effects of Low IFT and Wettability Alteration. Society of Petroleum Engineers. doi:10.2118/173797-MS.

Chevalier, T., Labaume, J., Gautier, S., Chevallier, E., & Chabert, M. (2018, April). A novel experimental approach for accurate evaluation of chemical EOR processes in tight reservoir rocks. In SPE Improved Oil Recovery Conference. Society of Petroleum Engineers.

Clark, N. J. (1969). Elements of petroleum reservoirs. Society of Petroleum Engineers of AIME.

Clark, A. J. (2009, January). Determination of recovery factor in the Bakken formation, Mountrail County, ND. In SPE Annual Technical Conference and Exhibition. Society of Petroleum Engineers.

Clarkson, C. R., & Pedersen, P. K. (2011, January 1). Production Analysis of Western Canadian Unconventional Light Oil Plays. Society of Petroleum Engineers. doi:10.2118/149005-MS.

Dehghanpour, H., Lan, Q., Saeed, Y., Fei, H., & Qi, Z. (2013). Spontaneous imbibition of brine and oil in gas shales: Effect of water adsorption and resulting microfractures. Energy & Fuels, 27(6), 3039-3049.

Dehghanpour, H., Lan, Q., Saeed, Y., Fei, H., & Qi, Z. (2013). Spontaneous imbibition of brine and oil in gas shales: Effect of water adsorption and resulting microfractures. Energy & Fuels, 27(6), 3039-3049.

Dehghanpour, H., Zubair, H. A., Chhabra, A., & Ullah, A. (2012). Liquid intake of organic shales. Energy & Fuels, 26(9), 5750-5758.

Desai, S. A New Sustainability Challenge: Water Management in Unconventional Shale Oil & Gas Operations.

Druetta, P., Raffa, P., & Picchioni, F. (2019). Chemical enhanced oil recovery and the role of chemical product design. Applied Energy, 252, 113480.

Ertekin, T., Abou-Kassem, J. H., & King, G. R. (2001). Basic applied reservoir simulation (No. Sirsi) i9781555630898) chapters 5 and 9.

Ezulike, D. O., and Dehghanpour, H. 2015. A Complementary Approach for Uncertainty Reduction in Post-Flowback Production Data Analysis. Journal of Natural Gas Science and Engineering, 27, Part 2, 1074-1091, ISSN 1875-5100, https://doi.org/10.1016/j.jngse.2015.09.059.

Fakcharoenphol, P., Torcuk, M. A., Wallace, J., Bertoncello, A., Kazemi, H., Wu, Y. S., & Honarpour, M. (2013, September). Managing shut-in time to enhance gas flow rate in hydraulic fractured shale reservoirs: a simulation study. In SPE Annual Technical Conference and Exhibition. Society of Petroleum Engineers.

Fakcharoenphol, P., Kurtoglu, B., Kazemi, H., Charoenwongsa, S., & Wu, Y. S. (2014, April). The effect of osmotic pressure on improve oil recovery from fractured shale formations. In SPE unconventional resources conference. Society of Petroleum Engineers.

Fakcharoenphol, P., Kurtoglu, B., Kazemi, H., Charoenwongsa, S., & Wu, Y.-S. (2014, April 1). The Effect of Osmotic Pressure on Improve Oil Recovery from Fractured Shale Formations. Society of Petroleum Engineers. doi:10.2118/168998-MS

Franz, Jr., J.H. and Jochen, V. (2005). When your Gas Reservoir is Unconventional, SO IS OUR Solution, Shale Gas White Paper. Schlumberger, Houston, TX.

Fritz, S. J. (1986). Ideality of clay membranes in osmotic processes: a review. Clays and clay minerals, 34(2), 214-223.

Galas, C., Clements, A., Jaafar, E., Jeje, O., Holst, D., & Holst, R. (2012). Identification of Enhanced Oil Recovery Potential in Alberta, Phase 2 Final Report. Prepared for Energy Resources Conservation Board by Sproule Associates Limited, Calgary.

Gandossi, Luca. "An overview of hydraulic fracturing and other formation stimulation technologies for shale gas production." Eur. Commisison Jt. Res. Cent. Tech. Reports 26347 (2013).

Gant, P. L., & Anderson, W. G. (1988, March 1). Core Cleaning for Restoration of Native Wettability. Society of Petroleum Engineers. doi:10.2118/14875-PA

Gdanski, R. D., Fulton, D. D., & Shen, C. (2006, January). Fracture face skin evolution during cleanup. In SPE Annual Technical Conference and Exhibition. Society of Petroleum Engineers.

Ghanbari, E., & Dehghanpour, H. (2016). The fate of fracturing water: A field and simulation study. Fuel, 163, 282-294.

Ghandi, E., Parsaei, R., & Riazi, M. (2019). Enhancing the spontaneous imbibition rate of water in oil-wet dolomite rocks through boosting a wettability alteration process using carbonated smart brines. Petroleum Science, 1-13.

Golabi, E., SEYEDIN, A. F., & AYAT, E. S. (2009). Chemical induced wettability alteration of carbonate reservoir rocks.

Guo, B., & Ghalambor, A. (2005). Natural gas engineering handbook vol. 22.

Habibi, A., Binazadeh, M., Dehghanpour, H., Bryan, D., & Uswak, G. (2015, September). Advances in understanding wettability of tight oil formations. In SPE Annual Technical Conference and Exhibition. Society of Petroleum Engineers.

Habibi, A., Dehghanpour, H., Binazadeh, M., Bryan, D., & Uswak, G. (2016, October 1). Advances in Understanding Wettability of Tight Oil Formations: A Montney Case Study. Society of Petroleum Engineers. doi:10.2118/175157-PA

He, K., Xu, L., Gao, Y., Yin, X., and Neeves, K. B. 2015. Evaluation of Surfactant Performance in Fracturing Fluids For Enhanced Well Productivity In Unconventional Reservoirs using Rock-on-a-Chip Approach. Journal of Petroleum Science and Engineering 135:531–541.

Held, P. (2014). Rapid critical micelle concentration (CMC) determination using fluorescence polarization. BioTek Application Note.

Holditch, S. A. (2003, November 1). The Increasing Role of Unconventional Reservoirs in the Future of the Oil and Gas Business. Society of Petroleum Engineers. doi:10.2118/1103-0034-JPT

Kathel, P., & Mohanty, K. K. (2013, September). EOR in tight oil reservoirs through wettability alteration. In SPE Annual Technical Conference and Exhibition. Society of Petroleum Engineers.

Kemper, W. D., & Rollins, J. B. (1966). Osmotic Efficiency Coefficients Across Compacted Clays 1. Soil Science Society of America Journal, 30(5), 529-534.

King, G. E. (2010, January). Thirty years of gas shale fracturing: What have we learned?. In SPE Annual Technical Conference and Exhibition. Society of Petroleum Engineers.

Kooi, H., Garavito, A. M., & Bader, S. (2003). Numerical modelling of chemical osmosis and ultrafiltrationacross clay formations. Journal of Geochemical Exploration, 78, 333-336.

Kuhn, H., Försterling, H. D., & Waldeck, D. H. (2009). Principles of physical chemistry. John Wiley & Sons

Knudsen, B. R., & Foss, B. (2013). Shut-in based production optimization of shale-gas systems. Computers & Chemical Engineering, 58, 54-67.

Lan, Q., Dehghanpour, H., Wood, J., & Sanei, H. (2015, August 1). Wettability of the Montney Tight Gas Formation. Society of Petroleum Engineers. doi:10.2118/171620-PA

Lan, Q., Ghanbari, E., Dehghanpour, H., & Hawkes, R. (2014, February 25). Water Loss versus Soaking Time: Spontaneous Imbibition in Tight Rocks. Society of Petroleum Engineers. doi:10.2118/167713-MS

Li*, X., Teklu, T. W., Abass, H., & Cui, Q. (2016, August). The impact of water salinity/surfactant on spontaneous imbibition through capillarity and osmosis for unconventional IOR. In Unconventional Resources Technology Conference, San Antonio, Texas, 1-3 August 2016 (pp. 3058-3076). Society of Exploration Geophysicists, American Association of Petroleum Geologists, Society of Petroleum Engineers.

Longoria, R. A., Liang, T., Nguyen, Q. P., &DiCarlo, D. A. (2015, July). When Less Flowback Is More: A Mechanism of Permeability Damage and its Implications on the Application of EOR Techniques. In Unconventional Resources Technology Conference, San Antonio, Texas, 20-22 July 2015 (pp. 1835–1843). Society of Exploration Geophysicists, American Association of Petroleum Geologists, Society of Petroleum Engineers.

Mahadevan, J., Sharma, M. M., & Yortsos, Y. C. (2007, December 1). Capillary Wicking in Gas Wells. Society of Petroleum Engineers. doi:10.2118/103229-PA.

Makhanov, K., Habibi, A., Dehghanpour, H., & Kuru, E. (2014). Liquid uptake of gas shales: A workflow to estimate water loss during shut-in periods after fracturing operations. Journal of Unconventional Oil and Gas Resources, 7, 22-32.

Malusis, M. A., Shackelford, C. D., & Olsen, H. W. (2003). Flow and transport through clay membrane barriers. Engineering Geology, 70(3-4), 235-248.

McGuire, P. L., Chatham, J. R., Paskvan, F. K., Sommer, D. M., & Carini, F. H. (2005, January). Low salinity oil recovery: An exciting new EOR opportunity for Alaska's North Slope. In SPE western regional meeting. Society of Petroleum Engineers.

McPhee, C., Reed, J., & Zubizarreta, I. (2015). Core analysis: A best practice guide (Vol. 64). Elsevier.

Milter, J., & Austad, T. (1996). Chemical flooding of oil reservoirs 6. Evaluation of the mechanism for oil expulsion by spontaneous imbibition of brine with and without surfactant in

water-wet, low-permeable, chalk material. Colloids and Surfaces A: Physicochemical and Engineering Aspects, 113(3), 269-278.

Montgomery, C. T. and M. B. Smith (2010). "Hydraulic fracturing: history of an enduring technology."
Montgomery, C. T., & Smith, M. B. (2010). Hydraulic fracturing: history of an enduring technology. Journal of Petroleum Technology, 62(12), 26-40.

Morrow, N., & Buckley, J. (2011). Improved oil recovery by low-salinity waterflooding. Journal of Petroleum Technology, 63(05), 106-112.

Morrow, N. R., & Mason, G. (2001). Recovery of oil by spontaneous imbibition. Current Opinion in Colloid & Interface Science, 6(4), 321-337.

Moussa, T. & Awotunde, A. (2018). Self-adaptive differential evolution with a novel adaptation technique and its application to optimize ES-SAGD recovery process. Computers & Chemical Engineering, 118, 64-76. Doi: 10.1016/j.compchemeng.2018.07.018

Mungan, N. (1964). Role of wettability and interfacial tension in water flooding. Society of Petroleum Engineers Journal, 4(02), 115-123.

Myers, D. (2005). Surfactant science and technology. John Wiley & Sons.

Nazar, M. F., Shah, S. S., & Khosa, M. A. (2011). Microemulsions in enhanced oil recovery: a review. Petroleum science and technology, 29(13), 1353-1365.

NEB, A., OGC, B., & MNGD, B. (2013). The Ultimate Potential for Unconventional Petroleum from the Montney Formation of British Columbia and Alberta. Energy Briefing Note.

Negin, C., Ali, S., &Xie, Q. (2016). Most common surfactants employed in chemical enhanced oil recovery. Petroleum. Penny, G. S., &Pursley, J. T. (2007, January). Field studies of drilling

and completion fluids to minimize damage and enhance gas production in unconventional reservoirs. In European Formation Damage Conference. Society of Petroleum Engineers.

Neog, A., & Schechter, D. S. (2016, April 11). Investigation of Surfactant Induced Wettability Alteration in Wolfcamp Shale for Hydraulic Fracturing and EOR Applications. Society of Petroleum Engineers. doi:10.2118/179600-MS

Nieto, J., Batlai, B., & Delbecq, F. (2013). Seismic lithology prediction: A Montney shale gas case study. CSEG Recorder, 38(2), 34-43.

Olsen, H. W., Yearsley, E. N., & Nelson, K. R. (1990). Chemico-osmosis versus diffusion-osmosis. Transportation Research Record, (1288).

Paktinat, J., Pinkhouse, J. A., Stoner, W. P., Williams, C., Carder, G. A., & Penny, G. S. (2005, January 1). Case Histories: Post-Frac Fluid Recovery Improvements of Appalachian Basin Gas Reservoirs. Society of Petroleum Engineers. doi:10.2118/97365-MS

Palisch, T. T., Vincent, M., & Handren, P. J. (2010, August 1). Slickwater Fracturing: Food for Thought. Society of Petroleum Engineers. doi:10.2118/115766-PA

Penny, G. S., Dobkins, T. A., & Pursley, J. T. (2006, January 1). Field Study of Completion Fluids To Enhance Gas Production in the Barnett Shale. Society of Petroleum Engineers. doi:10.2118/100434-MS

Peters, E. J. (2012). Advanced petrophysics: geology, porosity, absolute permeability, heterogeneity, and geostatistics (Vol. 1). Greenleaf Book Group.

Rahman, K., Gui, F., & He, W. (2014, November 10). Multistage Hydraulic Fracturing Optimization for a Shale Oil Field Integrating Geomechanics and Production Modelling. Society of Petroleum Engineers. doi:10.2118/172097-MS

Rivard, C., Lavoie, D., Lefebvre, R., Séjourné, S., Lamontagne, C., & Duchesne, M. (2014). An overview of Canadian shale gas production and environmental concerns. International Journal of Coal Geology, 126, 64-76.

Rosen, M. J., & Kunjappu, J. T. (2012). Surfactants and interfacial phenomena. John Wiley & Sons.

Rosen, Milton J., et al. "Ultralow interfacial tension for enhanced oil recovery at very low surfactant concentrations." Langmuir 21.9 (2005): 3749-3756.

Samuel, M., Polson, D., Graham, D., Kordziel, W., Waite, T., Waters, G., ...& Downey, R. (2000, January). Viscoelastic surfactant fracturing fluids: applications in low permeability reservoirs. In SPE Rocky Mountain Regional/Low- Permeability Reservoirs Symposium and Exhibition. Society of Petroleum Engineers.

Sanchez, J. M., & Hazlett, R. D. (1992). Foam flow through an oil-wet porous medium: a laboratory study. SPE reservoir engineering, 7(01), 91-97.

Sandengen, K., Kristoffersen, A., Melhuus, K., & Jøsang, L. O. (2016). Osmosis as mechanism for low-salinity enhanced oil recovery. SPE Journal, 21(04), 1-227.

Saarenketo, T. (1998). Electrical properties of water in clay and silty soils. Journal of applied geophysics, 40(1-3), 73-88.

Schmid, K. S., Gross, J., & Helmig, R. (2014). Chemical osmosis in two-phase flow and salinity-dependent capillary pressures in rocks with microporosity. Water Resources Research, 50(2), 763-789.

Schramm, L. L. (Ed.). (2000). Surfactants: fundamentals and applications in the petroleum industry. Cambridge University Press.

Schramm, L. L. (1992). Fundamentals and applications in the petroleum Industry. Adv. Chem, 231, 3-24.

Shah, D. (1977). 0. and Schechter, RS:" Improved Oil Recovery by Surfactant and Polymer Flooding. In AIChE Symposium on Improved Oil Recovery by Surfactant and Polymer Flooding. New (pp. 55-91).

Shaoul, J. R., van Zelm, L. F., & de Pater, C. J. (2011, November 1). Damage Mechanisms in Unconventional-Gas-Well Stimulation--A New Look at an Old Problem. Society of Petroleum Engineers. doi:10.2118/142479-PA.

Shen, A., Liu, Y., Bai, M., Liang, S., Wang, F., Cai, B., & Gao, Y. (2018). Surfactant Effects of Wettability Alteration and Low IFT on Countercurrent Imbibition for Tight Oil Formation. Energy & fuels, 32(12), 12365-12372.

Sheng, J. J. (2015). Status of surfactant EOR technology. Petroleum, 1(2), 97-105.
Shanmugam, G. (2012). Handbook of Petroleum Exploration and Production. New Perspectives, 9, 1-488. Chapter7.

Shaoul, J. R., van Zelm, L. F., & de Pater, C. J. (2011, November 1). Damage Mechanisms in Unconventional-Gas-Well Stimulation--A New Look at an Old Problem. Society of Petroleum Engineers. doi:10.2118/142479-PA.

Tangirala, S., & Sheng, J. J. (2019). Roles of surfactants during soaking and post leak-off production stages of hydraulic fracturing operation in tight oil-wet rocks. Energy & Fuels, 33(9), 8363-8373.

Taylor, R. S., McIntosh, G., Litun, R., Munn, D., Bennion, B., Piwowar, M., … Hoch, O. (2009, January 1). Montney Fracturing-Fluid Considerations. Petroleum Society of Canada. doi:10.2118/2009-154

Teklu, T. W., Li, X., Zhou, Z., Alharthy, N., Wang, L., & Abass, H. (2018). Low-salinity water and surfactants for hydraulic fracturing and EOR of shales. Journal of Petroleum Science and Engineering, 162, 367-377.

Vengosh, A., Warner, N., Jackson, R., & Darrah, T. (2013). The effects of shale gas exploration and hydraulic fracturing on the quality of water resources in the United States. Procedia Earth and Planetary Science, 7, 863-866.

Vledder, P., Gonzalez, I. E., Carrera Fonseca, J. C., Wells, T., & Ligthelm, D. J. (2010, January Low Salinity Water Flooding: Proof Of Wettability Alteration On A Field Wide Scale. Society of Petroleum Engineers. doi:10.2118/129564-MS

Washburn, E. W. (1921). The dynamics of capillary flow. Physical review, 17(3), 273.

Wijaya, N., & Sheng, J. J. (2019). Mitigating near-fracture blockage and enhancing oil recovery in tight reservoirs by adding surfactants in hydraulic fracturing fluid. Journal of Petroleum Science and Engineering, 106611.

Windland, H. D. (1972). Oil Accumulation in Response to Pore Size Changes, Weyburn Field, Sastkatchewan (No. F72-G, p. 25). Amoco Production Research Report

Wu, Y., Shuler, P. J., Blanco, M., Tang, Y., & Goddard, W. A. (2008, March 1). An Experimental Study of Wetting Behavior and Surfactant EOR in Carbonates With Model Compounds. Society of Petroleum Engineers. doi:10.2118/99612-PA

Xie, X., Weiss, W. W., Tong, Z. J., & Morrow, N. R. (2005, September 1). Improved Oil Recovery from Carbonate Reservoirs by Chemical Stimulation. Society of Petroleum Engineers. doi:10.2118/89424-PA

Xu, M., & Dehghanpour, H. (2014). Advances in understanding wettability of gas shales. Energy & Fuels, 28(7), 4362-4375.

Xu, C., Kang, Y., You, Z., & Chen, M. (2016). Review on formation damage mechanisms and processes in shale gas reservoir: known and to be known. Journal of Natural Gas Science and Engineering, 36, 1208-1219.

Yan, Z., Dai, C., Zhao, M., Sun, Y., & Zhao, G. (2016). Development, formation mechanism and performance evaluation of a reusable viscoelastic surfactant fracturing fluid. Journal of Industrial and Engineering Chemistry, **37**, 115–122.

Yarveicy, H., Habibi, A., Pegov, S., Zolfaghari, A., & Dehghanpour, H. (2018, March 13). Enhancing Oil Recovery by Adding Surfactants in Fracturing Water: A Montney Case Study. Society of Petroleum Engineers. doi:10.2118/189829-MS

Yu, W., & Sepehrnoori, K. (2013). Optimization of multiple hydraulically fractured horizontal wells in unconventional gas reservoirs. Journal of Petroleum Engineering, 2013.

Yuan, L., Dehghanpour, H., & Ceccanese, A. (2019, April). Imbibition Oil Recovery from the Montney Core Plugs: The Interplay of Wettability, Osmotic Potential and Microemulsion Effects. In SPE Western Regional Meeting. Society of Petroleum Engineers.

Zhou, Z., Abass, H., Li, X., Bearinger, D., & Frank, W. (2016). Mechanisms of imbibition during hydraulic fracturing in shale formations. Journal of Petroleum Science and Engineering, 141, 125-132.